

CZECH TECHNICAL UNIVERSITY IN PRAGUE



FACULTY OF MECHANICAL ENGINEERING
INSTITUTE OF MATERIALS ENGINEERING

**Print process parameters development for tool
steel L-40 in Laser Powder Bed Fusion**

Master's thesis

Author: Tomáš Kment

Supervisor: Doc. Ing. Jana Sobotová, Ph.D

2020/21

I. OSOBNÍ A STUDIJNÍ ÚDAJE

Příjmení: **Kment** Jméno: **Tomáš** Osobní číslo: **459863**
Fakulta/ústav: **Fakulta strojní**
Zadávací katedra/ústav: **Ústav materiálového inženýrství**
Studijní program: **Strojní inženýrství**
Studijní obor: **Výrobní a materiálové inženýrství**

II. ÚDAJE K DIPLOMOVÉ PRÁCI

Název diplomové práce:

Vývoj parametrů procesu tisku pro nástrojovou ocel L-40 v Laser Powder Bed Fusion

Název diplomové práce anglicky:

Print process parameters development for tool steel L-40 in Laser Powder Bed Fusion

Pokyny pro vypracování:

1. Theoretical part
2. Experimental part
 - a. Modification of printing parameters and selection of suitable for further testing, printing of test specimens
 - b. Metallographic analysis and evaluation of mechanical properties
3. Comprehensive evaluation of results and their discussion
4. Conclusions

Seznam doporučené literatury:

- [1]GIBSON, I., D. W. ROSEN a B. STUCKER. Additive manufacturing technologies: 3D printing, rapid prototyping, and direct digital manufacturing. Second edition. New York: Springer, [2015]. ISBN 978-1-4939-2112-6.
[2]YANG, Li, Keng HSU, Brian BAUGHMAN, Donald GODFREY, Francisco MEDINA, Mamballykalathil MENON a Soeren WIENER. Additive Manufacturing of Metals: The Technology, Materials, Design and Production. Cham: Springer International Publishing, 2017. Springer Series in Advanced Manufacturing. ISBN 978-3-319-55127-2.
[3]YAP, C. Y., C. K. CHUA, Z. L. DONG, Z. H. LIU, D. Q. ZHANG, L. E. LOH a S. L. SING. Review of selective laser melting: Materials and applications. Applied Physics Reviews. 2015, 2(4). ISSN 1931-9401. Dostupné z: doi:10.1063/1.4935926

Jméno a pracoviště vedoucí(ho) diplomové práce:

doc. Ing. Jana Sobotová, Ph.D., ústav materiálového inženýrství FS

Jméno a pracoviště druhé(ho) vedoucí(ho) nebo konzultanta(ky) diplomové práce:

Datum zadání diplomové práce: **27.10.2020**

Termín odevzdání diplomové práce: **23.12.2020**

Platnost zadání diplomové práce: _____

doc. Ing. Jana Sobotová, Ph.D.
podpis vedoucí(ho) práce

prof. RNDr. Petr Špatenka, CSc.
podpis vedoucí(ho) ústavu/katedry



prof. Ing. Michael Valášek, DrSc.
podpis děkana(ky)

III. PŘEVZETÍ ZADÁNÍ

Diplomant bere na vědomí, že je povinen vypracovat diplomovou práci samostatně, bez cizí pomoci, s výjimkou poskytnutých konzultací. Seznam použité literatury, jiných pramenů a jmen konzultantů je třeba uvést v diplomové práci.

Datum převzetí zadání

Podpis studenta



Declaration

I, Tomas Kment, declare that this master's thesis has been composed by myself and that it has not been submitted or published (whole or any part) in any previous degree application. All the parts inspired or published by any other documents or publications are stated with proper references. I also declare that presented data in this thesis experiment was obtained by myself in laboratories of Czech Technical University, Institute of Material engineering in cooperation with NCC MATCA and CARDAM Solution s.r.o. company (except the rare data for powder chemical and particle analysis). Rare data for mentioned part were delivered by University of Chemistry and Technology and Institute of Physics of the Czech Academy of Sciences.



Acknowledgement

I would like to thank to my master's thesis supervisor Doc. Ing. Jana Sobotová, Ph.D. for her professional attitude, patience, time and effort to realize master's thesis. I would also like to thank Ing. Štěpán Koláček from NCC MATCA for his extraordinary additive manufacturing skills and especially help with the project realization. Another person I would like to thank - Ing. Jan Krčil for his willingness and laboratory equipment advising despite the Corona virus restriction and policies. Also, special thanks goes to NCC MATCA (Institute of Physics of the Czech Academy of Sciences) and Cardam Solution s.r.o. company, for financing this project, which connected the theory approach with the practical task. For the final application opportunity, I would like to say thanks to Beneš a Lát a.s. company. One more thanks goes to Ing. Filip Rušar for his experienced advising during the experiment preparations and evaluations. Last but not least, I would like to appreciate support of my girlfriend and family members during the studies at Czech Technical University.



Annotation

Master's thesis is dealing with additive manufacturing technologies with focus on Laser Powder Bed fusion method (Selective Laser melting). Selective laser melting printer is located at Institute of Physics of the Czech Academy of Sciences (NCC MATCA), where author of this thesis performed as Additive manufacturing specialist under the cover of Cardam Solution s.r.o. company. The main subject of the investigation is licensed tool steel L-40 supplied by company Formetrix. Tool steel L-40 is processed with Selective Laser melting without further heat treatment (as-built state). Powder analysis is realized with final PSD curves, particle shape (SEM) and inner quality analysis. Powder chemical composition is checked with the use of EDX. Further process parameters are investigated on single-tracks and cubic samples, where the goal is to reach the lowest amount of porosity 0,2 % (99,80 % density). Highest reached cubic sample density was 99,98 %. In the final stage tensile and Charpy impact test samples were printed and processed. Despite the cubic samples with selected process parameter showed 99,96 % density, final mechanical properties did not meet with all supplier's specifications. The fracture surface analysis is placed at the end of the thesis with recommended counter measurements. Experiment part is closed with die core print pre-processing for high pressure die casting application.

Handed thesis is realized in cooperation of Faculty of mechanical engineering, Materials engineering institute, NCC MATCA (Institute of Physics of the Czech Academy of Sciences) and Cardam solution s.r.o. company. The final application is targeted for casting plant of company Beneš a Lát a.s.

Key words

Additive manufacturing; Laser powder bed fusion; Selective laser melting; tool steel; mechanical properties; process parameters



Content

1	Introduction	2
2	Additive manufacturing	3
2.1	History of additive manufacturing	4
2.2	Additive manufacturing technologies and materials.....	4
2.3	L-PBF.....	13
2.3.1	SLM (LMF) process.....	13
2.3.2	SLM (LMF) printer basic construction.....	17
2.3.3	SLM (LMF) process parameters	18
2.3.4	SLM (LMF) materials	27
3	Tool steels	35
3.1	Characterisation of tool steels	35
3.2	Tool steel L-40	44
4	Experimental part	51
4.1	Powder analysis.....	52
4.2	Single tracks build set up.....	55
4.3	Cubic samples build set up.....	56
4.4	Mechanical properties testing samples	58
5	Results and discussion	60
5.1	Powder particle size, morphology and chemical composition	60
5.2	Single tracks – results.....	64
5.3	Cubic samples – results	68
5.4	Mechanical properties - results	73
5.5	Final L-40 application	81
6	Conclusion.....	83
7	Literature	85



Faculty of mechanical engineering
Material engineering institute

Tomas Kment

1 Introduction

Additive manufacturing became worldwide known topic in the recent years. The most usual term to describe additive manufacturing is “3D printing”. One of the main 7 additive manufacturing groups is (Laser) Powder Bed fusion (L-PBF) – Figure 1. L-PBF is a technology used dominantly in engineering applications, because it can process most of the metals. One of the very important material groups for L-PBF are tool steels.

According to many problems with the tool steels printing process (cracking etc.) the development in material engineering is still going further. [1] The main interest was to find tool steel, that could be printed at the room temperature and it would stand all the requirements for long lifetime application (e.g. in the high pressure



Figure 1: Tool steel L-40 processed in L-PBF printer

die casting process). One of the latest releases was done by the NanoSteel company as steel L-40 (licensed by Formetrix). [2] L-40 was designed for dies, moulds and special components applications. L-40 specification should also meet the requirement on the room temperature printability. On the other hand, quality of the print (also printability) can differ on printer type. [2]

Goal of this thesis is to find process parameters for L-PBF printer located at Institute of Physics of the Czech Academy of Sciences (NCC MATCA) with final L-40 print density in minimum 99,80 %. The secondary goal is to print tensile and Charpy impact test samples to specify the final L-40 mechanical properties with selected process parameters. In occasion of this thesis, author participated as Additive manufacturing specialist under the supervision of Cardam Solution s.r.o.

Handed thesis was realized in cooperation between Faculty of mechanical engineering, Materials engineering institute, Institute of Physics of the Czech Academy of Sciences (NCC MATCA) and Cardam solution s.r.o. company. Author of this thesis would like to thank and appreciate all sides for efforts to make this project possible.

2 Additive manufacturing

Additive manufacturing, also known as 3D printing, rapid prototyping or free-form fabrication, is the revolutionary method of creating objects from 3D model data, usually layer-by-layer. [3] Instead of subtracting material (like machining), additive manufacturing is adding material. In general, technology uses a 3D model CAD data, where model is separated into the layers with finite thickness. The layers are sequentially joined to each other until the object is created. [4] This methodology allows to reach almost every shape required by the application or customers. The final product can require some post processing steps, that changes based on the type of additive manufacturing technology or application (will be discussed further).

For the last few years additive manufacturing became a very hot topic in the field of future applications. Developers of 3D printers are reaching bigger printing platforms, faster building rates, better quality and accuracy of the final parts. All these aspects are in connection to the price drop and complexity of materials available to print. [5]



Figure 2: Additive manufactured part from Ti-alloy [6]

The result of such development is that additive manufacturing came to various industry sectors such as aerospace, automotive, medical, tooling or jewellery. [3] The example of the parts made by additive manufacturing (SLM process) are shown in Figure 2. [6]

Nowadays additive manufacturing (according to the ISO/ATM52900-15 standard) is divided into seven categories and each of them will be described further [5]:

- 1) Binder jetting
- 2) Direct Energy Deposition
- 3) Material extrusion
- 4) Material jetting
- 5) Powder bed fusion
- 6) Sheet lamination
- 7) VAT photopolymerization

2.1 History of additive manufacturing

As many other technologies, additive manufacturing (AM) was developed on several places at the same time by various innovators. First two 3D printing technologies were invented in 1981 by H. Kodama. In 1984 an inventor from United States, Chuck Hull, filled his own patent for technology called Stereolithography (SL) – a form of VAT photopolymerization. Hull became widely known as the inventor of the 3D printing even though there were similar works before. Hull went on to found in 1986 and commercialized in 1987 with the first printer SLA-1. [5]

SL technology was using photosensitive resin and UV laser to selectively create solid layers and sequentially whole 3D object. In this occasion the Stereolithography file format (STL) was presented and it is still used nowadays in various applications. [5] Technology principle is shown in Figure 3. [7]

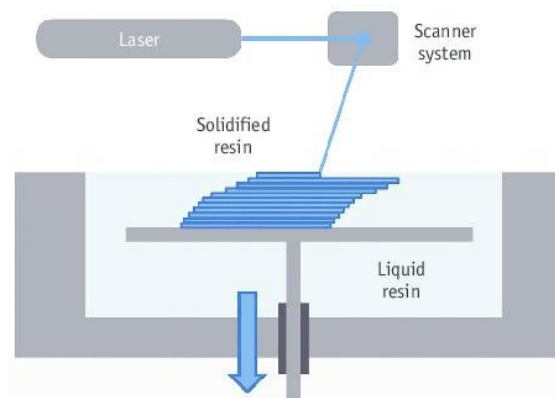


Figure 3: SL technology principle [7]

2.2 Additive manufacturing technologies and materials

Since 1984 (SL technology) until 2020, additive manufacturing made a huge step not only in the technology field, but also in processability of various materials like polymers or metals. In general, additive manufacturing can process following materials**:

- Resins, polymers and waxes
- Paper
- Sand
- Composites (also concrete)
- Metals
- Glass
- Chocolate and others

**Materials will be discussed in detail further.

As mentioned before, according the ISO standard ISO/ATM52900-15, there are 7 additive manufacturing technologies known in total. Technologies are summarized in Table 1. The Table 1 was mainly inspired by 3Dhubs website [8] .



Table 1: AM technologies - summary

Technology	Subtype	Energy source	Main Materials	Applications example	Companies example	Main benefits	Main disadvantage	Average layer thickness [μm]	Literature
<i>Vat photopolymerization</i>	SLA	UV light	Liquid resins or photopolymers	Concept models Medical scale models	Formlabs PRUSA research	Accuracy Surface quality	Limited and brittle materials	25 - 100 μm	[4], [8], [9], [10], [11]
	DLP	Digital projector							
	CDLP	Digital projector							
<i>Material extrusion</i>	FDM (FFF)	Heat source	Polymers Composites	Concept models Dimension control models Casting models	PRUSA research Stratasys	Building rates Price Strong polymer products	Part quality	50 - 400 μm	[4], [8], [10], [12]
<i>Material jetting</i>	MJ	UV light	Photopolymers	Plastic concept models	Stratasys	Multi-color print	Price	16 - 30 μm	[5], [8], [9], [10]
	NPJ	Heat (+Binder)	Metal Ceramic	Metal prototypes	Xjet	Accuracy and quality			
	DOD	Heat	Polymers Waxes	Casting models	Solidshape	Accuracy and quality			
<i>Binder jetting</i>	BJ	(Binder)	Metal Sand Ceramic	Prototypes Non-critical parts Sand moulds	ExOne Voxeljet	Building rates Building volumes Material diversity	Mechanical properties	100 μm	[5], [8], [10]
<i>Direct energy deposition</i>	LENS	Laser	Metals	Repairing Hybrid manufacturing	BeAM machines	Free shape starting surface High building rates	Quality - machining requirement	250 - 500 μm	[4], [5], [8], [9]
	EBAM	Electron beam			SCIAKI				
<i>Sheet lamination</i>	LOM	Heat Binder	Paper Polymers	Prototypes and concept models	Mcor	Building speed	Limited materials	100 - 200 μm	[4], [5], [8], [9]
<i>Powder bed fusion</i>	MJF	IR light + fuse agent	Metal Ceramics Polymers	Engineering concept models Final machine parts	HP	Price-building rate ratio	Metal diversity	70 - 100 μm	[4], [8], [9], [10], [11], [13]
	SLS	Laser	Polymers	Prototypes Functional parts	EOS	Isotropic properties Self-supporting	Price	80 - 120 μm	
	DMLS/ SLM (LMF)	Laser	Metals	Topology optimized parts Tooling Medical application	EOS/SLM solutions	Mechanical properties Metals processability	Build volume Anisotropy	30 - 50 μm	
	EBM	Electron beam	Metals	Medical application Topology optimized parts Tooling	GE additive	Stress free parts Metal processability	Cool down time Anisotropy	50 - 200 μm	



- *VAT Photopolymerization*

Technology VAT photopolymerization was shortly presented in the history of additive manufacturing. It is obvious that this technology was just at the beginning of the 3D printing. Nevertheless, it has still strong place in the field of additive technologies

In general, Photopolymerization processes use advantage of liquid resins or photopolymers, that are chemically reacting with the light at certain wavelength and become solid. The reaction itself is called photopolymerization (origin of the technology name). [4] Printing process is based on the sinking of the building platform into the resin



Figure 4: SLA printed model parts [14]

about the distance equal to the layer thickness. For each one step energy source cures the material and creates a solid layer of specific shape. The layers afterwards create a whole 3D object. [14] Example of the printed parts is shown in Figure 4.

Based on various configurations and light sources, VAT Photopolymerization is divided into subtype technologies like SLA (Stereolithography), DLP (Digital light processing), CDLP (Continuous Digital light Processing) and others. Resins and photopolymers are processable in this additive manufacturing technology.

The main advantage of VAT photopolymerization is accuracy, surface quality and simplicity. As disadvantages we can mention brittle parts, degradation on the sunlight and postprocessing requirements. [8]

- *Material extrusion*

Material extrusion is one of the most widely used additive manufacturing process worldwide. The most spelled shortcuts in this fields are FDM and FFF. FDM (Fused deposition modelling) was developed by Stratasys company (USA) and only this company can use the name for the technology. [15] FFF (Fused Filament Fabrication)



was invented by the company RepRap and the name can be freely used. Besides the names the technologies are completely the same.

FDM (or FFF) process starts with material loading in the solid state (can be liquid). Material is most usually in the form of pellets, granules, powder or wire. The material is transported to the extrusion head. In the extrusion head with the specific heat material becomes semi-solid (or liquid).

Afterwards the material is extruded with positioning of extrusion nozzle with specific flow and diameter. Higher diameter means higher throughput, but also worse part quality. After extrusion material solidifies another layer can be placed. [4]

- ① Filament spools
- ② Main filament
- ③ Support filament
- ④ Extrusion head
- ⑤ Printed part
- ⑥ Support structure
- ⑦ Build platform

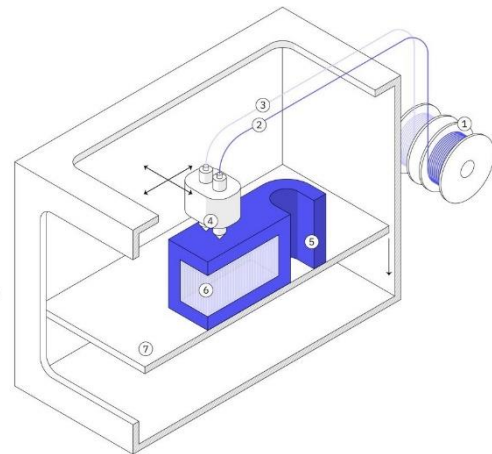


Figure 5: FDM technology principle [8]

Process is shown in Figure 5. [8]

Among the thermoplastic materials commonly used are acrylonitrile butadiene styrene (ABS), polylactic acid, polycarbonate, polyphenylsulfone, polyamide, polystyrene, and Ultem 9085. Several printers allow to use two different materials during one printing process. [5]

FDM technology is easy-to-handle, office friendly, cost effective, it has relatively high building rates with connection to durable, strong products. The weakest point of FDM is the low accuracy compare to the other AM technologies (connected to the diameter of the extrusion nozzle) and anisotropy of the printed parts. [8]

FDM technology was also the key-point of the Czech 3D printing inventor Josef Prusa. His printer Prusa i3 (Figure 6) became one of the most worldwide used printer ever. [12]

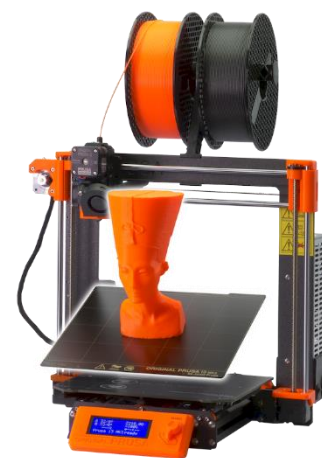


Figure 6: Prusa i3 printer [12]



- *Material jetting*

Material jetting is a process that is very similar to the original 2D printing mechanism. First successful printer with material jetting technology was introduced in 1994 by Solidscape and it was using melted wax droplets to create objects. [4], [16]

In classical material jetting, droplets of photosensitive materials (like photopolymers etc.) in the liquid droplets form are deposited with the use of the printing head to certain location. Material is cured with UV light afterwards. When the certain layer is created, the building platform lowers. Printing mechanism is shown in Figure 7. [16]

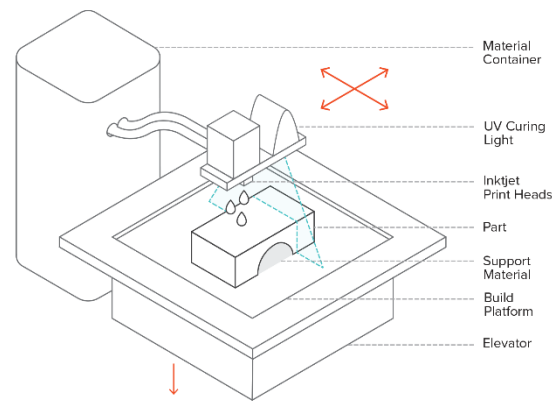


Figure 7: Material jetting technology [16]

Second subtype technology is Nanoparticle jetting (NPJ). NPJ printing mechanism was developed by the company Xjet. The process uses inkjet-style head to deposit thousands of droplets of a proprietary liquid containing metallic, ceramic nanoparticles or support nanoparticles. The temperature in the build chamber can be as high as 300 °C (570 °F), which causes the liquid to evaporate as the nanoparticles are deposited. After the initial printing process, a component still contains a level of porosity, as well as support material attached (“green part”). Therefore, final heat treatment is required. [5]

Third subtype method Drop on demand (DOD) is described in detail in [5].

Material jetting (MJ) is very accurate (± 0.1 mm) and it is considered as one of the most precocious AM technology (mainly in surface quality). On the other hand, MJ always requires support structures and it is considered as one of the most expensive. [16]

MJ can also use several types of materials in one process (full-colour printing) -mainly polymers and waxes (especially for casting models and prototypes). There are also technologies in MJ using metals – like NPJ. [8]



- *Binder jetting*

Binder jetting (BJ) is additive manufacturing process, that was originally developed at MIT (Massachusetts Institute of Technology) as Three-Dimensional printing (3DP). In principle BJ applies a binder into a powder deposited on the powder bed. Binder provides a bonding mechanism to the powder particles (binder also contains a small number of powder particles). Once the layer is created the powder bed lowers and process is repeated. [4] The process of printing is shown in Figure 8 [17].

After the printing process the printed parts are left in the building chamber for a certain time to fully bond the powder particles. Afterwards the parts are de-powdered. The resulted parts contain the building material, but also the bonding agent (binder) – the part has low mechanical properties. These parts are called “green parts” and they require the post processing process. Post-processing can differ, but in general it means to evaporate the binder in the furnace. Afterwards the part is usually sintered, but the process can differ. [17]

The final product contains a certain amount of porosity (for sintered parts around 3 %). [17] This leads to the BJ general disadvantage – mechanical properties of the final parts (mainly for metals) are lower than for other AM technologies. For example, [17] shows that Yield strength for Stainless steel 316 in BJ + sintered part is 214 MPa. On the other hand, for DMLS or SLM process (will be introduced further) is 470 MPa. [17]

BJ is using a nozzle to deposit the binder into the powder. This is the reason, why BJ is considered as one of the highest productivities in AM (several nozzles can be used) despite lower mechanical properties. Printers for BJ are also allowing larger building chambers than other AM technologies like SLM. [4]

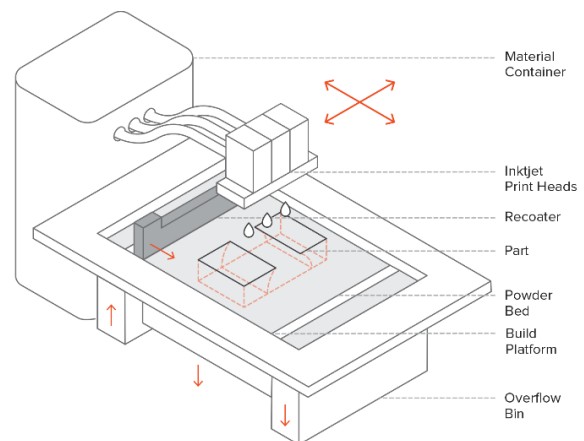


Figure 8: Binder jetting technology [17]

BJ can process various materials like metals, sand or tungsten carbide. The advantage is that printer does not have to produce the heat to connect the powder particles. BJ is used not only for metal parts, but also for sand mould casting etc. [4], [17]



- *Direct energy deposition*

Direct energy deposition (DED) is an AM technology that can be used for materials like ceramics or metal composites, polymers etc. Nowadays DED is used mainly for production of metal parts. DED additive manufacturing systems deposit material on to a platform (or component) from a nozzle, in which the feed material is melted. The metal feedstock is generally melted with laser (Laser Engineered Net Shape = LENS) or electron beam (Electron Beam Additive Manufacture = EBAM). [5], [8]

The melted material is directed into the melt pool where cools down and solidifies. Electron beam-based systems use a metal wire feed, and the process must be performed in a vacuum to prevent the electrons in the electron beam interacting with or being deflected by air molecules. Laser systems use either wire or powder feed, and either require a fully inert chamber. Wires are used because of the economic benefits. [5]

DED technology allows high deposition rates against the Powder bed fusion (PBF) – up to 9 kg/h (for PBF 0,2 kg/h). Higher deposition rate relates to loss of accuracy – final machining is required most of the cases. One of the big advantages of DED is that flat surface is not required for deposition. This can be used in hybrid manufacturing systems or repairing dies and other metal components. [5]

- *Sheet lamination*

At the beginning of the AM commercialization, in 1991 technique called Laminated Object Manufacturing (LOM) was published. The technology consisted of placing material sheets on the building platform, that were bonded and cut by the laser. [4]

In general process remained the same until nowadays, except various techniques are used for various materials. The main difference in the various techniques we can find in the order of material bonding (or joining) and forming (shape cutting). Based on that we can find processes “bond-then-form” and “form-then-bond”. [4] All the technology principles are described in [4].

From material perspective various groups were already processed like plastics, metals, ceramics, paper or composites. The last two mentioned are mainly used today. Advantage of the technology is in low shrinkage, low induced stress and material variation. The disadvantage is accuracy and inhomogeneity. [4]



- *Powder bed fusion*

Powder bed fusion (PBF) is one of the most common used AM technology in engineering applications. PBF started in 1980s at the University of Texas (USA). The first published PBF technology was named SLS (Selective Laser Sintering) and it was using a polymer powder material to create objects with laser. [4]

Nowadays, all technologies considered to PBF share the same principle. Powder bed fusion uses energy source to fuse (sinter or melt) the powder particles. [8] The powder of certain height (equal to one layer thickness) is placed on the powder (building) bed. The sintered particles represent a layer of specific shape and are placed in specific way on each other until the whole object is formed. The technology can be divided into 3 groups based on thermal (energy) source used for joining the material particles. Each group can be also classified in order of melting or sintering the powder particles. [4]

Thermal sources in PBF: [4], [8]

- Laser – Selective laser sintering/melting or laser metal fusion (SLS/SLM or LMF), Direct Metal Laser Sintering (DMLS)
- Electron beam – Electron Beam Melting (EBM)
- Others (binders etc.) – Multi Jet Fusion (MJF)

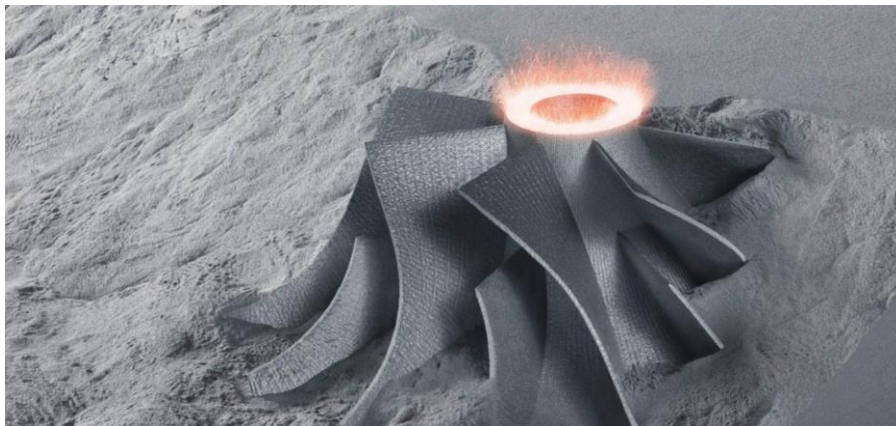


Figure 9: LMF (SLM) process part production [18]

The most common energy source are lasers. One of the parts being built in LMF (or SLM) process with TruPrint printer is shown in Figure 9 [18]. Presented thesis is also dealing with Laser-Powder Bed Fusion (L-PBF) and it will be described in detail in the next chapter. EBM will be shortly introduced and MJF description can be found in [5].



Electron Beam Melting (EBM)

EBM process is based on focussing of an electron beam in certain areas of printing bed with deposited powder (average particle size of 45-105 μm). [19] These areas are fully melted and solidified. In electron beam gun the tungsten filament is heated to emit electrons accelerated at high voltage (60 kV), resulting in an electron beam (carrying high kinetic energy). [19] The energy is then transferred into the powder and the solid layer is formed. [19]

Whole process is happening in the preheated vacuum chamber. In air or even an inert atmosphere, the electrons would get deflected as they would interact with the gas molecules. Before each powder layer is melted, the electron beam is defocused to scan the powder bed area. This causes the powder particles to slightly sinter together and provide the bed support for the part being built. [19] Mentioned operation reduces the requirement for supports. [5]

After the certain layer is completed, the process repeats on the lowered bed about the height of one-layer thickness with newly deposited powder.

Completed part is then left in the building chamber to cool down (based on material, size etc.). Electron beam melting process is shown in Figure 10. [5]

The main advantage of EBM is low residual stress in the final parts (due to pre-heating), relatively high building rates (suitable for larger components), reduction of support requirements. Disadvantages can be found in material processing (only conductive materials can be processed), cooldown time, powder recycling difficulties. [5]

As mentioned before, the thesis is dealing with Laser-Powder Bed Fusion (L- PBF). The next chapter describes the technology in detail.

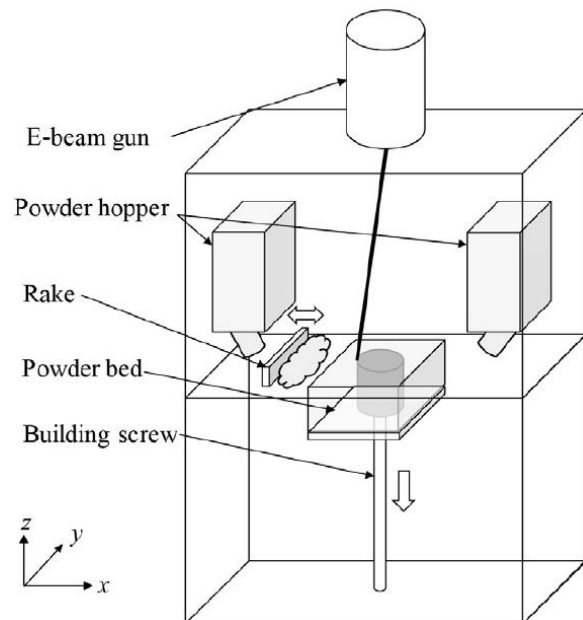


Figure 10: EBM process [5]



2.3 L-PBF

Powder bed fusion uses a high energy power source to selectively melt or sinter powder on the powder bed. [5] As mentioned, the most common used energy source is laser – Laser Powder Bed Fusion or shortly L-PBF. [4] Since 1980s L-PBF technology developed in a way of materials, building rates, product sizes, accuracy, etc. Many different approaches were presented and can be included into the L-PBF. Even though they share the same basic set of characteristics, difference can be found in a way of joining the powder material particles:

- SLS = Selective laser sintering
- DMLS = Direct metal laser sintering
- SLM/LMF = Selective laser melting/Laser metal fusion

SLS is originally polymer-based process marketed by company 3D systems and EOS. [4] As it is also referred by [4], [5] and [8], SLS process is mainly used for non-metal materials (exceptions can be found). This thesis is dealing with metal processing technology SLM (or LMF), so the SLS will not be described in detail. Even though can be said, that SLS is very similar to DMLS or SLM (LMF) technologies. More information about Selective Laser Sintering can be found in [8] or [5].

2.3.1 SLM (LMF) process

All L-PBF (even PBF technologies) share the same basic process principle. In this thesis we will focus more on SLM (LMF) and how it differs from DMLS. As first it is important to understand the process flow of the process.

- *Process flow and difference between SLM and DMLS*
-

a) Modelling and Pre-Processing

First step is creating and validating a CAD model. The CAD model is converted to proper format (usually STL or AMF). Model is then transferred into the pre-processing software (“slicer”). In this software the whole printing process is set up. It includes model manipulation, model repairing, positioning on the platform, scaling, adding support structures, slicing and setting most of the printing parameters. As an example of such a software - Magics by Materialise can be mentioned. Support structures in L-PBF of



metal parts are applied mainly to extract the heat from the model and avoid warpage due to thermal stress (object is anchored to the building plate). Support structures in this case do not support the part against the gravity and overhanging like in SLA or other methods. [19]

Afterwards the model with the support structures is sliced into a given number of layers with specific height. These slices create 2D cross-sections with the model. The thickness of the typical layer in SLM (even DMLS) process is 25 μm up to 75 μm . [19] The thickness also has to correspond to other printing parameters mentioned further.

Once the pre-processing steps are done, the machine preparation follows. [19] First printer needs to be cleaned from previous printing operations. Afterwards the printer is filled with the powder material. The shielding gas parameters needs to be checked too. Hardware preparation steps vary with the printer. Routine check should be also done before every printing operation, to ensure safety working space. [19]

b-1) Printing

Once the preparation process is done, the printing can start. The recoating mechanism applies exact layer of material powder. Most of the machines have process control, that takes picture every recoating cycle and use the reflectivity information to determine full coating areas (or pause the process to prevent failure). Printing operation is happening in the building chamber (pre-heating is possible) in the presence of the shielding gas (inert gas) like argon or nitrogen to prevent material oxidation. [19]

When the new layer of the material is ready, the laser beam starts to pass through the powder bed in x and y directions (Figure 11 [20]) and fuses the powder.

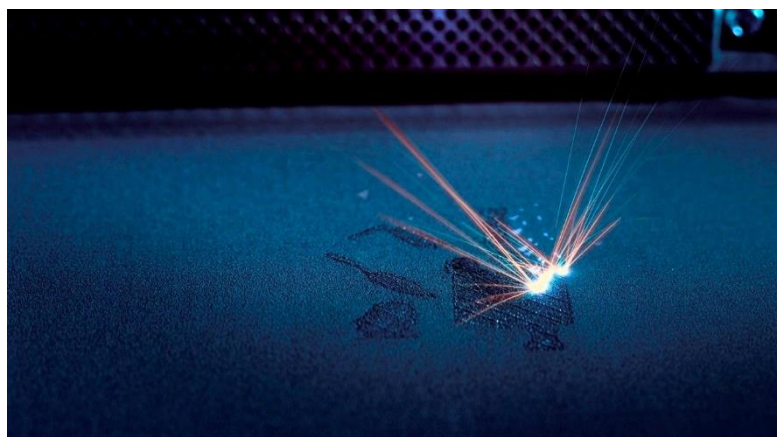


Figure 11: Printing process [20]



Information about the positioning of the laser is delivered through the special code, that is very similar to CNC G-code. Once the layer is created, the powder bed moves about the layer height in z direction. [4], [5] The printing platform can be also filled with different parts that are being built with different parameters. Printing is also the only moment, when SLM (LMF) and DMLS can be clearly divided.

b-2) Difference between SLM (LMF) and DMLS

SLM and DMLS are often considered as one technology processing metal materials, but difference still can be found. As it is mentioned in ALL3DP magazine [20], the difference between DMLS and SLM is the temperature that is being used for powder fusion. DMLS does not fully melt the powder, but the temperature is high enough to fuse the particle surfaces. On the other hand, SLM (LMF) process is reaching higher temperatures and fully melts the powder. LMF technology has no difference against the SLM method. As it is mentioned on TRUMPF official website [18], LMF fully melts the powder. Author of this thesis presumes, that in DMLS powder also melts in certain areas, but not in the full volume. Different names for the technologies seem unnecessary (only in marketing purposes), but the origin reason comes from the history and development of these technologies. [20]

DMLS was developed by company EOS and it was commercialized in 1995. SLM technology was developed at the same time by Fraunhofer Institute for Laser Technology in Aachen. [20] SLM faced issues that were not related to the technology itself but to the breaking of licensing agreements. [20] While EOS emphasizes DMLS, they also hold an interest in the SLM technology through their licensing arrangements with Trumpf GmbH (Trumpf named the technology Laser Metal Fusion – LMF). [20]

Generally, can be said, that in the final product is no difference between SLM, DMLS and LMF. Especially if we consider the sensitivity of the process parameters. Technologies using the melting mechanism will be working better with pure metals and DMLS will be restricted to alloys. [20] On the other hand, SLM (LMF) are reaching higher temperature, that leads to higher gradients and induced stresses.



c) Part removal

The printing time is based mainly on the part size, layer height and technology. Once the printing operation is done, L-PBF allows almost immediate de-powdering and part removing (advantage against EBM). Typically, the parts are removed from the powder on the building platform (Figure 12). The remained powder is reusable after certain sieving operations. [19]

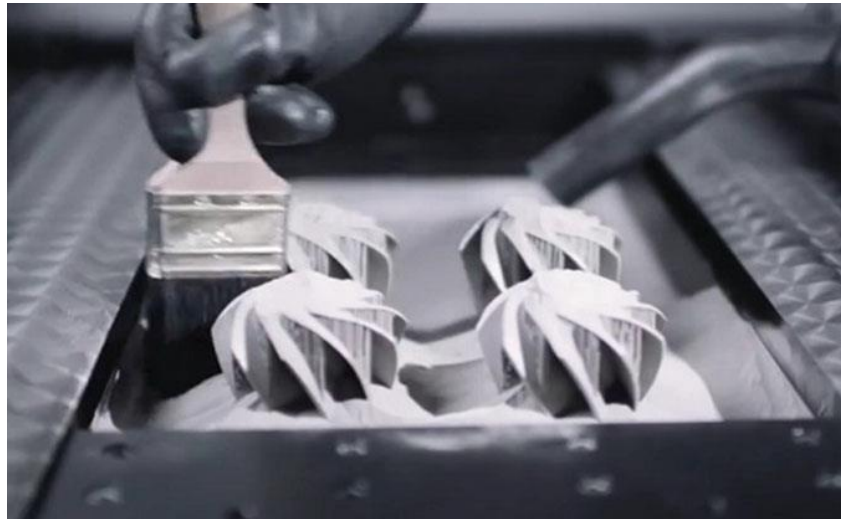


Figure 12: SLM part removing [19]

d) Post-processing

One of the main advantages is L-PBF produces near-net shape products. That means the parts are almost finished. Necessary processing operation is the support structures and the trapped powder removing. The supports can be removed manually or with the machining (based on requirements). Machining is usually used for surface finishing- Final parts can also show some residual stresses that are not suitable with the final application. The proper heat treatment to relief the stress or reach final mechanical properties can be applied. [19] The whole process flow is summarized in Figure 13.

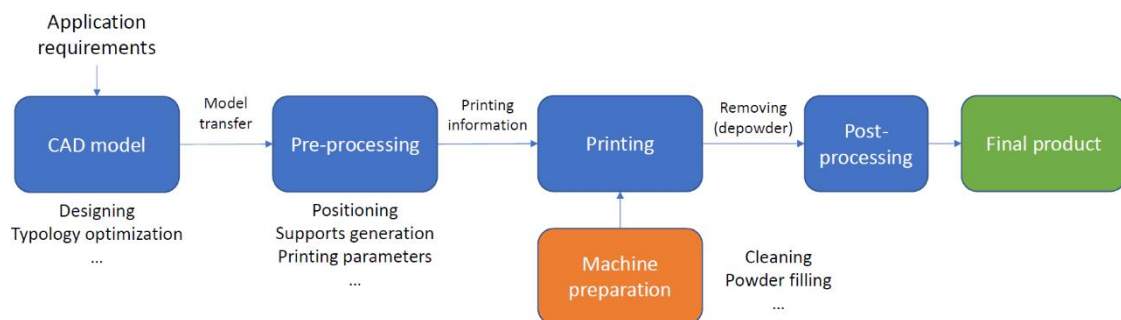


Figure 13: Process flow chart

2.3.2 SLM (LMF) printer basic construction

To fully understand principle of SLM (LMF), the printer construction basics should be explained.

The basic parts of the SLM (LMF) machines:

- Laser
- Scanner mirrors and lens
- Powder bed with platform
- Powder and overflow bin
- Recoating blade or roller
- Preheating source
- Shielding gas pumps and filters
- Construction (doors, ...)

Laser is the energy source used for metal powder fusion. The laser beam is directed with scanner mirrors through the lens in x and y directions on the powder bed. Powder bed is the place, where the material powder is deposited and fused. Deposition is realized with recoating blade (other mechanism can be placed). Powder is delivered from the powder tank (or bin) with help of the piston moving in Z direction. Exceeded powder is dropped in the overflow bin. Preheating source can be placed in several mechanisms like induction

spool in the powder bed or infrared light source. Shielding gas inflow and outflow is also placed in the printer. All the equipment is secured in the build construction with certain vibration damping. Other parts like manipulation equipment can be found, but it unnecessary to describe. The basic scheme of the SLM (LMF)

is shown in Figure 14. [5], [8]

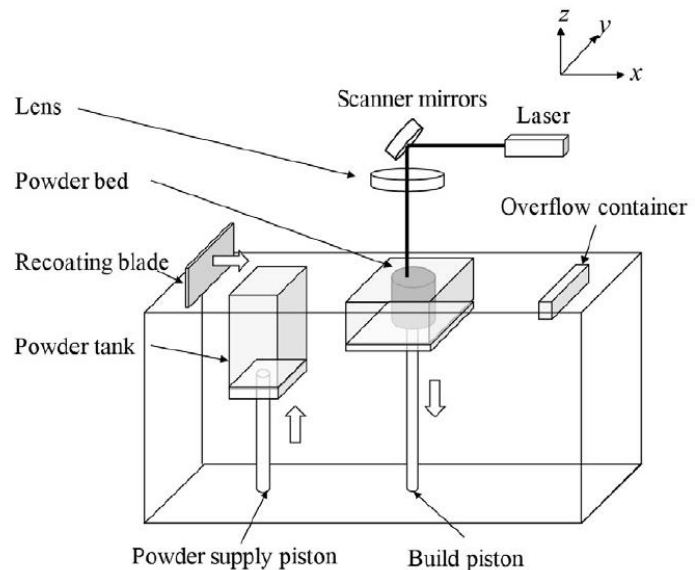


Figure 14: SLM printer scheme [5]



2.3.3 SLM (LMF) process parameters

The main goal of the handed thesis is the development of the process parameters for the tool steel L-40. The process parameters are critical according to the final product mechanical properties, microstructure, surface quality, process productivity etc. To fully understand the discussed topic, there needs to be deeper understanding of the main parameters, that the following experiment will be dealing with.

As it is mentioned in [19], for metal powder bed fusion technologies, there are more than 20 described process parameters in connection to the final part quality. On the other hand, there are also more than 20 parameters, which are not described and influence the final product. Handed thesis is dealing mainly with the material and printing strategy parameters. In this chapter we will be discussing parameters, that will occur in the later experiment.

In this thesis we will divide the process parameters in to following groups:

- a) Machine related parameters
- b) Powder related parameters
- c) Laser and scan strategy parameters
- d) Other parameters

a) Machine related parameters

As the SLM technology goes further in the development, the machine producers are forced to specify more parameters connected to the printer itself. Printer set up is usually delivered by the manufacturer, but users can adapt it very easily. Machine parameters are mostly dealing with the process stability and control. For example, the oxygen content in the printing chamber, specific printer components temperatures, recoater type and speed etc. In our case we will be discussing two parameters from this group – shielding gas and printing chamber pre-heating.

Build chamber pre-heating is commonly applied to avoid cracking and thermal distortions which is caused by rapid cooling in SLM. [21] Preheating also can help to reduce the amount of porosity in the part processing, because of the lack of fusion (low energy input). The study [21] also mentions, that preheating could provide more stable



melt pool during the printing process. In the commercial SLM machines, the preheating is very limited and usually is not greater than 200 °C. [21] This is mainly caused by inability of the bigger platforms to provide homogenous temperature fields.

Melting in SLM process leads to quick temperature cycles, where material is selectively melted and solidified in short time period. We can assume, that in high carbon steels (like tool steels) the martensite (or bainite) transformation is happening even in the build chamber environment. Martensite/bainite transformation leads to higher induced stress, where in combination with temperature gradients the cracks can appear. The cracks with connection to preheating is shown in Figure 15 for M2 HSS steel. [22]

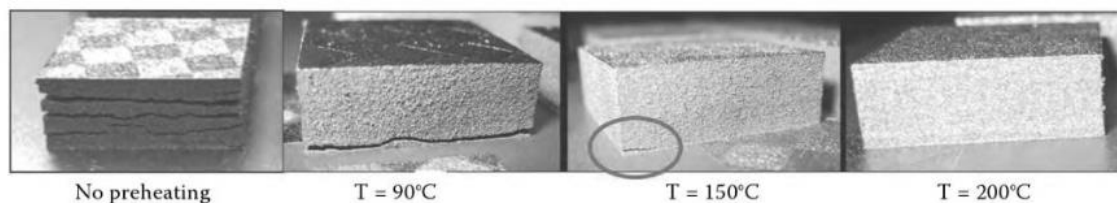


Figure 15: Cracks elimination with preheating for M2 HSS steel [22]

For example, study [23] of H13 tool steel, which has very similar applications like steel L-40, showed sensitivity to higher pre-heating against the structure homogeneity and mechanical properties. On the other hand, in the mentioned study [21], the preheating had no influence on the Maraging steel 18Ni300. [21] This could be caused mainly by the carbon content, where in Maraging steels is very limited.

As it was mentioned, the main issue with the pre-heating is to keep the temperature field homogeneous and do not increase the temperature gradient among the build platform. This is especially based on the type of preheating mechanism. [24]

According to discussed problems, in this study the build preheating will not be considered. Especially if the process parameters can be set up in the room temperature, it avoids instability and part failure in case of pre-heating deviations. The ability of the metal to be printed during the room temperature also brings big advantage to be transformed on other printers. Preheating will be applied only in case the main object of this thesis – L40 tool steel – will be unprintable at the room temperatures. As it will be discussed further, L-40 was developed in purpose of the best possible printability.



The second discussed parameter in machine parameters group is shielding gas (SG). During the LMF (SLM) process, the melt-pool must be covered by the shielding gas to avoid reactions mainly with the oxygen. Steels reactivity with oxygen is increasing in higher temperatures. On the other hand, depends on the alloy itself e.g. Titanium will require more precise shielding than steels.

LMF (or SLM) uses as inert atmosphere argon or nitrogen. The inert gas is directed to the building chamber on the building platform with the certain flow (inner circulation). The gas is filtered during the printing from secondary products through filter system. Direction of the shielding gas flow can affect the final product and create the defects in certain areas. Especially the secondary products from the previous printed areas can be transferred by the SG on the following printing areas. Some studies also showed the effect of the shielding gas flow on mechanical properties of the processed material. The biggest issue is the flow among the build chamber- it is not constant. The purity of the shielding gas is also big question, so the oxygen content should be always checked. [25]

As an example, study [26] can be mentioned. In this study it was proved, that position of the test sample on the building platform has high impact on the final density. This study also showed the impact of the shielding gas flow velocity, where the porosity significantly decreased with the increasing velocity. This is very valuable experience, but it will always be based on the printer construction.

In this thesis the gas flow influence will be constantly set (even it is not constant always). All the experiments for process parameters development will be designed to avoid influence of the SG flow. During the experiment the samples will be observed to observe any repeating defects on the certain platform position. As a shielding gas nitrogen will be used with the flow of 2,5 m/s.



b) Powder-related parameters

Powder-related parameters are the first variabilities, that is the manufacturer dealing with in matter of the product material. The critical factors are particle shape, particle size and chemical composition. The last mentioned is probably the most important, because chemical composition defines the processability for specific AM technology.

The weldability of various metals and alloys can vary significantly, and it is a good indicator (not the only one) which metals are processable by SLM. [27] Especially for steels, the weldability is chemically dependent. If the carbon content increases, the processability of the steel decreases. Chemical purity of the material is also highly important, because oxygen, hydrogen or sulphur can cause failures during the building. The chemical purity depends directly on the powder production technology (gas atomization, water atomization etc.) and storage. For example, [28] have studied the oxygen content in Ni-Based alloy for WA and GA powders. Oxygen content in WA powder was 95 times higher than in GA (1,90 [wt. %] vs 0,02 [wt. %]). [28]

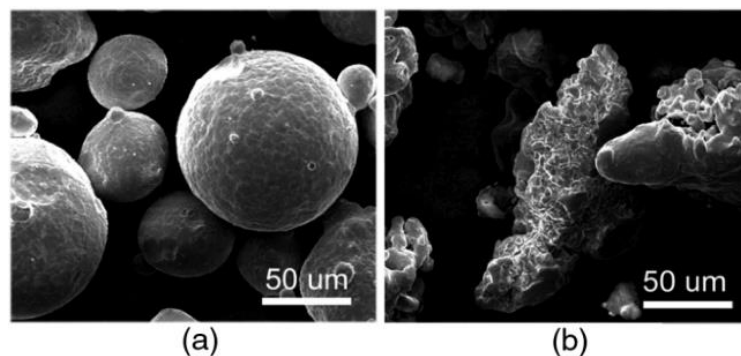


Figure 16: a) Gas atomized powder b) Water atomized of H13 tool steel [29]

The metal powder particles shape for AM is preferred to be spherical. Spherical shape allows powder bed machines to spread homogenous fine layers. [27] The shape of the particles highly depends on the powder production technology, where gas atomization is reaching best combination of shape, density and reproducibility. [3] The comparing example of H13 tool steel powders (WA and GA) investigated by [29] is shown in Figure 16. The water atomized powders are distributing unstable and irregular shapes, with higher oxygen content. [29] WA powders have an advantage in the lower production cost, but the printing process is still a big question of stability.



Last parameter we will be discussing deeply is the particle part size which is mostly defined with particle size distribution (PSD) curves. Generally, there are two types of PSD curves – cumulative and differential. The (PSD) is a curve, that is summarizing the particle sizes and its distribution presented in the amount of the powder. The example of the differential PSD curve is shown in Figure 17. The x axis in Figure 17 represents the powder size and y axis the % of differential or cumulative volume. For specific dimension on the x axis the volume percentage can be found. Second curve is the cumulative PSD curve, which describes how much volume of the powder has “lower size than”. These values are usually placed into differential PSD curve in D_{10} , D_{50} and D_{90} values. For example, $D_{10} = 30 \mu\text{m}$, means that 10 % of the particles in the measured volume has lower size than $30 \mu\text{m}$. [3], [30] From authors experience mostly used curve is differential with the use of D_{10} , D_{50} , D_{90} values.

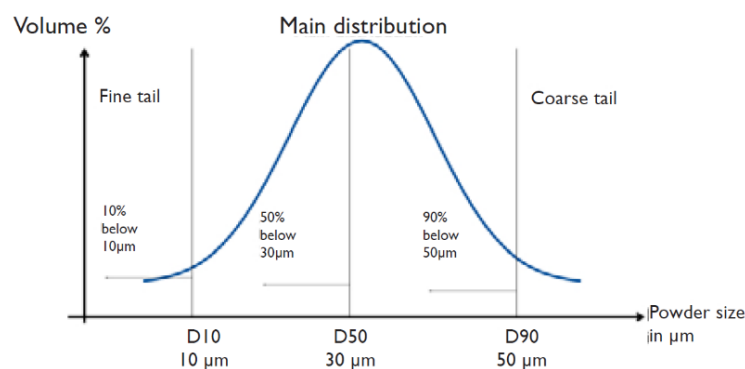


Figure 17: PSD curve [3]

Powder particle size is very important in matter of layer thickness, because it is considered as approximate layer height limit. [19] Layer thickness will be described in laser related parameters.

Even though there are more variabilities, that could be investigated, we will try to minimize and consider them as a stable (constant). In this thesis the particle shape, size distribution and chemical composition will be investigated. For example, powder absorptivity will not be considered. As it is also mentioned in [19], this value is mainly based on particle shape and chemical composition. It can be also said that material powder in the further process is constant parameter that is accepted or not. Powder investigation is always voluntary, and it should be applied mainly in the case of the new material (or supplier) to ensure the final product quality. In the ordinary case or certified supplier, the powder parameters can be guaranteed.



c) Laser and scanning parameters

In the laser and scanning related parameters we can find more variable values, that must be considered always. The laser set up has to adapt not only to the material (powder), but also to the design of the printed object.

As a laser and scan related parameter we can mention laser spot diameter, laser wavelength, laser pulse with

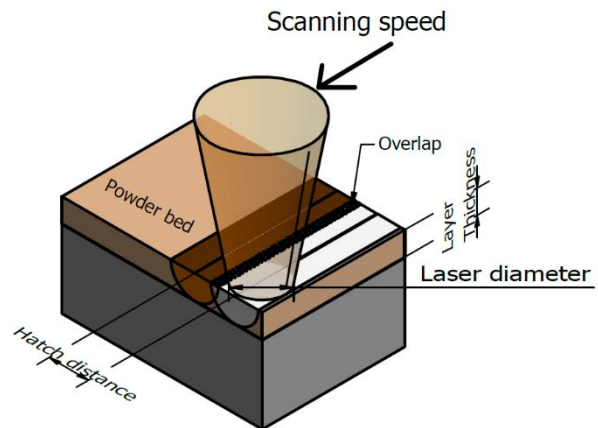


Figure 18 SLM process parameters example

certain frequency (or continual), scanning speed, hatch distance etc. All the mentioned parameters will be influencing the printing process and its stability.

According to many publications (e.g. [31]) the main factors to be optimized in the SLM process is laser power, hatch spacing (or overlap), scanning speed and layer thickness. [4], [31] The mentioned parameters are shown in Figure 18.

Parameters in Figure 18 can be connected into one general criteria – Volume Energy density (VED). VED is definition of energy input to the volume 1 mm³ of the processed material. Simplified definition is used as: [32]

$$VED = \frac{P}{v \cdot h \cdot t} \text{ [J/mm}^3\text{]}$$

Where P is the laser power [W], v is scanning speed [mm/s], h is hatching distance [mm] and t is the layer thickness [mm]. [32] VED equation shown above is not accurate, because it doesn't use for example absorptivity. On the other hand, VED is very usable estimation to optimize the printing process and reach appropriate quality.

Additional value used in this thesis in the following experiment is the linear energy density. The linear energy density will be considered as $E_L = P/v$ [J/mm]. It is very approximate value to determine the energy input for single vector. E_L is usable mainly in the first printing experiments with the new material. Various studies have shown that there exist optimal laser power/scanning speed ratio for the SLM process. [19] Other



laser-related parameters like laser wavelength etc. will not be discussed in this thesis, but in some cases, they play very important role.

As it was mentioned before, the main 3 parameters (layer thickness is kept constant) need to be adapted to certain material and geometry. That means on the border of the printed objects the parameters will be chosen differently than in the volume area. Therefore, the up-skin, down-skin, border and in-skin parameters are usually separated in the software set up. In this thesis we will be discussing dominantly in-skin parameters that form most of the manufactured object. The rest can be followed by certain recommendation or it can be investigated separately. In the following paragraph the main 3 laser related parameters will be defined.

Laser power is the most important parameter option of the printing process, because it determines the amount of the energy output towards the powder bed. Scanning velocity provides an information, how quickly the laser beams moves around the powder bed (how long is the beam spot area exposed to the laser). Hatch spacing defines the distance between the centres of each printed line (vector). Usually the overlapping is used, and it is highly dependent on the laser beam diameter and its HAZ. [19] The layer thickness is kept constant and it influence mainly the part dimension quality and printing process time (higher layer thickness leads to faster building speed).

In the process parameters development, the range of VED is set and the parameters are adapted to cover full range of possible values. For this purpose, the cube samples are printed and analysed (microstructure, porosity, hardness), where the process parameters are different for each cube. The example platform from this thesis experiment is shown in Figure 19. This set up will be more discussed in the experiment part.



Figure 19: L-40 cubic samples from experiment

From description above is certain, that laser-related parameters are defining usually the amount energy transferred into certain volume of the material. Scan-related parameters points to strategy of the laser beam movement in each layer. It defines the strategy how



the printed object is built. Hatch distance is the main scan-related parameter and it was described in previous paragraphs. Scan pattern, scanning sequence plays very important role in the thermal gradient distribution and temperature fields distribution. [19] Ideal printing strategy would provide homogenous temperature field. This ideal strategy is unreachable. [19] We can also assume, that anisotropy of the final part will be affected by the scan-related parameters (like with part orientation), because the grain structure will be oriented in specific direction.

The main scan-related parameters are scanning pattern, hatch distance, hatch offset etc. [4] Based on the geometry the vectors are generated for each layer. Scan pattern is defined as hatch pattern, the planned deposition paths associated with one or a series of layers. [27] Scan strategy is the design and selection of scan paths to optimize conditions such as accuracy, warping, residual stress anisotropy etc. [27] Scan strategy overview can be found in [33]. The most commonly used scanning strategies are Meander, Stripes and Chessboard (Figure 20). [34] The meander strategy is used mainly in thin wall structures. The stripes and chessboard strategy are used for wider parts, but the strategy keeps the vector lines shorter (lower temperature gradients). [34]

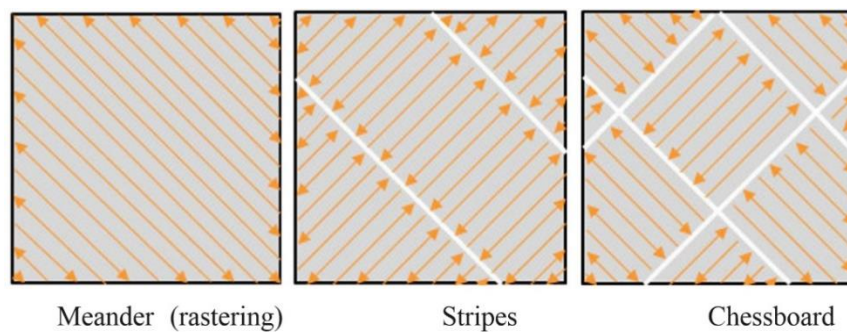


Figure 20: Types of scan strategies [34]

In many studies, the strategy is based on dividing the area into squares which are randomly fused by laser. This strategy helps to alleviate preferential build-up of residual stress. [4] To avoid a heat concentration and high temperature gradients, the rotation of scan strategy is usually used in combination with shifting to the certain direction. For example, with angular offset scanning strategy, the scanning vector

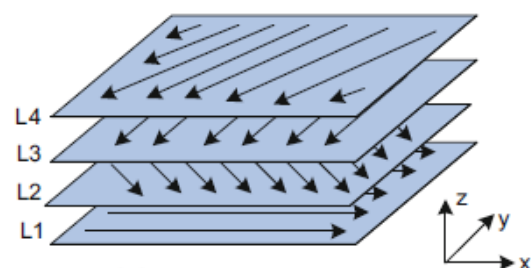


Figure 21: Angular offset scan strategy [19]



rotates in a predetermined direction about certain angle (Figure 21). [19] The most common angles for rotation are 45°, 67° and 90°. [35]

The scanning strategy is very complex problematic and can't be shortly covered in this chapter. It is always considered for specific component. It should avoid heat concentrations and defects generations like small pin holes. Especially the pin holes are critical in the areas, where several vectors meet every layer. This effect is avoided with described layer rotation and shifting.

d) Others

In the last group of parameters, we can consider all other parameters like for example building platform material. The experimental part will be investigating only the first 3 groups.

From the previous text it is obvious, that SLM process has many parameters that highly impact the printed part. Some of them can be monitored during the printing process, but most of them can be evaluated only after printing. All the parameters that will be handed thesis dealing with are summarized in the Table 2. Author realizes that these parameters are not full description for the printing process, but it is an accurate description for this thesis experiment and future component manufacturing.

Table 2: Printing parameters dealing in this thesis

Parameter type ↓	Variable parameters	Constantly set parameters
Machine-related	Pre-heating **	Shielding gas flow Recoating speed
Powder related	-	Powder absorptivity Particle size Chemical composition Particle shape
Laser and scan related	Laser power Hatch spacing Scanning speed	Layer thickness Scan strategy
Others	-	-

** Pre-heating can be applied based on the results for no pre-heating



2.3.4 SLM (LMF) materials

SLM (LMF) is mostly metal processing technology. The last years of development of the lasers enabled to process also ceramics and composites. In this chapter only metals will be introduced with no deeper explanation. Tool steels, which are topic of this thesis, will be described in detail afterwards.

- *Aluminium alloys*

Al-alloys have been in the group of interest in the last years. Combination of strength, density and corrosion resistance makes Al-alloys in combination with AM attractive for engineering applications. Al-alloys can be divided into two main groups – heat treatable and non-heat treatable. This is mainly due to chemical composition that causes formation of different phases. For heat-treatable alloys precipitates occurs in the microstructure and affects mechanical properties. These heat-treatability affects also the processability of the alloy by SLM. On the other hand, high reflectivity and thermal conductivity (heat dissipation) in the powder bed causes limitations in processability of the Al-alloys in general.

The most recent investigated Al-alloy for SLM (LMF) technology was AlSi10Mg. AlSi10Mg is mainly selected because of its weldability (factor for processability in SLM), hardenability, corrosion resistance and lightweight. For example, study [36] reached almost fully dense parts with various combination of process parameters. As a conclusion the processing window was presented with reaching tensile strength of 310 MPa (for density 97,6 %). EOS for example provides the material data sheet for their printers with tensile strength of 460 MPa in as built state. [36] As another example AlSi9Cu3 was also investigated in some studies.

As an interesting fact can be mentioned, that Al-alloys in the powder formation can be explosive. Al-alloy powder in presence of oxygen can cause ignition or explosion, because of the material reactivity. [27]

- *Titanium alloys*

Titanium alloys are one of the most popular, easy to print metals. Titanium has very good weight/strength ratio, corrosion resistance and biocompatibility. On the other hand, titanium has poor machinability and it is expensive. AM brings for titanium very



cost-effective manufacturing process, where complex shape parts can be produced with printing instead of conventional methods connected with scrap or exceed material. Buy-to-fly ratio is a term used in aerospace to compare the volume of material at the beginning of the production and in the end use product. For conventional manufacturing it can be 40:1, but for AM it can be 4:1. [37] In case of high-cost titanium AM is cost-saving solution. [37]

Ti-alloys are divided into 3 basic categories α , $\alpha + \beta$ and β , where α is formed with HCP crystal structure and β is formed with BCC crystal structure. Ti-based alloys manufactured by SLM mostly lead to the formation of acicular shaped martensitic α' (HCP) instead of equilibrium α or lath type martensite phase as the cooling rate is very high (105-106 K/s). β titanium alloys are not used in many cases, because powder manufacturing for these alloys is more difficult. [37]

In general, SLM processed Ti-alloys ductility is considered lower than for conventional methods, because the density of the part is not 100 %. [37]

The most common studied and applied Ti-alloy is Ti-6Al-4V. The alloy is mainly used for biomedical application as an orthopaedic prosthesis (Figure 22 [38]), but also in aerospace industry. For example, Ti-6Al-4V was investigated in [39]. The resulted tensile strength was 1334 MPa and elongation was 6,4 %. Strength was higher in SLM than for EBM (around 150 MPa difference), because SLM has higher cooling rates resulted in α' phase with small amount of β . [39]



Figure 22: Ti-6Al-4V hip system stem [38]

As another example study [40] can be mentioned. In this study Ti-5Al-2.5Sn (fully alpha phase) was investigated.



- *Ni-based alloys*

Ni-based usually contains combination of nickel and chrome content with other chemical elements. These alloys have very good creep resistance, tensile strength, corrosion resistance, good machinability and weldability (SLM processability factor). The most usual applications are in aerospace (engines), combustion chambers and chemical industries. [27] In the aerospace applications SLM is mainly used for reaching the special cooling systems to increase the engine life-time. [41] One of the blade designs by Siemens company is shown in Figure 23. [42] Ni-based alloys are strengthened in 2 common ways. First with the use of chemical elements like Cr, Co, Mo, W, Ta (intermetallic phases) in the face centred cubic Ni γ matrix. Second type of strengthening is solid solution strengthening to reach γ' phase by Ta, Ti and Nb in combination of grain boundary strengthening with carbides etc. [41]



Figure 23: SIEMENS 3D printed blade [42]

Ni-based alloys are usually well processable in SLM method. Recent studies were focused mainly on solid solution hardened superalloys and the γ'' strengthened IN-718. In high load application higher content of γ' (Al+Ti elements) is required. The processability of Ni-based alloys decreases with higher γ' content. The cracks start to occur during the processing and preheating has to be applied. [41]

In the processability manners, study [41] did a large research on several batches of IN-738 alloy. In this study various cracks and porosity content was reached. It was proved, that suitability of the IN-738 can't be same for all powder manufactures. This information can be very important in matter of all material processing via SLM.

Another study which was dealing with Ni-based alloy Hastelloy X is [43]. In this case process parameters (laser power and scanning speed) were studied and the results were compared to wrought parts. The tensile strength of the printed Hastelloy was higher,



but elongation was lower against wrought one. Material properties increase with increasing laser power and decreasing scanning speed. Difference in the microstructures were observed. [43]

- *Other Non-iron based metals*

As other metals processable with SLM (LMF) copper, gold, shape memory alloys like Nitinol or cobalt alloys can be mentioned. [27] All these materials have their own specifications, why they should be used in Selective laser melting. For example, copper



Figure 24: Copper AM processing [44]

is very challenging material for laser processing technologies. This is caused mainly due to copper high reflectivity and thermal conductivity, where material is unable to melt with standard laser configurations (higher energy source is needed.). Copper could be used mainly for its thermal conductivity in injection moulding or heat exchangers. The first SLM was shown by the Fraunhofer ILT in Aachen, where modifications in SLM process had to be applied. These modifications were not published. Anyway, Fraunhofer ILT claims, that they can produce copper parts with 99,9 % density. Copper being processed is shown in Figure 24. [44], [45]

Another interesting material is Nitinol (alloy of nickel and titanium). This shape memory alloy can return into previous undeformed shape with use of heat. The mechanism is mainly based on phase transformation between austenite and martensite. The application of NiTi alloys is directed to the medical fields. Nitinol is very sensitive to atmospheric impurities (oxygen especially). Study [46] did an investigation in this issue for two different atmospheres with different oxygen contents. It was proved, that SLM parameters affect the phase transformation temperatures. This conclusion also proves,



that process parameters can influence other factors than internal defects like cracks or porosity, but also physical properties. [46]

• *Iron-based materials*

The last group of materials mentioned in this chapter will be iron-based materials. Iron-based materials are the most used materials in engineering applications worldwide. Obviously for this reason they are the most required materials for SLM processing. In the previous chapters of this thesis it was mentioned that the processability of the materials in SLM can be indicated by weldability. In case of steels it is generally known, that with increasing carbon content in steels decreases the weldability (crack tendency etc.). According to that, released studies were mainly oriented on low and medium carbon steels: stainless steels, maraging steels and tool steels. [27]

High carbon steels are still in the development for processing. The limitations of the printer's construction are sometimes met in processing likewise material (preheating limit in connection to build volumes etc.). Such a development is dealt for example in Fraunhofer ILT in Aachen. Fraunhofer ILT

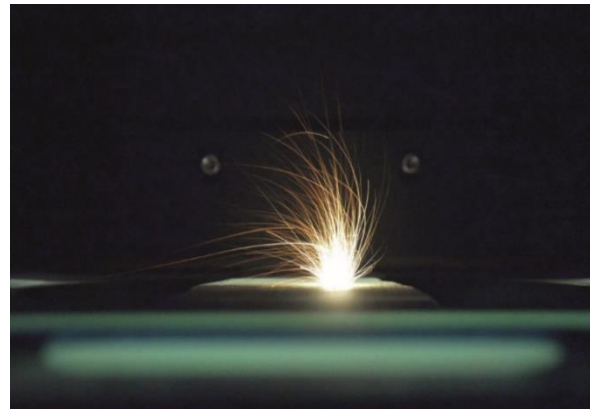


Figure 25: High carbon steel processing in SLM [47]

mention that they can process even steels with carbon content of 1,38 wt. % [47] To accomplish the crack-free printed objects laser powers higher than 400 W and preheating of 500 °C has to be used. [47] The processing of high-carbon content steel is shown in Figure 25.

• *Stainless steels*

Stainless steels offer high variations of mechanical properties, corrosion resistance, wear resistance etc. Stainless steels are generally classified as steels that contain more than 12 wt. % of chrome in solid solution. They are divided in 4 main groups based on microstructure: ferritic, austenitic, martensitic and duplex (combination of phases).

The microstructure is affected by the chemical composition (also by heat treatment). The main alloying element is chrome and nickel. Alloying elements are basically divided



into ferrite or austenite stabilization elements. Carbon content is based on type of stainless steel.

Ferritic steels

Ferritic steels are the steels with very low carbon content (up to 0,1 %) and high chrome content (between 13 - 30 %). [48] The microstructure is basically one phased and it is formed by BCC crystals of ferrite. Ferritic steels have very low plasticity, notch toughness and they cannot be hardened. On the other hand, they contain lower amount of expensive alloying elements (like nickel), they have good corrosion and heat resistance. Application of ferritic steels are mainly in case of higher mechanical properties and corrosion resistance requirements (exhaust pipe systems etc.). [48]

Ferritic steels are very difficult to weld, because they become brittle in higher temperatures and grain growth occurs in longer temperature expositions. Unsuitable phases like sigma can be formed during exposition also. We can assume that all these aspects make ferritic steels unsuitable for Selective laser melting or any other L-PBF technology. [49]

410L steel was purpose of the investigation in study [50]. Ferritic structure with martensite areas was observed. Very low impact strength was reached with further improvement after heat treatment. Build samples failure was dominantly brittle. Two phase transformation and inner stress presence were pointed as the main cause. [50]

Martensitic steels

Martensitic steels contain higher amount of carbon (0,1 % up to 1,5 %) and high amount of chrome (between 12 % and 18 %). [48] The microstructure is formed by nonequilibrium phase martensite (body-centred tetragonal crystal) with amount of retained austenite and also precipitates can be present. [48] The chemical composition of the martensitic steels allows to extend martensitic transformation to the room temperature ranges. Martensitic transformation is not followed by diffusion and it happens almost in no time duration. Martensite forms needle-like grains, which are very suitable as grain strengthening mechanism.



Martensitic steels are typical for its high strength, wear resistance, corrosion resistance and low plasticity. Corrosion resistance is the lowest from mentioned 4 types of stainless steels (caused by higher carbon content). From available literature we can also expect that corrosion resistance can be affected by AM method against conventional manufactured parts [48] Martensitic steels were the purpose of many studies (e.g. AISI 420, 17-4 PH, 15-5 PH etc.).

Very interesting study [51] was performed on 17-4 PH steel. 17-4 PH is precipitation hardened martensitic steel, that contains 3-5 % of copper. Copper is the cause of precipitation hardening. This steel has all advantages of martensitic steels extended of stability up 300 °C. [51] This study used a new oxide dispersion strengthening with oxygen content in the build atmosphere 500 ppm (induced dispersion of nano Mn-Si oxide). [51]

Austenitic steels

Austenitic steels are the most common stainless steels worldwide (70 % production of the stainless steels). [48] Chemical composition is based on chrome and nickel content. Nickel is austenite forming element. The carbon is present in very low amount (usually up to 0,08 %). [48] The austenite microstructure with certain amount of austenite forming elements becomes stable in room temperatures. These steels perform with ductility, high corrosion resistance in atmosphere (even in higher temperatures), but also in several acids. On the other hand, sensitivity to corrosion cracking in temperature exposition between 500 – 950 °C or intergranular corrosion can be observed. [48]

From SLM perspective austenitic steels have been widely used, because of their processability and properties. In the recent year 316L and 304L were dominantly investigated. 316L performs high ductility, corrosion resistance and bio-capability. It is used in medical, jet engines, food industry, automotive etc. One of the manufactured parts is shown in Figure 26. [52], [53]



Today 316L is basic material for many powder producers. On the other hand, powders and their properties are still being developed. For example, in paper [54] the WA and GA powders were compared. Very similar mechanical properties and densities were reached with WA powder. Only issue was in different chemical composition in some elements (corrosion behaviour influence) and surface roughness. [54]



Figure 26: 316L additive manufactured part [52]

- *Maraging steels*

Maraging steels are considered as high strength steels (up to 2000 MPa) with good ductility and in certain chemical composition also corrosion resistance. [48] These steels have low carbon content with high amount of nickel. Ductile nickel martensite is formed after quenching, where in the next step intermetallic phases strengthen the matrix. Maraging steels are suitable for SLM process, because of their good weldability. 18Ni300 steel as an example of SLM processing can be mentioned. Specimens manufactured from Maraging steel 18Ni300 are in the Figure 27. Maraging steels are also applied as hot working tools for high pressure die casting (discussed further). [37], [55]



Figure 27: 18Ni300 SLM printed samples [21]

Tool steels and especially tool steel L-40 is purpose of this thesis, so tool steels will be discussed separately in the next chapter.

3 Tool steels

Tool steels are one of the most important materials for production engineering. Every metal component has to be manufactured with the use of tools (casting, machining, forging etc.). The lifecycle of every tool is critical for time scheduling, finance expenses and part quality. All the mentioned aspects are mainly based on material and its heat treatment. It can be said that tool steels are also one of the most precise iron-based metals in the material



Figure 28: MAPAL 3D printed bell tool [56]

engineering industry. Large range of tool steels are available on the market for various applications. Additive manufacturing brought completely new challenge into the topic of geometry possibilities. One of the 3D printed tool can be seen in Figure 28. [56]

Nowadays, tool steels are very attractive materials especially for SLM (LMF), DMLS process. Tool shapes that can be reached with the use of AM are incomparable to the traditional manufacturing. With the use of these AM technologies the lifetime of the tools can be significantly increased (will be introduced further).

Generally, tool steels contain carbon in higher amounts. Higher carbon content leads to the tendency of crack-forming during the SLM process. As it was mentioned before, an approach of preheating helps to eliminate the cracks, but processing of such a steel is still big challenge and it is one of the dominant research topics in AM industry. [57]

3.1 Characterisation of tool steels

To deeply understand the topic of tool steels, in this chapter all characteristics will be introduced. Subject of this thesis investigation (steel L-40) will be introduced at the end.

- *Designation system and types of tool steels*

Designation of tool steels is presented in EN 10027 in 2 parts. System of EN 10027-1 divides tool steels into 4 basic groups based on chemical composition. As an example, steel X63CrMoV5-1 can be mentioned. System of EN 10027-2 divides steels into



numbered groups (according to their applications and characteristics). Equivalent code for the same steel as in previous example is 1.2362. [58], [59]

There are several mechanisms how to divide tool steels into groups. For example, [58] shows mechanism used by tool suppliers, but also type of tool steels based on solidification mechanisms. According to standard ISO 4957:1999 the tool steels can be divided into the following groups [60]:

- a) Non-alloyed cold-work tool steels
- b) Alloy cold-work steels
- c) High-speed steels (HSS)
- d) Alloy-hot work steels

a) Non-alloyed cold work tool steels

In the standard defined as special steels, suitable for working or processing of materials, for handling and measuring workpieces. These steels exhibit for this purpose high hardness, wear resistance and toughness. [60]

This group of tool steels usually contain from 0,3 up to 1,5 % of carbon, up to 0,4 % of manganese and silicon. [61] Quenching of these steels is performed from temperatures A_3 for hypoeutectoid and slightly above A_1 for hypereutectoid. Tempering between 160 - 280 °C is applied afterwards. [61] Usual reached hardness is between 56 and 60 HRC. [61] Structure is formed by perlite in the core and martensite on the sides of the tool (for higher thicknesses there is not hardenability to reach martensite in the full volume). These steels are applied on hand tools, screw taps etc. They cannot be used for high demand applications like dies. [62], [61]

In this group C45U, C90U or C120U as an example can be mentioned. [60]

According to the mentioned low application requirements, it would be inefficient to process such a steel with expensive technology like SLM. No publications were found in the literature for this topic. On the other it would be interesting to produce tools according to user requirements by printing it in the moment of need instead of buying it regularly in the shop.



b) Alloy cold-work steels

Alloy cold-work steels are defined in the standard as non-alloy or alloy tool steels for applications in which the surface is generally below 200 °C (during application). [60] Steel 21MnCr5 or X100CrMoV5 can be found in this group as an example. [60]

Generally, this group is very similar to the non-alloyed one, but steels have better hardenability (from 60 up to 64 HRC) and lower hardness drop with increased temperatures. [62], [61] Usual chemical composition is carbon (0,4-2 %), chrome, tungsten, molybdenum etc. Summary of alloying elements usually doesn't exceed 3 to 5 % (except high chromium steels). [62] The properties are reached with quenching (oil or air) and tempering. [60] Special type in this group are chromium alloyed steels, where the chrome content is up to 13 %. [61] Application of alloy cold-work steels is usually for extrusion mandrels, extrusion cylinders, stamps etc. [61]

According to the literature, there were several studies trying to process alloy cold-work steels. Two examples with main processing parameter are shown in Table 3.

Table 3: Alloy cold-work steels processed by SLM (examples)

Steel	VED	Layer thickness	Pre-heating	Defects	Source
X110CrMoVAI8-2	238 J/mm ³	30 μm	240 °C	Small pores	[63]
X65MoCrWV3-2	245 - 269,5 J/mm ³	30 μm	200 °C	0,5 % porosity Cracks for RT	[64]

c) High speed steels (HSS)

HSS are defined in EN ISO 4957:2000 as steels used mainly for machining and forming processes. Because of the chemical composition they have the highest high-temperature hardness and temper resistance up to 600 °C. [60] This definition is very questionable according to the new hot-work steels on the market.

Chemical composition is usually based on carbon content (more than 0,7 %), tungsten and molybdenum. High speed steels are very typical with their temperature stability and high hardness (60 up to 66 HRC). [61] Heat treatment consists of quenching (up to



1280 °C) and repeating tempering (usually 3 times). [61] The most used is HS6-5-2 and HS7-4-2-5 for higher machine powers. [58]

High speed steels are in the scope of investigation for SLM processing. Special shapes with conformal cooling channels can be produced for optimal machining conditions. This could lead to increasing of the tool lifetime.

Investigation of processing parameters were presented by many authors. Very interesting study was done by J.Saewe et. al. [57] on high speed steel AISI M50 (or 80MoCrV42-16). In this study AISI M50 was successfully produced by SLM machine. The influence of HIP (hot isostatic pressing) was investigated. HIPed samples increased the mechanical properties significantly (porosity reduction), but the properties were still lower than for conventionally manufactured samples. [57]

Example of the processed HSS with process parameters are shown in Table 4. Detail of crack forming in M2 HSS based on preheating is in Figure 29. [1]

Table 4: HSS processed by L-PBF examples

Steel	VED	t [μm]	Preheating	Defects	Source
M50	69 J/mm ³	30	500 °C	Pores	[57]
M2	51-111 J/mm ³	30	-	Cracks	[1]
	185 J/mm ³	30	200 °C	2% porosity	

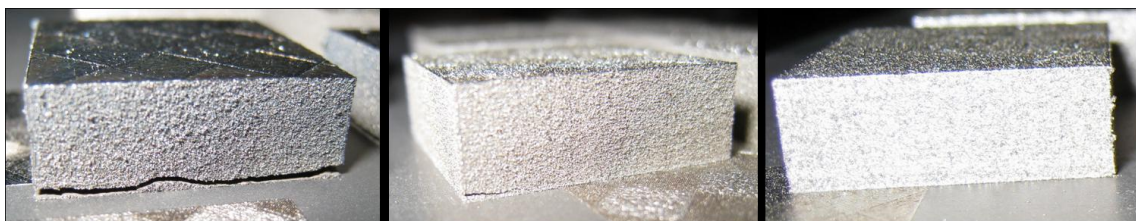


Figure 29: M2 HSS parts produced with a pre-heating temperature of 90°C (left), 150 °C (middle), 200 °C (right) [1]

d) Alloy-hot work steels

Alloy-hot work steels are defined in [60] as steels for applications in which the surface temperature is over 200 °C. General requirements for hot work steels are softening resistance in high-temperature exposures and resistance to thermal shocks, thermal



stability, hardness (in elevated temperatures), wear-resistance, diffusion resistance, machinability etc. [65]

In chemical compositions these steels usually contain carbon from 0,3 up to 0,7 %. [62] For further alloy-hot work steels can be divided into chromium, tungsten and molybdenum hot work steels. Chromium hot work steels contain around 5 % of chrome with combination of other alloying elements. Tungsten hot-work steels contain between 9 and 17 % of tungsten. Molybdenum hot-work steels are not that usual, and they content approx. 5 % of molybdenum. [62], [65]

From application perspective chromium steels keep hardness on the same level up to 425 °C and tungsten hot-work steels up to 620 °C. [65] On the other hand for die cooling application the chromium steels are preferred because of the cracking resistance. Chromium steels are generally the most used hot-work tool steels. Although the hardness is not the highest possible, chromium hot work steels have outstanding toughness and thermal shock resistance. [65]

This group of tool steels is very sensitive on processing quality, where any small defect can reduce the lifetime of the tool. In AISI classification hot-work steels are classified with letter H (e.g. H11, H13 etc.). [65] Typical application of such a steel is for example as forging tools, injection moulding or in high pressure die casting tools. High pressure casting die application is the purpose of this thesis and it will be discussed further. [65]

Simplified comparison of the tool steel is shown in Table 5 to simply understand main application requirements and difference in the basic groups of tool steels.

Table 5: Simplified comparison of the tool steel types [65]

Steel	Type	C [%]	Main alloying element	HRC	Cracking resistance	Machinability	Toughness	Softening resistance	Wear resistance
D2	Cold-work	1,5	Cr	54-61	Highest	Low	Low	High	High
M2	HSS	0,8	Cr, Mo, W	60-65	Medium	Medium	Low	Very high	Very high
H11	Hot-work	0,4	Cr	38-54	Highest	Medium - High	Very high	High	Medium



• *Chemical composition of tool steels*

It can be said that processing and application suitability of the tool steel is dominantly influenced by the chemical composition. The most common alloying elements are Cr, Ni, W, Mo, V and less used is Mn, Si, Co. [58] Effect on properties by each alloying element (published by J.Sobotová [58]) is summarized in Table 6.

Table 6: Alloying elements in tool steels and their effect on properties [58]

	Hardness and strength	Plasticity and ductility	Wear resistance	Machinability	Polish-ability	Carbide-forming	Hardenability	Softening resistance	Corrosion resistance
C	+	-	+	-	-	yes	+		
Cr	+					yes	+	+	+
Si						no	+	+	
Mn						yes	+		
V		±	++	-	-	yes	+	++	
Mo		-				yes	+	+	
W		-				yes	+	+	
Ni	+	+				no	+		
Co	+	-				no	-	+	

“+” means increasing and “-” means decreasing

• *Heat treatment of tool steels*

Heat treatment of tool steels requires high experience. In manufacturing process, heat treatment is critical step to achieve homogenous structure and to increase the wearability or to reach good machinability.

Usual heat treatment for tool steels is Normalizing, Annealing, Stress relief annealing, (HIP = hot isostatic pressing), Quenching and tempering.

Normalizing

Normalizing is applied mainly on the tools that have been manufactured by forging. Forging causes inhomogeneous microstructure and in high forging temperature also coarse grain structure. With normalizing more homogenous, fine-grained microstructure with not orientated carbides is reached. Normalizing performs usually with heating up to A_3 or A_{cm} temperature and air cooling. [65] For AM production of tool



steels normalizing is usually not applied. Also, for many tool steels normalizing is to recommend at all (e.g. H11, H13 etc.).

Annealing

Tool steels are designed to be wear-resistant. This causes very low machinability of the material. For the purpose of improved machinability, the annealing heat treatment is applied. Simultaneously, the microstructure is uniformed for subsequent hardening operation. Annealing result is material with decreased hardness and improved machinability. The starting microstructure can consist of lamellar or plate-shape particles of cementite in perlite or bainite even martensite. The final microstructure is formed by dispersed spherical carbides in ferrite matrix. It is realized with heating to temperatures between 750 – 900 °C with subsequent slow furnace cooling. [65]

Stress relief annealing

The processing of the tool-shape brings in manufacturing certain stress that can be source of the micro/macro cracks or distortion (also the heat treatment). That is why the stress-relief treatment is applied after machining and grinding operations. In SLM (LMF) stress-relief is very common and important heat treatment, because these AM methods performs high temperature gradients resulted in residual stresses. Objective of the stress relief is to reduce the residual stress without causing changes in microstructure. Material is heated usually between 550 and 750 °C with subsequently slow cooling. [65]

HIP (Hot isostatic pressing)

Hot isostatic pressing (HIP) is a process to densify powders or cast and sintered parts in a furnace at high pressure (100-200 MPa) and at temperatures from 900 to 1250 °C for example for steels and superalloys. [66] The gas pressure acts uniformly in all directions to provide isotropic properties and almost 100 % densification. [66] Hot isostatic pressing is an optional step in the tool steels processing with AM This method decreases inner defects, porosity etc. (Figure 30). Many publications showed an effect of HIP application and increasing the ductility of the final product. HIP process is very common to apply in case of AM of the metal components.

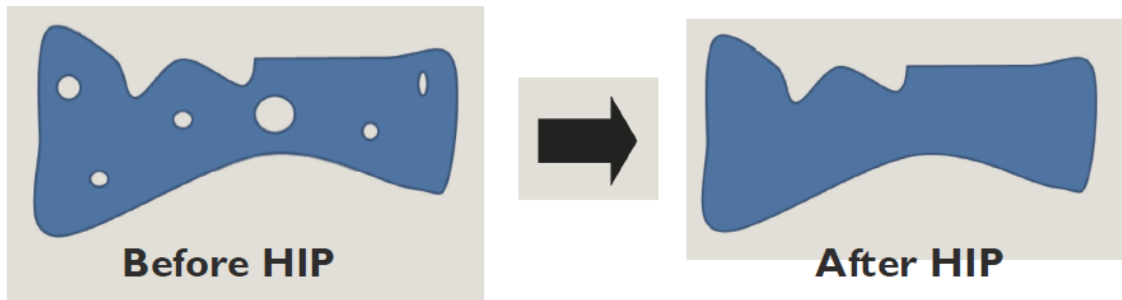


Figure 30: HIP part effect [66]

Hardening (Quenching and tempering)

Hardening is one of the most common heat-treatments according to steels. It is realized by three following steps: austenitizing, quenching (cooling) and tempering. Each step causes changes in mechanical properties and microstructure. Conditions of the hardening must be considered according to application requirements.

Austenitizing is realized with heating to the proper temperature. For hypereutectoid steels it is above A_{cm} and for hypoeutectic slightly above A_3 . Austenitizing temperature and time should also be set to avoid grain coarsening. The use of Fe-Fe₃C diagram is approximate and the alloying of the steel has to be considered. During the austenitizing the uniform heating should be applied. If the temperature of the tool is not uniform, the temperature gradients could cause stress to be generated (or cracking). [65]

After the proper heating the material is quenched. Quenching is rapid cooling of the material to reach high hardness with supersaturated microstructure (martensite or bainite). Full single-phase microstructure is unreachable, because certain amount of austenite is always stabilized even in room temperatures (called retained austenite). Ability of the steel to reach at least 50 % of the martensitic structure is called hardenability. There are several quenching mechanisms based on cooling conditions. Despite the high cooling rates in AM the quenching usually needs to be done. Quenching is very complex problematic and it can't be described properly on one page. More information about quenching can be found in [65].

Tempering is the final step applied on the quenched tool steel. At the start the supersaturated microstructure formed mainly by martensite or bainite is presented. The material has very high hardness and low ductility. For tempering material is heated



slightly above A_1 temperature. Supersaturated microstructure is unstable and starts to change. The carbon atoms start to rearrange, carbides start to precipitate, retained austenite is transformed, martensite tetragonality decreases (tempered martensite). These mechanisms usually do not occur in one tempering step and has to be divided (two or three). Primary goal of the tempering is to increase toughness and ductility. [65]

Hardening is used for almost every tool steel, mainly to be able to control final properties of the tool. In AM the hardening usually follows HIP or stress relief heat treatment. In the Figure 31 and Figure 32 can be seen typical heat treatment for hypoeutectoid steel (including manufacturing) for the conventional tool and SLM manufactured tool.

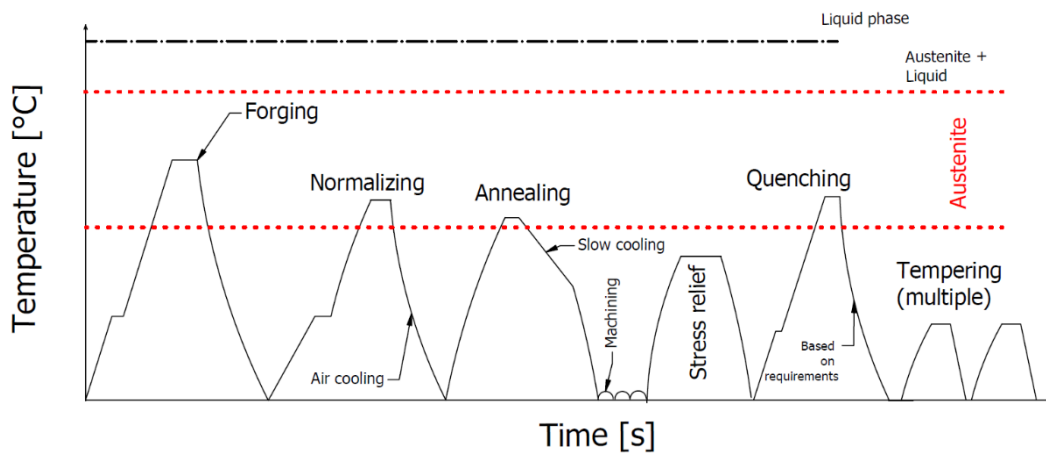


Figure 31: Conventional tool heat treatment (normalizing is not suitable for every tool steel)

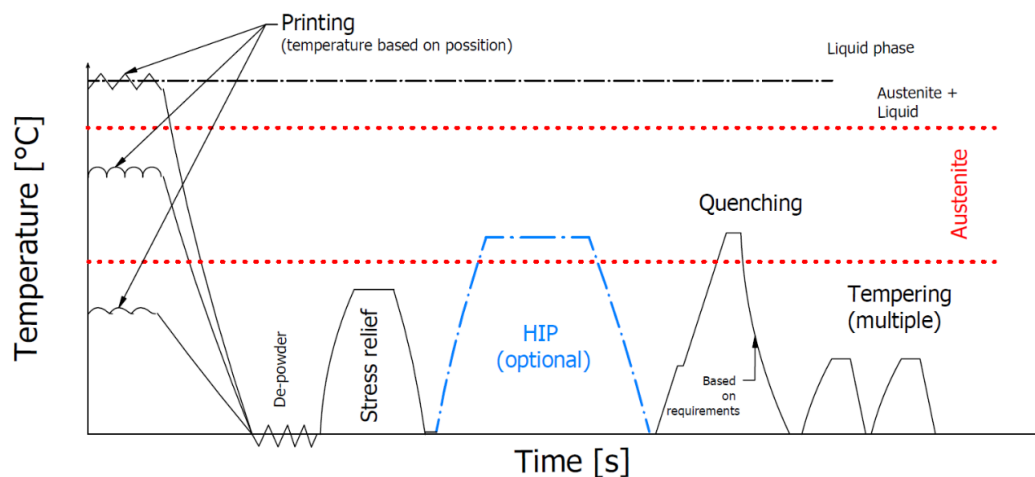


Figure 32: SLM manufactured tool heat treatment

It can be summarized, that heat treatment is critical for the final tool quality. In this thesis the heat treatment will not be investigated, because the goal is to reach suitable properties directly after the printing process. Investigated steel L-40 was designed for this purpose.



3.2 Tool steel L-40

L-40 is one of the latest releases in the tool steel development. It was patented by the company Nanosteel and nowadays it is licensed by the company Formetrix. L-40 was designed as high-performance steel, providing high hardness in combination with



Figure 33: L-40 bolt threading tool [2]

increased ductility directly after printing process. L-40 was also tailored to be printable crack-free in the room temperature. Especially this advantage brings new alternative to lower performance maraging steels and hard to print tool steels like H13. [67] L-40 development target was to provide L-PBF material powder for tools, dies, molds and special components manufacturing. One of the L-40 application in form of compression die for bolt threading is shown in Figure 33. [67], [2]

• *Chemical composition and powder parameters*

L-40 is distributed in powder form with approximate price 60 Euro/kg (price can vary). The powder size specification is clarified as $D_{10}=20\ \mu\text{m}$, $D_{50}=33,4\ \mu\text{m}$ and $D_{90}=54,2\ \mu\text{m}$. The chemical composition of L-40 is given by Formetrix approximately, because actual composition is protected. Specified chemical composition is summarized in Table 7.

Table 7: L-40 chemical composition declared by Formetrix [2]

Element	Cr	Ni	Mo	Cu	Nb	C	N
	> 10.5 %	< 5 %	< 5 %	< 1 %	< 1 %	< 1 %	< 1 %

It is obvious, that based on Table 7 deeper discussion can't be done, because chemical composition is not described in detail. On the other hand, we can expect that carbon content will be much lower, than in typical H13 or H11 tool steels (according to room temperature printability). This chemical strategy is also mentioned in [67]. L-40 is based on lower carbon content, which usually leads to crack formation in the print. The main alloying element is chrome, which is very suitable and typical for hot work steels (heat resistance). Other elements and their influence on mechanical properties were



described in the Chapter 3.1. Chemical composition will be investigated in the experiment part of this thesis, but it can't be published according to the protected rights.

• *Mechanical and physical properties*

As it was mentioned before, L-40 is tailored tool steel for L-PBF technologies. It is ferrous alloy powder with final print case hardenability up to 70 HRC. Formetrix declares various properties in heat treated or in as-built state (after printing). Heat treatment is voluntary based on the application requirements. Parameters for heat treatment are not standardized, but they can be delivered from powder distributor. Heat treatment is not the purpose of this thesis and it won't be applied.

For heat treated state the tensile strength is clarified 1650 MPa in combination with 10 % of elongation. [2] In as-built state the tensile strength is declared as 1500 MPa with elongation minimum at 14 %. [2] Hardness is clarified for as built state between 46 and 48 HRC and after heat treatment 50 up to 52 HRC. [2] All other specifications provided by Formetrix are summarized in Table 8.

Table 8: L-40 mechanical and physical properties clarified by the company Formetrix [2]

	As built	Heat treated
Mechanical properties		
Hardness - HRC	46-48	50-52
R _m [MPa]	1500	1650
R _{p0.2} [MPa]	1300	1350
Elongation [%]	>14	10
KV [J]*	60	18
Physical properties		
Thermal Expansion Coefficient [ppm/°C]*	11,3	10,2
Thermal Conductivity [W/mK]*	16,3	18,2
Specific Heat [J/Kg.K]*	451	424

* at 20 °C (or room temperature)

The physical properties in combination with mechanical properties were especially designed for tool application. For example, thermal conductivity is highly important in high pressure die casting, because die material can transfer the heat quickly to the coolant in the cooling channels.

- *L-40 applications*

Industry sector and material development are usually dealing with questions related to final applications. On the Formetrix official website [68] three applications were shown with multiple results.

- Aluminium die casting tool (Figure 34 - left)
- Compression Dies (Figure 34 - middle)
- Hot stamping die (Figure 34 - right)

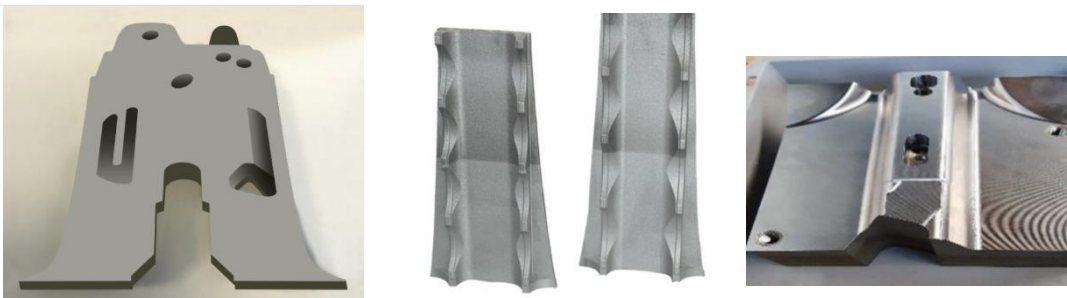


Figure 34: L-40 application examples by Formetrix [68]

Based on the authors professional experience we will focus directly on aluminium die casting with conformal cooling application (Figure 34 on the left).

During the aluminium high pressure die casting process (HPDC), the die is cooled down with the cooling channels placed inside the die. Simplified production die thermal cycle is shown in Figure 35. The temperatures in Figure 35 are just based on authors experience and don't have any connection to the specific production. The cycle also differs based on the position in the die.

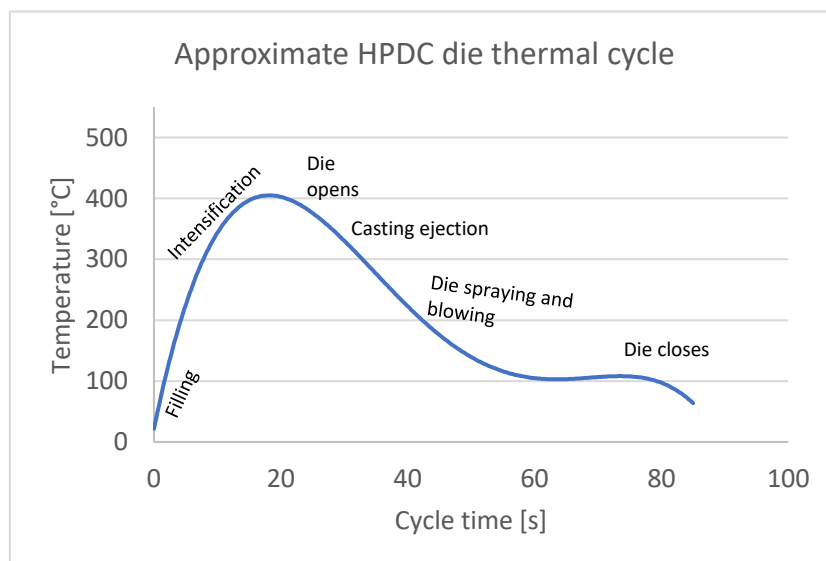


Figure 35: Approximate HPDC (aluminium) die thermal cycle



Aluminium in the HPDC die can reach even 200 km/h in the liquid state. It is obvious that die material will be highly deformed by the process. According to [69] the main failures in die material are:

- Thermal fatigue (thermal cracks)
- Gross fracture
- Erosion
- Die soldering

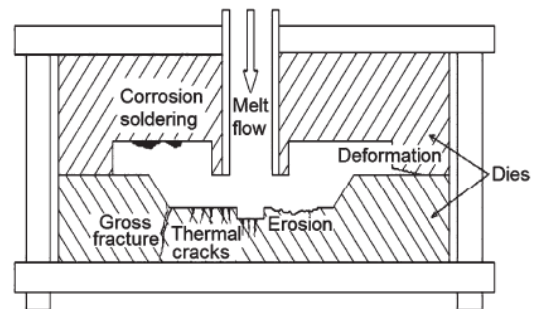


Figure 36: Die failure mechanisms [69]

To avoid all the mentioned defects and meet required die-lifetime it is necessary to reach all the requirements for the die material.

The main requirements are:

- Heat-resistance
- Temper resistance
- Thermal conductivity
- Hardness (even in high temperatures) and toughness
- Thermal shock resistance
- Fatigue resistance

All the deformation mechanisms are highly based on the die and casting construction. Especially the cooling system of the die is critical factor for die operating temperatures. Proper cooling can highly reduce the die failures, but also decrease the operating temperatures. In lower operation temperatures steel can provide more suitable mechanical properties (some steels lose hardness and strength in higher temperatures). Another benefit of proper cooling can be lower cycle and maintenance time.

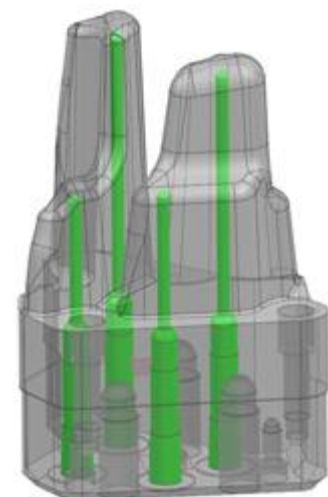


Figure 37: Conventional cooling [70]



The conventional die cooling systems are manufactured by drilling. Drilling allows to create cooling channels just in the straight lines (x, y, z direction). This method is easy, but it is limiting the cooling channels ability. Conventional cooling system as one of the die cores is shown in Figure 37. [70]

The resulted temperature field in the conventional manufactured tool can be very unbalanced. This can lead to high die soldering, die stress, long solidification time etc.

Additive manufacturing brought a completely new possibilities into die manufacturing. As it was mentioned before, AM allows to reach almost every shape required by the application. The cooling channels can be placed in almost every area of the die part with variability of diameter and especially closer to the surface. This brings benefits in the form of lower operation temperatures (especially surface), lower cycle time, maintenance etc. The mentioned idea of proper area cooling is called conformal cooling and example of this application is shown in Figure 38. [70]

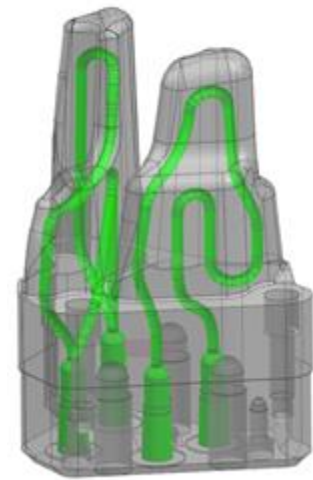


Figure 38: Conformal cooling tool [70]

L-40 could provide mentioned suitable properties with easy printability. In conformal cooling this could bring the conformal cooling technology to another level, because without difficult post-processing L-40 could be delivered in the die set with suitable properties. As it also mentioned on website [68], L-40 can be printed on wrought materials, so the proper combination of properties can be met.

Further L-40 applications can be found in [68].

- *L-40 in literature*

Mentioned before, L-40 is one of the latest releases in the material engineering world and there are only a few publications dealing with this topic.

One of the researches was published at the conference EuroPM in 2019. Publication [71] is dealing with the influence of powder atomization process and printing parameters. For the experiment two types of powder atomization were used – WA and GA. The targeted size distribution was $D_{10} = 20 \mu\text{m}$ and $D_{90} = 50 \mu\text{m}$. [71]



Chemical composition remained the same for both types of powders, only the oxygen content was different. This topic was discussed in Chapter 2.3.3. In this study the WA powder contained about 300 % more oxygen than GA powder. Experiment was performed on EOS M290 L-PBF printer. Following parameters were used [71]:

- Laser power between 150 and 350 W
- Scanning speed from 200 to 1000 mm/s
- Layer thickness 30 and 40 μm
- Stripe overlap 20, 30 and 40 %

The experiment set consisted of the same 4 parts like in this thesis, where single tracks, cubic samples, tensile test bars and Charpy samples were analysed.

The results from two different types of powders were clear. The WA powder performed higher particle size - $D_{90} = 71,9 \mu\text{m}$ (for GA $D_{90} = 57,3 \mu\text{m}$). The single tracks performed best results with linear energy density $E_L = 0,3 \text{ J/mm}$. In order of cubic samples, 4 different parameters with overlap 30 % and 40 % reached the highest density. In comparison of final GA and WA in cubic samples, the WA samples performed with maximum porosity content 1,07 %. GA printed samples showed maximum 0,03 % of porosity. This result was obtained on the area 1 mm^2 of the investigated sample (not suitable for deeper quantification). [71]

The results of the study experiment were mechanical properties (Table 9). Even GA powder didn't meet all the specifications in the Formetrix description (Yield strength, KV value). WA also didn't meet descriptions. Powder performed with critical drop in the Impact energy values (values for elongation were not presented). [71]

Table 9: Resulted mechanical properties from various atomization powders in publication [71]

	L-40 GA	L-40 WA
R_m [MPa], Z direction	1800 (± 200)	1900 (± 200)
$R_{p0,2}$ [MPa], Z direction	1250	1250
KV [J], XY direction	49 (± 3)	13 (± 2)
KV [J], Z direction	27,5 (± 3)	8,5 (± 2)
HRC	45 (± 3)	52 (± 4)



• *Comparison L-40 with alternative tool steels*

Be able to consider the contribution by L-40 to the tool steel material perspective, the alternative steels should be introduced and compared. Talking about tool steels for generally high tool application tools we can talk about H11, H13 tool steels and M100, M300 maraging steels. In Table 10 and Figure 39 three of the most relevant steel examples are compared. AB stands for as built state and HT for heat treated state.

Table 10: Various tool steels comparison from various sources

	L-40		H13		MS300	
	As Built	HT	As Built	HT	As Built	HT
HRC	47	51	53	N/A	34,8	53,5
A [%]	14	10	12,4	N/A	12,4	5,6
KV [J]	60	18	14,4	N/A	N/A	N/A
Source	[2]	[2]	[72]	-	[73]	[73]

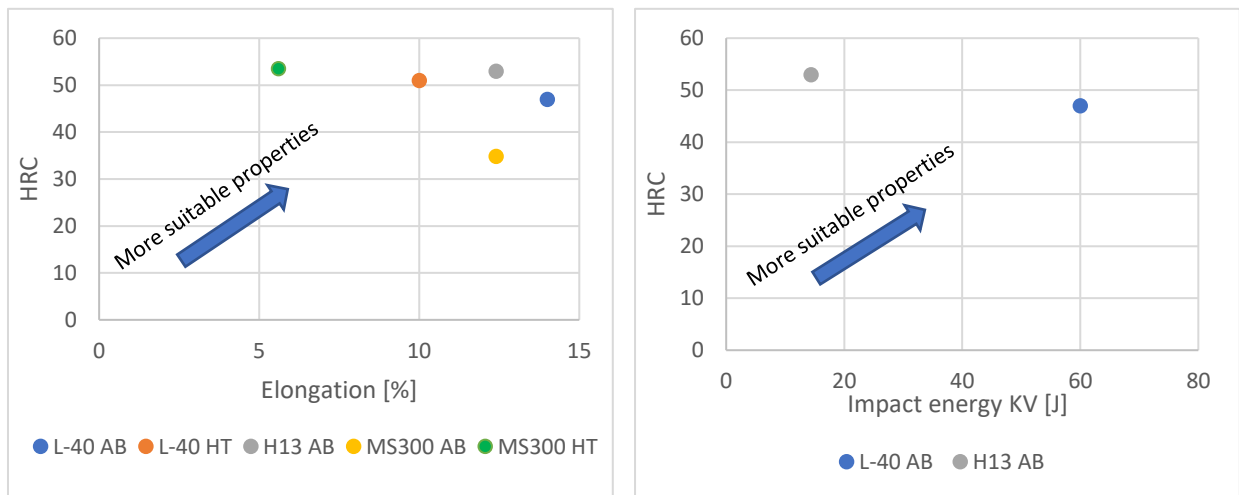


Figure 39: Various tool steels comparison from various sources – left: HRC and elongation, right: HRC and Impact energy

From Figure 39 (left) it is obvious that MS300 steel in as built state has relatively low hardness against H13 and L-40. In heat treated state MS300 provides more hardness but the elongation (ductility) goes rapidly down. L-40 and H13 are comparable in matter of hardness and ductility. In case of impact energy (KV) L-40 keeps its resistance against strong impacts. Simply said - it is more ductile for as-built state. In combination with room temperature printability L-40 keeps its advantage (H13 type tool steels usually crack on common printers at room temperature). [68]

In the next chapters L-40 will be investigated with various experiments to reach the best print quality according to the process parameters on the specific SLM printer.



4 Experimental part

The experimental part of the handed thesis is dealing with the discussed tool steel L-40 processed by the SLM (LMF) technology. The experiment was realized in cooperation between Material engineering institute at CTU and NCC MATCA under the supervision of CARDAM solution company. The purpose of the experiment was to investigate the processability of the tool steel L-40 for industrial applications.

The experiment is divided into 4 parts:

1. Powder analysis
2. Single tracks
3. Cubic samples
4. Tensile and Charpy specimens

In the first part of the experiment the input powder material is analysed. As the following the powder material is processed with various parameters and geometries. The main goal of the experiment is to provide printing parameters according to maximum density and possible efficiency of the printing process. Experiment parameters are suited for specific printer and for other printers should be investigated separately. In some cases, the transferring mechanisms to other printers can be applied.

All the printing experiments were realized on the TruPrint 1000 printer by TRUMPF company owned by NCC MATCA located at Institute of Physics of the Czech Academy of Sciences. TruPrint 1000 is one of the smaller printers available on the market, which makes it suitable for experimental or small parts purposes. The build volume is cylindrical with 98 mm diameter and



Figure 40: TruPrint 1000 by Trumpf company [18]

100 mm height. The laser spot is 55 μm in diameter, maximum laser power 200 W. Materials like Al-alloys, stainless steels, tool steels or Ti-alloys can be processed with this printer. Further information can be found in [18].



During the experiments light microscopy was used to analyse single-tracks and cubic samples. For this purpose, the digital light microscope OLYMPUS DSX1000 located in Material engineering institute at CTU was used. OLYMPUS DSX100 is suitable for scanning lower and medium magnification observations. For closer microstructure observation the light microscope NEOPHOT 32 was used.

Other experimental procedures will be explained separately in the following articles.

4.1 Powder analysis

In the powder particle analysis following experiments were realized:

- Particle size and distribution (PSD curves) – Laser diffraction
- Particle shape and inner quality – Scanning electron microscopy (SEM)
- Chemical composition – Energy dispersive X-Ray analysis (EDX)

• *Particle size*

To determine powder particle size and distribution the laser diffraction method was applied. This method is very popular nowadays, because it provides quick, dynamic and repeatable measurements. The principle is based on the laser beam directed on the measured sample in the measurement cell. The light scatters according to the particles size with different angles. Small particles perform with larger scattering angles and larger particles with smaller angles (Figure 41). The intensity of the scattered light is recorder by the detectors. [74]



Figure 41: Light scattering in laser diffraction measuring method for larger and smaller particles [74]

The signals from various detectors are analysed. To calculate the particle size distribution two different methods can be used - Fraunhofer or Mie. In the experiment the Fraunhofer theory was used, which doesn't require optical properties of the sample.



The main output from the laser diffraction are the cumulative and differential PSD curves discussed in Chapter 2.3.3. [30], [74]

The analysis was realized on the Particle Sizer Analysette 22 NanoTec by company Fritsch located at University of Chemistry and technology. The machine uses laser diffraction in the water, where the repeatability of the measurement is for $D_{50} \leq 1\%$. The mentioned analyser can measure sizes between 20 nm and 1 mm. [75]

- *Shape and inner quality analysis*

The particle shape importance was discussed in the process parameters Chapter 2.3.3. According to the regular powder particle sizes (10-80 μm) the scanning electron microscope (SEM) was used. SEM image and magnification are reached with focused electron beam of primary electrons. The electrons are passing into the material and interact with atoms, which allows to receive information. [76]

The electrons are generated in the electron gun. Electrons (or primary electron) are concentrated into the beam with the use of anode and the beam is directed on the sample surface. The sample is than analysed point by point, row by row (scanning). Signals are recorded with the use of detectors. All points form the full image of the observed area. The depth in which the electrons can penetrate is defined mainly by primary electrons energy and the atomic number of the material. The most important signals to receive information about the surface of the sample are the secondary electrons (penetrated and escaped from the material) and reflected electrons. Secondary electrons are the most usual to form the topography image of the sample. [76]



Figure 42: FEI Quanta 3D FEG [78]

The resolution of the SEM image is highly dependent on the distinctiveness of the microscope. Another important technical aspect for SEM is also that samples has to be electrically conductive. In the case the sample is not conductive, the negative charge starts to accumulate, and the electric field deviate the primary electrons from the



surface. The main benefit from the SEM is that electron beam has lower wavelength so it can reach much higher magnitude. [76]

In this experiment the SEM FEI QUANTA 3D FEG (Figure 42) was used to observe the shape of the powder particles. Powder particles were analysed in 2 different ways. First the dry powder was observed to identify the particle shape. Secondary the powder was fixed, grained, polished and observed from the inner quality perspective.

- *Chemical composition*

As the last step of the powder analysis the chemical composition was checked before the printing operations. For this purpose, the Energy Dispersive X-Ray (or EDX) analysis was applied.

In the SEM several interactions between observed material and electrons can be found. One of the specific is the X-ray caused by the inelastic interaction between the electrons. Emitted X-ray of specific energy is then processed with the detector where electrical pulse is then assigned to specific spectrum value. In multi-channel analyser are pulses divided according to their size (full spectrum is created). Spectrum is formed by the peaks of characteristic rays for specific chemical element (e.g. Figure 43). On the x axis the energy is shown and on the y axis the number of photons for this value (chemical element) is displayed. The area under the peaks can be transferred to specific volume element content. The evaluation of the EDX analysis requires experience, because some false peaks or peak covers can occur. It is also obvious that this method defines chemical composition locally on the observed sample. To get quantitative result the electron beam has to move in the certain area, so the composition map can be generated. [76]

In this thesis the EDX analysis was applied on the SEM. The analysis was done on the fixed powder particles that were observed in the purpose of inner quality.

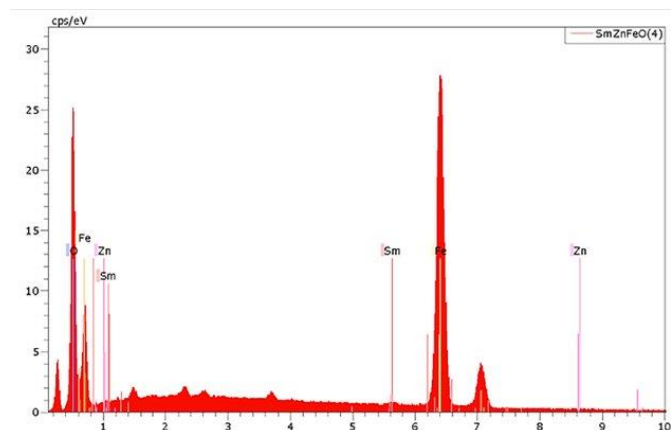


Figure 43: SEM peaks example [79]

4.2 Single tracks build set up

All the printed parts in SLM process are produced layer-by-layer. The layer itself consists of certain vectors combination, assigned to specific parameters. It can be said that vectors are base structure to form any geometry in SLM (LMF). In the process parameters development is common to realize building of such single vectors with specific laser power and scanning speed (the rest of the parameters are constant). The printed single vectors are called single tracks. Combination of certain power and scanning speed can be called linear energy E_L [J/mm] density (even it is not accurate). Linear energy for specific combination can be determined like $E_L = P/v$ [J/mm].

In the experiment single tracks for the layer thickness of 40 μm were performed with combination of laser power 160 W up to 200 W and scanning speed 100 mm/s up to 1200 mm/s. Pre-processing was realized with the use of software Magics. The single tracks were separated on the platform into 4 sections for representing specific laser power. The layout of the platform with gas flow and recoater direction from pre-processing software Magics is shown in Figure 44.

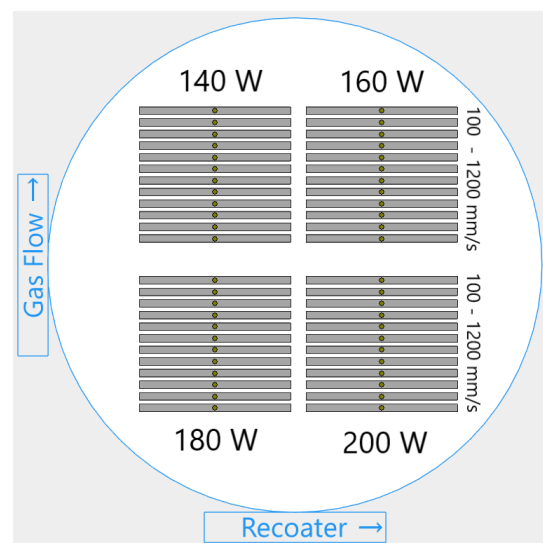


Figure 44: Single-track in software Magics

Before the experiment the printer preparation was done, and it will be explained further. Important fact to be mentioned is that first layer and its accuracy is highly problematic and had to be carried out. The recoater must be tough (will not deform during movement) to ensure exact layer thickness is placed. According to that, the original recoater was replaced with ceramic one. Also, the powder deposition and movement of the recoater was performed manually. The final layer after manual powder deposition is shown in Figure 45.



Afterwards the printed single tracks were analysed with the use of microscopy in upper view and perpendicular cut. Single tracks were sorted into 5 stages of quality (described further). It is also important to mention, that single-tracks experiment part is voluntary, and it provides very rough look out on the material printability. Based on author's experience, in many cases the final parameters don't match the best single

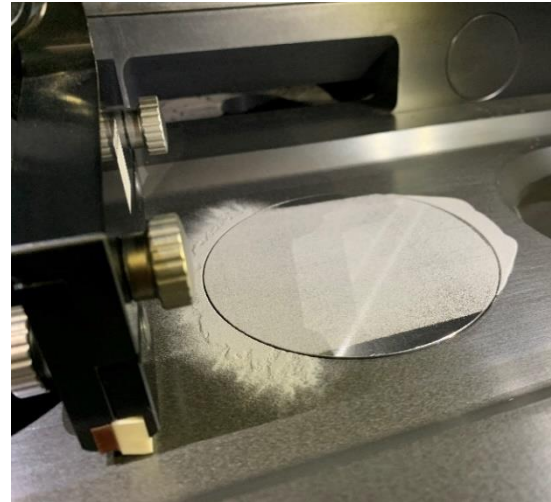


Figure 45: Deposited first layer

tracks parameters. On the other hand, single tracks provide very good estimation for further experiment part.

4.3 Cubic samples build set up

All the experiment parts are directly connected to each other. The cubic (volume) samples 10 mm x 10 mm x 5 mm were printed based on the results from the single-tracks experiment. The cubic samples were placed with the use of block and cone supports to dissipate the heat and stick the cube to the platform. All the pre-processing operations dealing with geometry and process parameters were performed in the software Magics.

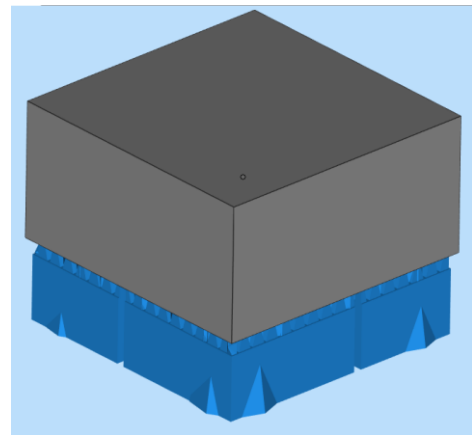


Figure 46: Cubic samples

It is obvious, that against the single-tracks, cubes are considered as volume samples. That means there are more parameters to be considered in the printing set up. Values that were modified for each cubic sample were in-skin (infill) of the samples. The modified parameters (in in-skin) were laser power (180 and 200 W), scanning speed (500 - 1400 mm/s) and hatching distance (60, 75 and 90 μm). 1400 mm/s scanning speed was extended based on single-tracks results. The rest printer set up values were used from Trumpf factory settings for steel 1.2709. The up-skin (upper finish layers), down-



skin (bottom finish layers) were disabled. The reason for variations only in in-skin parameters is, that most of the volume is formed by the in-skin set up. The additional values for up-skin and down-skin can be investigated further.

For mentioned in-skin parameters first 42 variations were defined and placed on 2 building platforms. The energy density VED was varied in the range of 36 up to 104 J/mm³ (later up to 167 J/mm³). In the experiment process more variations of the

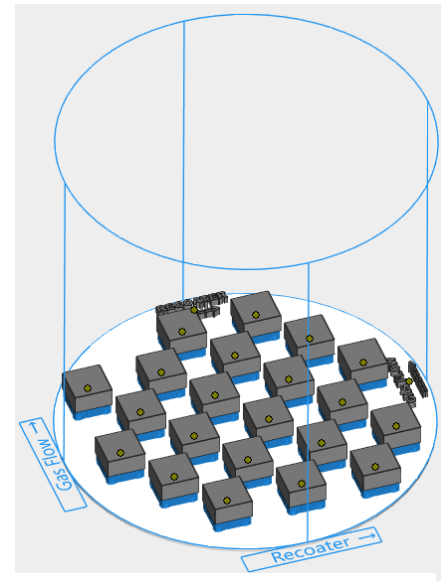


Figure 47: Cubic samples set up

parameters were needed to investigate, so the third platform with 21 samples was printed. Samples on each platform were placed in the chess layout. The final platform geometry definition in software MAGICS can be seen in Figure 47.

Before the print the machine was cleaned to eliminate any possible deviations. The build chamber was vacuumed from remained powder, the filters were cleaned and the laser protecting glass was polished. Afterwards the powder was placed into the supplier bin and the correction of the building platform was done. Once the machine was ready to use, definition code was imported, and the building chamber was filled with nitrogen. Final printing process of the cubic samples is shown in Figure 48.

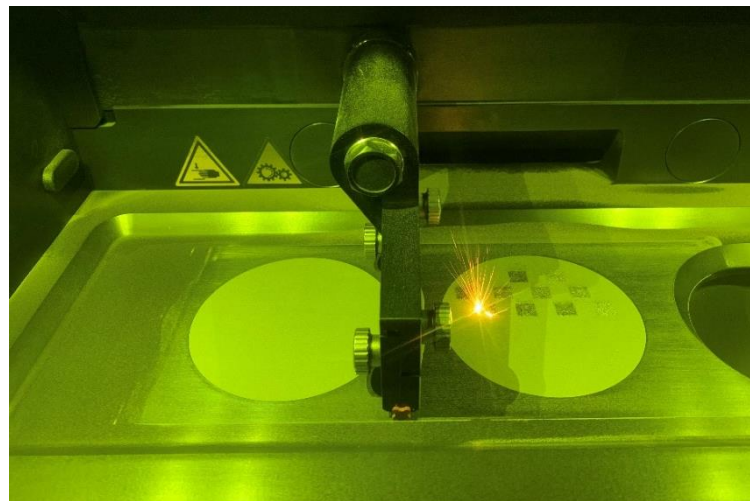


Figure 48: Printing process of the cubic samples

After the printing process the samples were post-processed and inspected with the light microscopy. The main goal was to specify the porosity and the hardness of the samples. The porosity was analysed in the software NIS-Elements.

4.4 Mechanical properties testing samples

As it was written in previous chapter, all experiment parts are directly connected. That means the final stage of process parameters development in handed thesis is based on the lowest porosity results (in combination with highest productivity) from the cubic samples experiment part. These parameters were used to build mechanical testing samples for two mechanical properties test methods – tensile and Charpy impact test.

Mechanical test samples print parameters were for in-skin $P=200\text{ W}$, $v=500\text{ mm/s}$, $h=75\text{ }\mu\text{m}$, with disabled top-skin and down-skin parameters. The whole in-skin parameters set up was only bordered by one line with parameters $P=125\text{ W}$ and $v=500\text{ mm/s}$. As it was also mentioned at the beginning of the thesis (e.g. Table 1), Laser Powder bed fusion performs anisotropy in the final prints. For this reason, 3 groups of mechanical samples were printed with different platform orientation angle - 0° , 45° and 90° . Platforms pre-processed in software Magics are shown in Figure 49. Total print time for left platform was approximately 13 hours, for middle platform 18 hours and for right platform 13,5 hours.

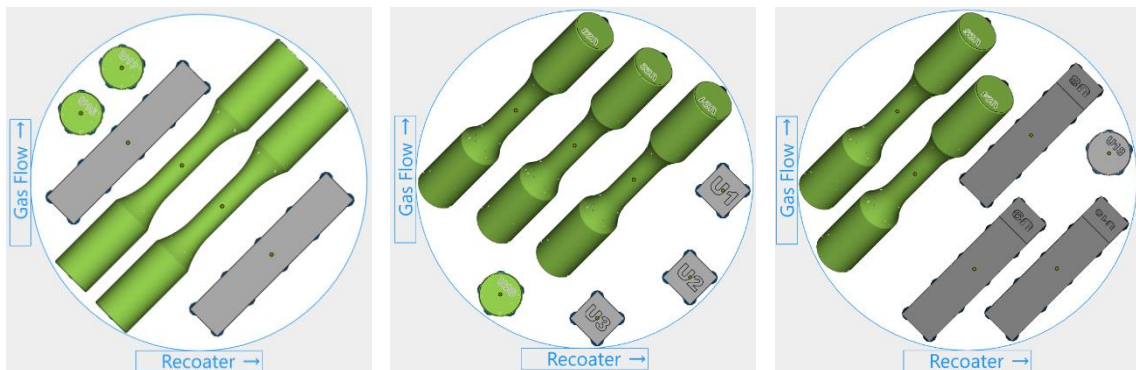


Figure 49: L-40 platform examples pre-processed in software Magics

All the printed samples were obviously supported by the proper structures, that had to be slightly optimized with later platforms processing (thickness of the support structures etc.), because the samples were breaking away from the platform.

Final printed test samples were de-powdered, removed from the platform and support structures, machined and tested. Tensile test was performed according to the standard ČSN EN ISO 6892-1 with starting sample diameter $d_0=6\text{ mm}$ and $L_0=22\text{ mm}$ (not standardized length). The whole definition of the tensile test method can be found directly in ČSN EN ISO 6892-1 and will not be described in detail. Targeted values were



tensile strength R_m [MPa], yield strength $R_{p0,2}$ [MPa] and elongation A [%] The tensile test was realized at CTU in the laboratories of Material engineering institute with INSTRON 5582.

Charpy Impact test was realized on standardized dimensioned sample with U-type notch at the CTU Material Institute laboratories with the use of PH300/450-Charpy (300 J maximum). Whole 15 samples were tested at the room temperature of 21 °C. The targeted value was to define absorbed impact energy KU [J] for all 15 samples (3 x 5 samples with different build platform angle).

According to the mechanical properties results, Charpy test specimens were investigated in cross-section under the light microscope. This experiment part was added to define reasons and counter measurements for future prints with enhanced properties.



5 Results and discussion

In this chapter all the results will be presented with the followed discussion. The results were completely prepared by the author of this thesis (except the chemical composition and powder morphology which was done externally).

5.1 Powder particle size, morphology and chemical composition

As it was mentioned before 3 experiments were realized on the supplied gas atomized L-40 powder by Formetrix – laser diffraction, particle shape/inner quality observation with SEM and chemical composition analysis with EDX.

- *Particle size and distribution*

The resulted PSD curves from laser diffraction are shown in Figure 50.

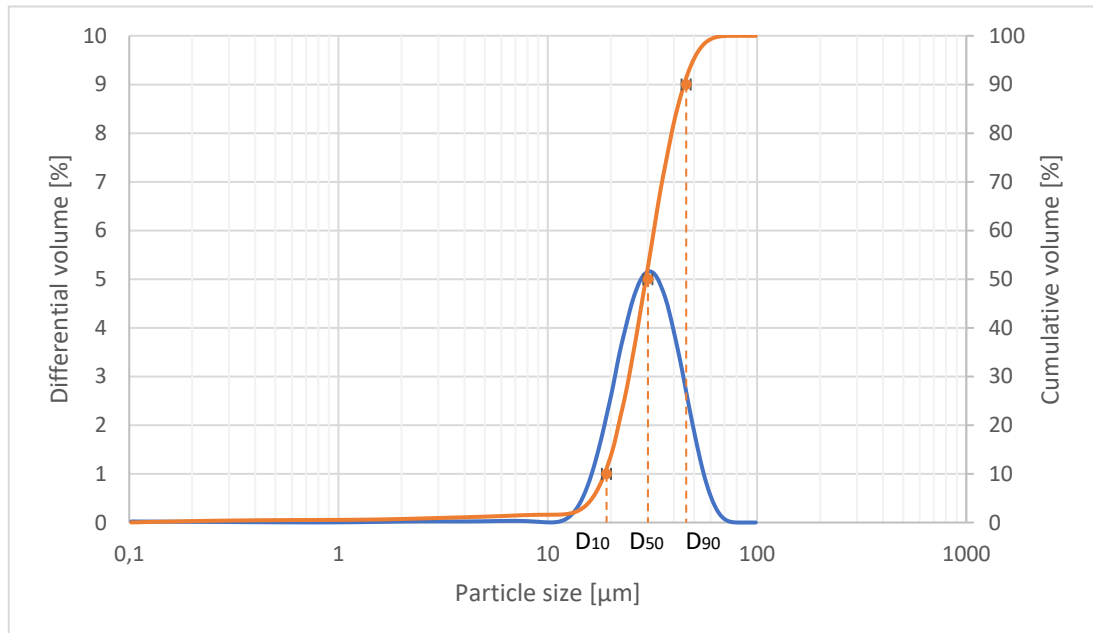


Figure 50: PSD resulted curve (orange – cumulative, blue – differential)

Particle sizes are summarized and compared with specifications in following Table 11.

Table 11: Comparison of measured and specified powder particle size

	D10 [μm]	D50 [μm]	D90 [μm]
L-40 specification	20	33,4	54,2
L-40 measured value	19,1	30,1	45,9

From differential PSD curve (Figure 50- blue) is obvious that particle sizes are dominantly between 20 and 55 μm (almost 90 % of the powder particles). Narrow range of the main particle size distribution is suitable for process stability. Cumulative curve (orange)



defines D_{10} , D_{50} and D_{90} values. Highest curve gradient will be met in the D_{50} area, which is suitable powder property for printing process.

Values in Table 11 correspond with the supplier's definitions and generally are slightly lower than the specification. As it was mentioned before, particle size and its distribution are also critical for minimum layer thickness. From measured values we can assume that layer thickness of 40 μm for the experimental printing experiments will be suitable.

- *Particle morphology and inner quality*

Mentioned in previous chapters, the powder particle shape was observed with use of scanning electron microscope. Obtained pictures example are shown in Figure 51.

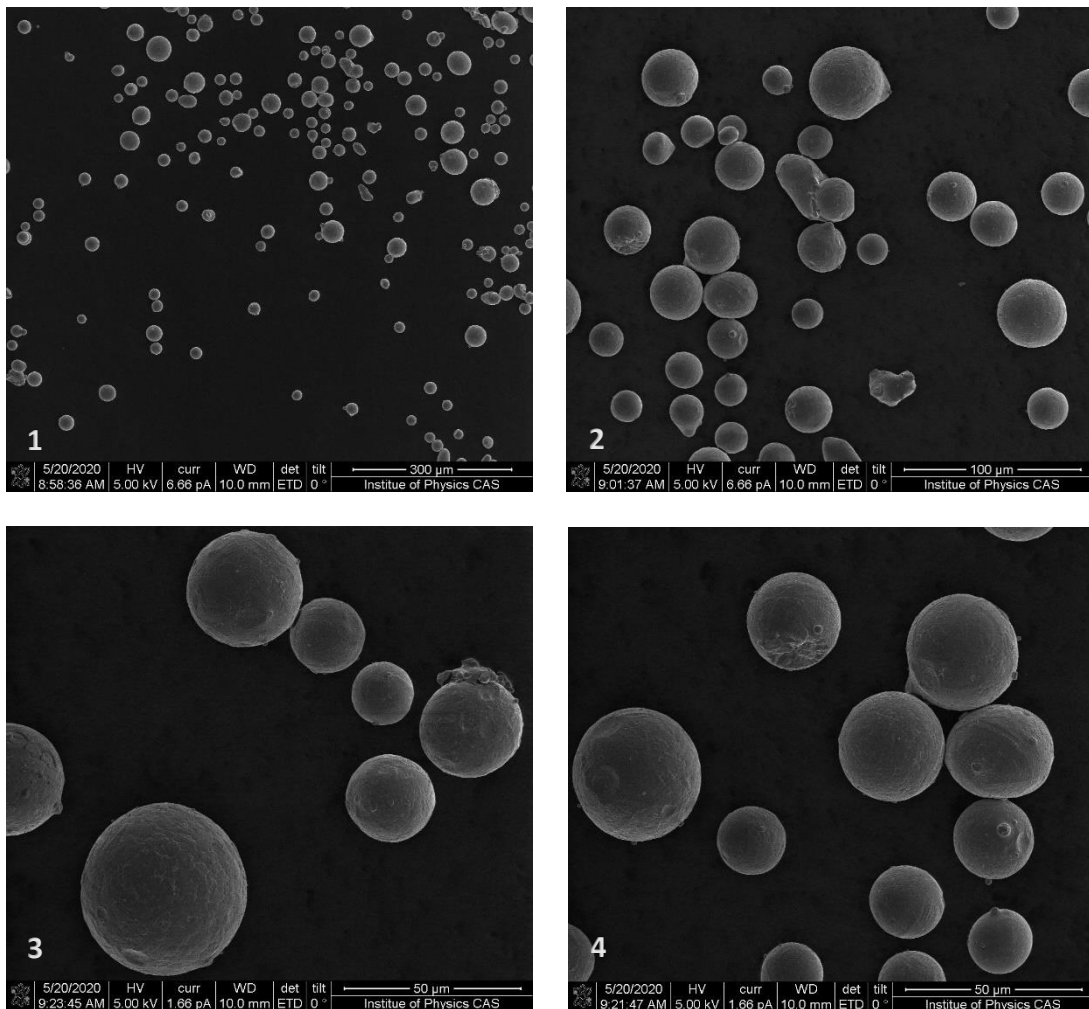


Figure 51: L-40 powder particles in different magnifications [SEM]

In the Figure 51 various powder particles can be seen. Most of the particles are spherical. Few irregular particles can be seen for example in the picture 1 and 2. In the picture 1



and 2 also some agglomerations can be seen. In picture 2, 3 and 4 we can also find some satellite particles. All these deviation forms are caused by the manufacturing process (gas atomization) and are presented in almost all metal powders. Generally, can be said that powder form is appropriate to gas atomization process, where mostly spherical particles are presented with few irregularities and deviations.

The second part of shape and quality observation on the SEM was realized with the fixed, grained and polished powder particles. Pictures of the powder inner quality are shown in Figure 52.

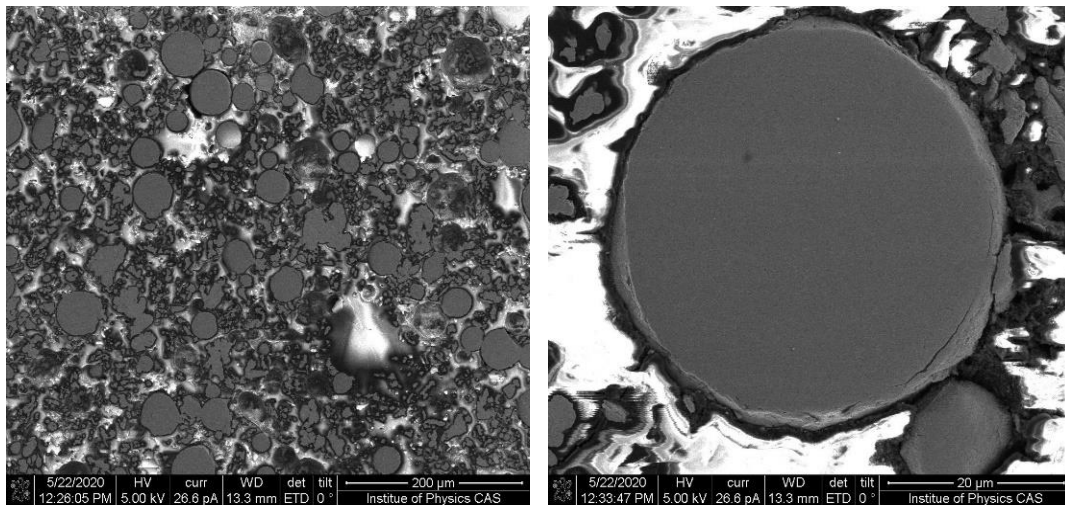


Figure 52: Fixed, grained, polished L-40 powder particles [SEM]

Generally, there is almost no porosity in the particles (or spongy particles). It can be said that density of the particles will be nearly 100 % (as mostly). On the right side of Figure 52, there is a detail of spherical particle. Around the particle in Figure 52 small oxide layer can be seen, which is connected to the oxygen content during gas atomization, but also to the storing method of the powder.

- *Chemical composition*

In the last step of the L-40 powder investigation experiment, the chemical composition was analysed with the use of EDX and optical chemical spectroscopy. EDX was realized on the fixed powder particles from previous experiment part. As it was mentioned, the chemical composition is given by the supplier Formetrix and it is protected. For mentioned reason the evaluation is simply summarized in Table 12 without EDX peaks records.



Table 12: L-40 powder chemical composition control

Element	Cr	Ni	Mo	Cu	Nb	C	N
Content [%]	> 10.5	< 5	< 5	< 1	< 1	< 1	< 1
Control	OK	OK	OK	OK	OK	OK	OK

From EDX analysis it was also clear, that chemical composition is more complex than it is mentioned in Table 12. The limits by Formetrix are only one sided, so the complex control can't be realized. It would be also suitable to check powder oxygen content. This experiment could not be realized, because of the laboratory restriction caused by coronavirus.

With the chemical composition analysis, the powder experiment was finished. To sum up L-40 powder completely met the specifications given by the supplier. The particle size and distribution matches D_{10} , D_{50} and D_{90} with no wide range of main distribution. Particle shape is mostly spherical with few irregular particles, agglomerations and satellite particles. These deviations correspond with the powder manufacturing method. Chemical composition could not be fully investigated, because of the protected rights.

5.2 Single tracks – results

Printed single tracks on the building platform are shown in Figure 53. As it was mentioned before, the platform was separated into 4 sections based on laser power P [W]. Single tracks were observed in upper view and cross-section with the use of light microscopy. Goal of the upper view was to determine the thickness of the single tracks.



Figure 53: Printed single tracks

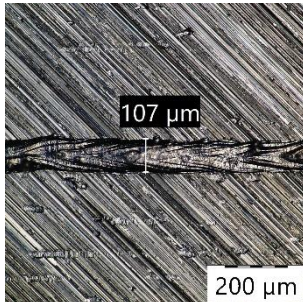
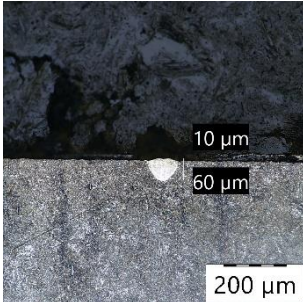
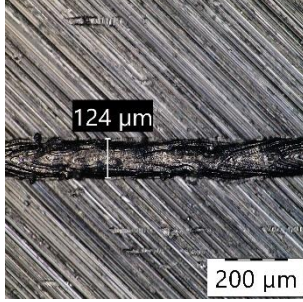
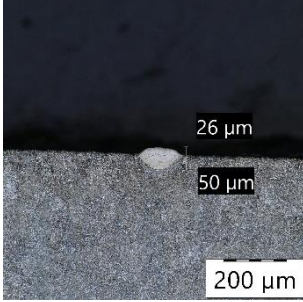
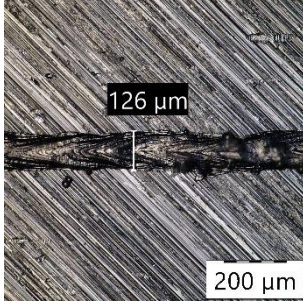
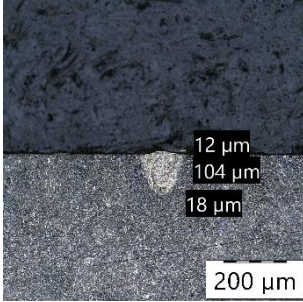
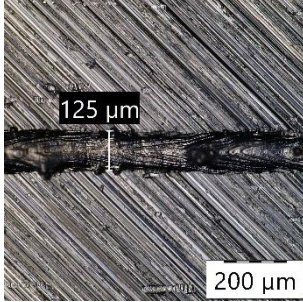
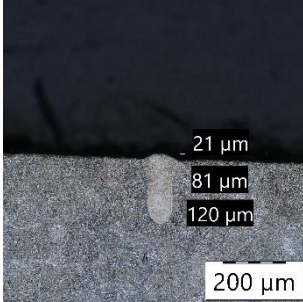
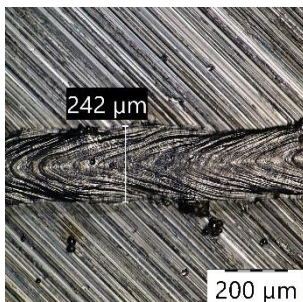
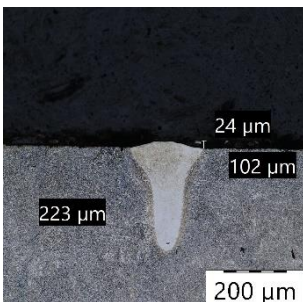
In the cross-section (perpendicular cut to the single tracks) the height depth and heat affected zone (if occurred) was investigated. The cut sections were fixed, grinded, polished and etched. The etching was highly problematic, because of 2 different materials (platform and the single track). The best etching results were achieved with the use of vilella (Picric Acid based etchant) for 10 minutes. Author realizes that the etching quality could be improved, but in this experiment part the structure phase is not the main purpose.

The single tracks were divided into 5 specific groups based on the measured values and the single tracks appearance. The groups with the description are shown in the Table 13 on the next page. Each description is followed by an example picture in the upper and cross-section view. The values of the dimensions in the cross-section view are always in the order from the top of the image (height, depth and heat affected zone if occurred). The height values of the single tracks were not used for classification, because during the preparation some of them were deformed.

From the Table 13 can be also seen, that the single tracks have the height values generally below $20\ \mu\text{m}$. This value doesn't correspond with the layer thickness made by the recoater ($40\ \mu\text{m}$) even approximately. This could be caused by the one-layer deposition discussed before. We can expect that the first layer thickness was lower and not fully homogenous on the platform. Even with the manual deposition, the first layer could be slightly removed away from the gas flow starting mechanism (filling the chamber with nitrogen).



Table 13: Groups of single tracks

	Description	Upper view and cross-section view example	
1	Single track is in the depth less than 100 μm with no or very low laser passing into the basic material. Width of the single track is up to 115 μm .		 <p data-bbox="1426 293 1453 562">P=200 W, v= 1100 mm/s</p>
2	Single track is very shallow in the depth (less than or equal 50 μm) with no or very low laser passing into the basic material. Width of the single track is up to 130 μm .		 <p data-bbox="1426 613 1453 882">P=180 W, v= 600 mm/s</p>
3	Single track is medium in the depth (up to 115 μm) with the slight laser passing into the platform basic material. Width of the single track is less than 145 μm .		 <p data-bbox="1426 965 1453 1234">P=140 W, v= 600 mm/s</p>
4	Single track is large in the depth (up to 130 μm) with the laser passing into the platform basic material. Width of the single track is less than 170 μm .		 <p data-bbox="1426 1317 1453 1585">P=180 W, v= 500 mm/s</p>
5	Single tracks has very large depth (more than 130 μm) with the high laser passing into the platform basic material. The width is more than 170 μm .		 <p data-bbox="1426 1668 1453 1937">P=200 W, v= 200 mm/s</p>



Assigned groups to specific single-track parameters are shown in Table 14. The numbers and colours are matching the group description in Table 13. If the single-track performed at least 1 condition from certain group, it was considered to the higher number one.

Table 14: Single-tracks results for specific laser power and scanning speed

		P [W]			
		140 W	160 W	180 W	200 W
v [mm/s]	100	5	5	5	5
	200	5	5	5	5
	300	5	5	5	5
	400	4	5	5	5
	500	4	4	4	4
	600	3	4	2	4
	700	2	2	3	4
	800	2	2	2	3
	900	2	2	2	2
	1000	2	2	2	1
	1100	2	2	1	1
	1200	2	2	1	1

From Table 14 is obvious, that lower scanning speeds (100 – 400 mm/s) are generally causing powder and base material overheating. This leads to the wide and deep single tracks with heat affected zone (HAZ) and melted base material in the shape of key-hole. Generally, can be said that linear energy input is too high even for values slightly above 0,3 J/mm. For mentioned reasons all laser powers with 100-400 mm/s are not suitable for further investigation.

More interesting areas starting to occur in higher scanning speeds. In 140 and 160 W area, single tracks start to show better results even from scanning speed 700 mm/s. For 180 W and 200 W the values improve from scanning speed 900 mm/s.

The best results were achieved in the area of the two highest scanning speeds for 180 and 200 W of laser power. The single tracks performed regular shape with, appropriate depth, constant thickness and almost no HAZ or key-hole effect. As an example, single-track for 200 W and 1100 mm/s is shown in Figure 55. The same single track was scanned in the 3D with the use of digital microscope (Figure 54). On the left side the topology scan is shown. On the right the deviation in height is visualized with colours is displayed. It is obvious that single track is almost constant in height and it is keeping the line order.

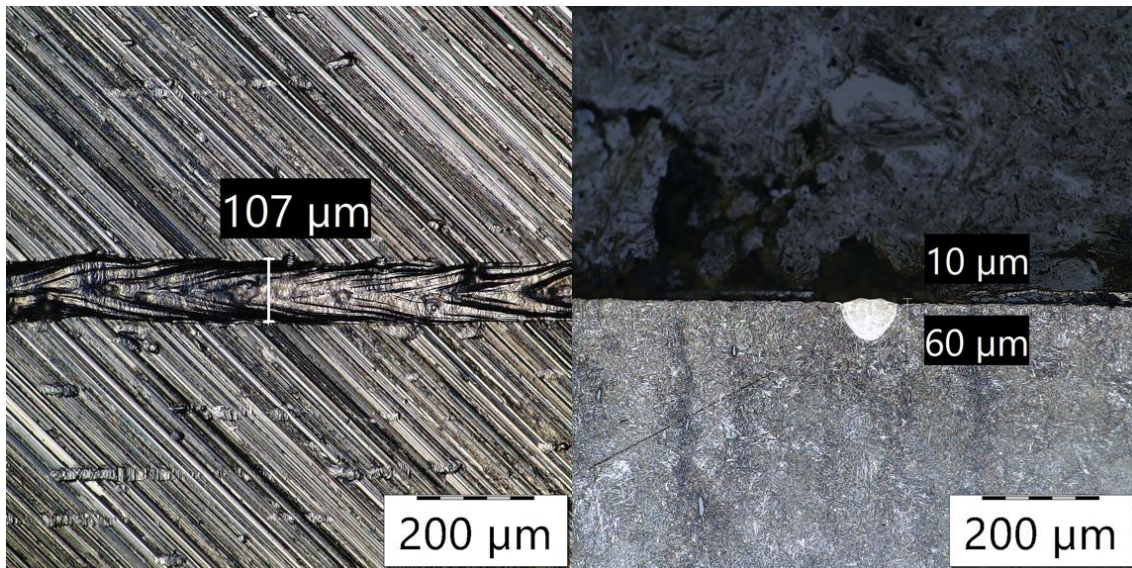


Figure 54: The best achieved L-40 single track $P=200$ W and $v=1100$ mm/s

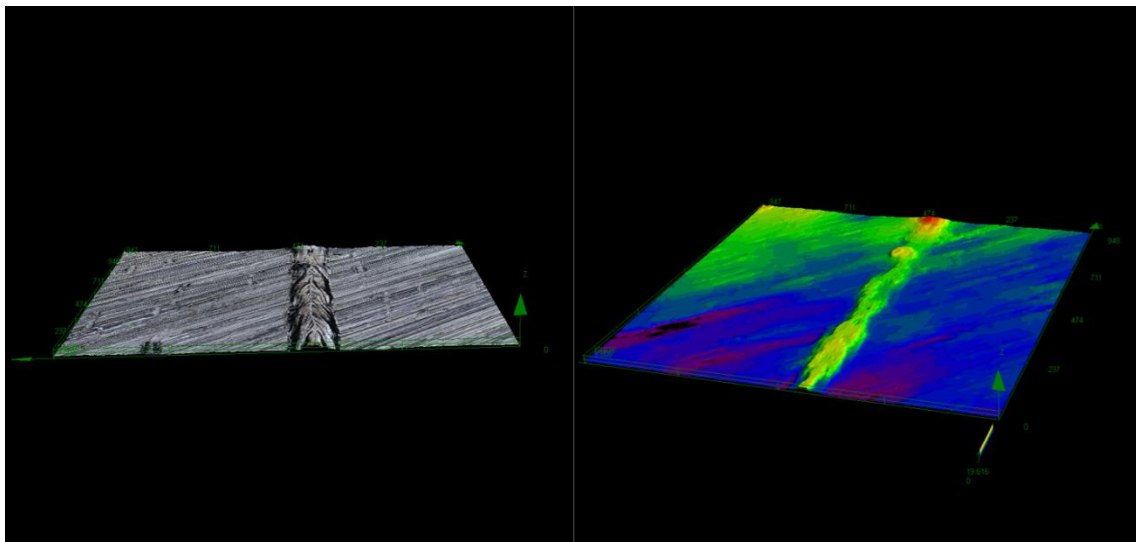


Figure 55: 3D scan of the best achieved L-40 single tracks

To sum up, the single-track experiment met the expectations. The variations of laser power and scanning speed were classified into 5 specific groups. The values of 180, 200 W and 900-1200 mm/s were selected as the area of further interest. Higher scanning speeds were chosen, because in the summarizing Table 14 improvement at the bottom right corner is evident. The important fact to be mentioned, is that the cracks or failures in the single tracks were not observed. This fact suggests the printability of the L-40 steel in the room temperature. On the other hand, single-tracks experiment gives very rough estimation of the real process parameters. It has to be mentioned that single track height did not correspond with the layer height value and this could cause high deviation from final process parameters reached (will be discussed).

5.3 Cubic samples – results

The second part of the experiment was dealing with the volume cubic samples. The whole process set up and preparation was described in Chapter 4.3. Final printed platform is shown in the Figure 56. On the left side is the platform during de-powdering process and on the right side the final platform with the samples.



Figure 56: Final printed L-40 platform for 200 W – on the left de-powdering, on the left finished platform

As it was mentioned, in the first phase of this experiment two platforms were printed for 180 W and 200 W laser power, 800-1400 mm/s scanning speed and 60, 75, 90 μm of hatch distance. Afterwards experiment processing required more detailed process window investigation, so the third platform with extended (lower) scanning speeds 500-900 mm/s for 60, 75 μm of hatch spacing was printed. The first outlook resulted porosity based on VED is shown in Figure 57 for all 63 printed samples. From this graph it can be clearly said that with increasing VED value porosity amount decreases.

Complete separated results for each printed cubic sample with specific parameters are shown in Table 15, Table 16. The non-etched metallography pictures with assigned porosity and volume energy density are summarized in Table 17 on the page 72.

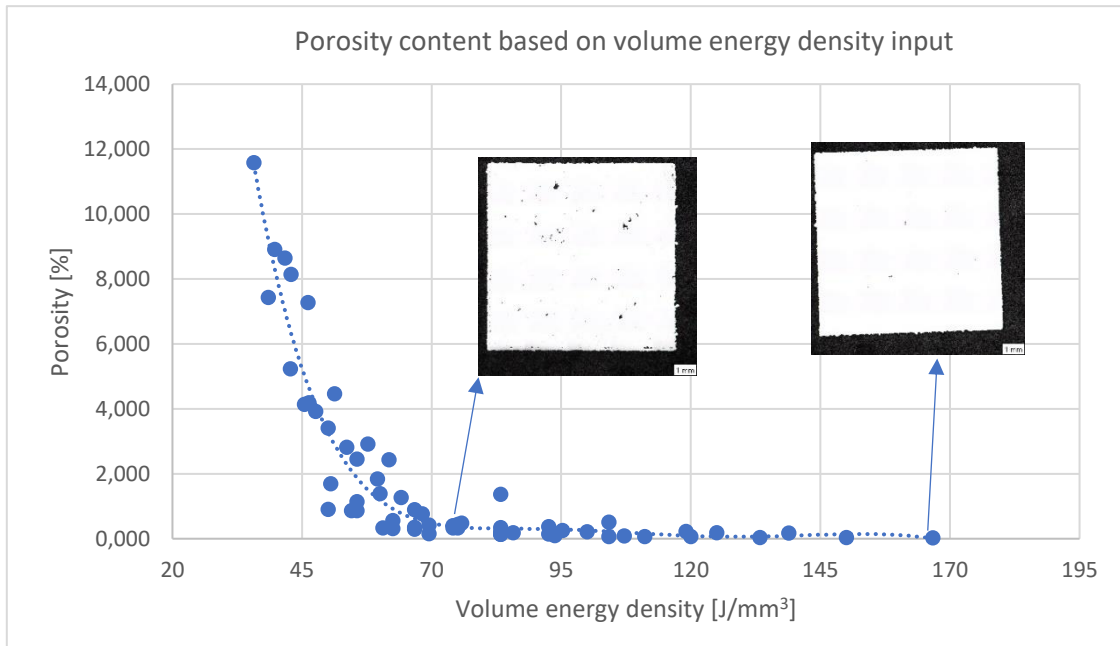


Figure 57: Porosity based on VED value for all L-40 samples

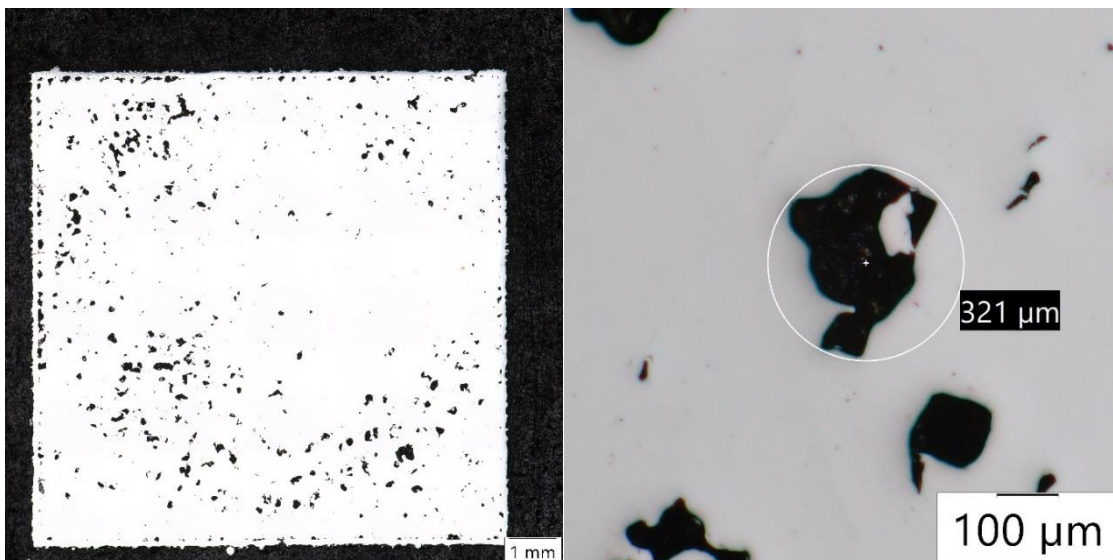


Figure 58: Irregular shape porosity

From the result values in Table 15 and Table 16 is obvious that with higher scanning speeds porosity content increases. Generally, can be said that scanning speed more than 1000 mm/s leads to unsuitable porosity content (porosity mostly above 0,3 %). The cause of this unsuitable porosity for higher scanning speeds was identified via the light microscopy and volume energy density evaluation. As the scanning speed increases, volume energy density gets lower and the powder has no energy to fuse. This trend is also obvious from the results in various hatch spacing parameter. As the hatch spacing increases the energy density goes down. In Table 15, Table 16 and Table 17 is easy to



observe increased porosity content for higher 90 μm of hatch spacing. Direct prove is shown on metallography picture in Figure 58. In Figure 58 irregular porosity with partly melted are can be seen.

As it is also mentioned in [77], shown type of irregular porosity is caused by low energy input. Powder has not enough energy to fully fuse. That is also the reason why the experiment parameters were extended with one lower scanning speed platform.

On the other hand, the samples with increasing energy input performed with lower stable porosity content. Generally, the best results were achieved with lowest scanning speed 500 mm/s for 60 and 75 μm of hatch spacing. The VED input for these parameters were 133-167 J/mm³.

We can assume that suitable energy input to reach the 99,9 % density is minimum 120 J/mm³. Secondly, lower volume energy density input than 120 J/mm³ leads to unsuitable and unpredictable amount of porosity. From hatch spacing perspective the value 90 μm is not suitable to use in production, because the powder bed area is not fully melted. One of the main conclusions from Table 17 is also that tool steel L-40 is printable at the room temperature environment on the TruPrint 1000 printer. This can be said based on no crack appearance on every printed sample.

Table 15: L-40 cubic samples -porosity values for laser power 180 W in %

180 W	Scanning speed [mm/s]									
h [μm]	500	600	700	800	900	1000	1100	1200	1300	1400
60	0,04	0,18	0,08	0,11	0,13	0,33	0,76	0,31	2,91	2,82
75	0,06	0,21	0,18	0,41	0,29	1,39	0,86	3,40	7,27	8,14
90	N/A	N/A	N/A	0,56	2,45	0,90	4,14	8,64	7,43	11,58

Table 16: L-40 cubic samples -porosity values for laser power 200 W in %

200 W	Scanning speed [mm/s]									
h [μm]	500	600	700	800	900	1000	1100	1200	1300	1400
60	0,02	0,17	0,22	0,28	0,37	1,36	0,47	0,15	1,27	1,84
75	0,04	0,07	0,25	0,26	0,40	0,89	0,33	1,14	4,46	3,92
90	N/A	N/A	N/A	0,41	2,43	0,87	1,69	4,18	5,23	8,91



Another purpose of the experiment was hardness measurement. The measurement was performed on the sample with the lowest porosity sample ($P=200W$, $v=500$ mm/s, $h=60$ μm), because the porosity could devaluate the measurement. Final as-build hardness from 5 measurements was $44\pm 0,5$ HRC which corresponds with the Formetrix specifications in [2] .

In the last step the sample with the lowest porosity content was observed after polishing and etching. The etching was realized with Vilela for 10 secs. Final metallography picture is shown in Figure 59.

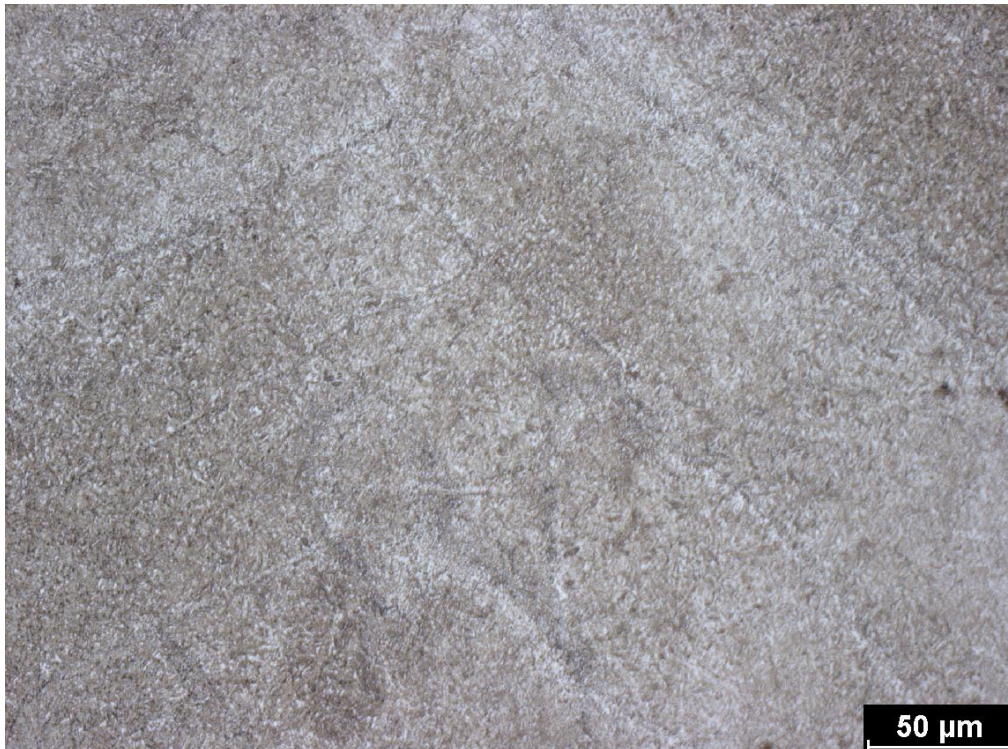


Figure 59: L-40 as-build microstructure on the lowest porosity cubic sample, $44\pm 0,5$ HRC

The structure in Figure 59 is formed by the combination of martensite, bainite and retained austenite. Retained austenite content can't be determined with the use of light microscopy and could be done via SEM. For future applications the analysis should be done, because retained austenite can lead to dimension inaccuracy or hardness changes during the heat exposure. In Figure 59 epitaxial grain boundaries can be slightly observed. The structure is very fine grained which is typical for powder metallurgy manufacturing methods.



Table 17: Metallography pictures summary of samples up to v=1100 mm/s assigned to E [J/mm³] and porosity value [%]

P [W]	180 W			200 W		
h [μm]	60	75	90	60	75	90
500			N/A			N/A
E [J/mm ³]	150	120	-	167	133	
Porosity [%]	0,04	0,06	-	0,02	0,04	
600			N/A			N/A
E [J/mm ³]	125	100	-	139	111	
Porosity [%]	0,18	0,21	-	0,17	0,07	
700			N/A			N/A
E [J/mm ³]	107	86	-	119	95	-
Porosity [%]	0,08	0,18	-	0,22	0,25	-
800						
E [J/mm ³]	94	75	69	104	83	69
Porosity [%]	0,11	0,41	0,56	0,28	0,26	0,41
900						
E [J/mm ³]	83	67	62	93	74	62
Porosity [%]	0,13	0,29	2,45	0,37	0,40	2,43
1000						
E [J/mm ³]	75	60	50	83	67	56
Porosity [%]	0,33	1,39	0,9	1,36	0,89	0,87
1100						
E [J/mm ³]	68	55	45	76	61	51
Porosity [%]	0,76	0,86	4,14	0,47	0,33	1,69

5.4 Mechanical properties - results

As it was mentioned in Chapter 4.4, based on the best porosity results from the cubic samples experiment, process parameters were selected for mechanical test samples print. The print was realized on 5 different platforms (according to build space) with 3 types of samples orientation - 0°, 45° and 90°. Three examples of printed platforms (corresponding with Figure 49) are shown in Figure 60.

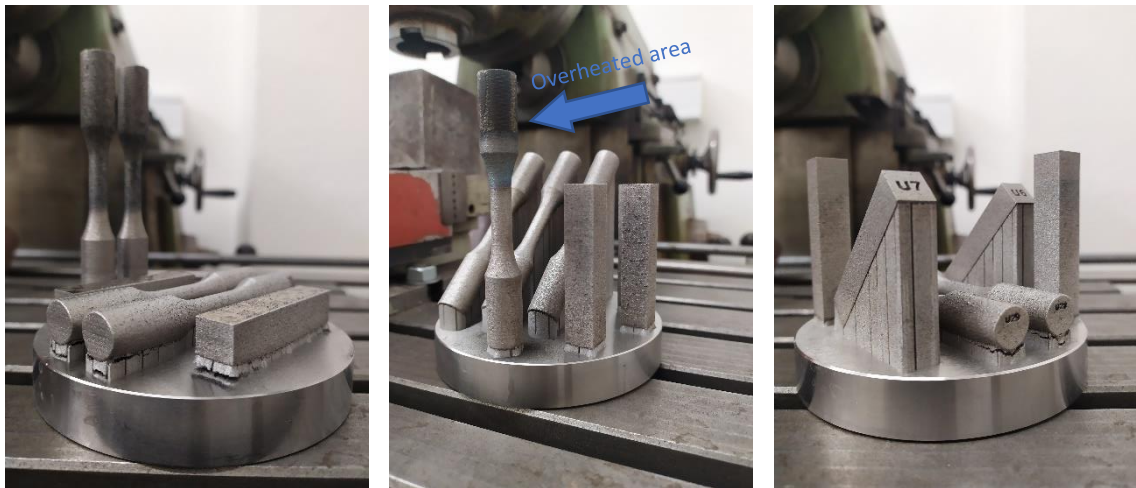


Figure 60: SLM printed platform examples from tool steel L-40 (total print time in hours: left-13, middle-18, right 13,5)

As it can be seen in Figure 60, the parts oriented vertically (90° build angle) performed with high overheated area and induced stress (mainly in upper part). This can be observed by the colour deviation in Z direction. Horizontal samples (0° build angle) performed with support structure failure during the print (high stress induction). On the other hand, the colour deviation didn't occur, so the overheat was lower than for vertical samples. The specimens with 45° build angle performed with almost no support crack and low colour deviation in Z direction. That leads to the fact that supports under the whole sample transferred the heat successfully and the stress induction was lower.

As it was also mentioned in Chapter 4.4, printed specimens were machined and tested according to the previous description – tensile test and Charpy impact test. Example of used machined samples are shown in Figure 61.



Figure 61: L-40 machined SLM testing samples



Specimens processing was interrupted by one factor, that has to be mentioned. The machining of the tensile test samples was done with the same roughness on the grip side as on the testing 6 mm diameter length. That resulted into smooth specimen/grip tool interaction, which caused the specimen sliding during the force loading. For this reason, the force-elongation record was affected, and yield stress value could not be specified in the most of cases. Author realizes the mistake, but according to coronavirus restrictions the experiment would be highly delayed. Yield strength is published only if at least 3 values from 5 samples was identified. Author would recommend test at least 3 more samples (with thread grips) for each orientation, to identify the yield strength.

The resulted values from the tensile strength test are shown in Table 18 and in Figure 62. Important fact to all mechanical testing results is that Formetrix did not state mechanical properties in order of build direction - compared values has to be considered carefully.

0° build angle samples reached the highest mechanical properties from all 3 sample groups. Tensile strength is approximately as supplier clarifies. On the other hand, elongation is about 3,6 % lower and Yield strength about 123 MPa lower. Standard deviation is appropriate to the measured values, except the elongation $\pm 1,2$ %. This problematic will be discussed further.

45° build angle samples did not meet supplier's specified values in tensile strength about 116 MPa (7,7 %) and in elongation about 5,0 %. Standard deviation for all values is appropriate to the test method.

90° build angle samples performed the lowest values from all 3 groups and missed the target properties about 318 MPa (21 %) and in elongation in minimum about 9,0 %. Standard deviation also showed the lowest stability at all (especially 1,4 % for elongation value). It can be expected that the values from supplier are not stated for 90° build angle.

Table 18: L-40 as-built state mechanical properties – tensile test

Build angle	R _m [MPa]	A [%]	R _{p0,2} [MPa]
0°	1479 ± 48	10,4 ± 1,2	1177 ± 72
45°	1394 ± 49	9,0 ± 0,9	-
90°	1182 ± 81	5,0 ± 1,4	-
Formetrix [2]	1500	>14	1300

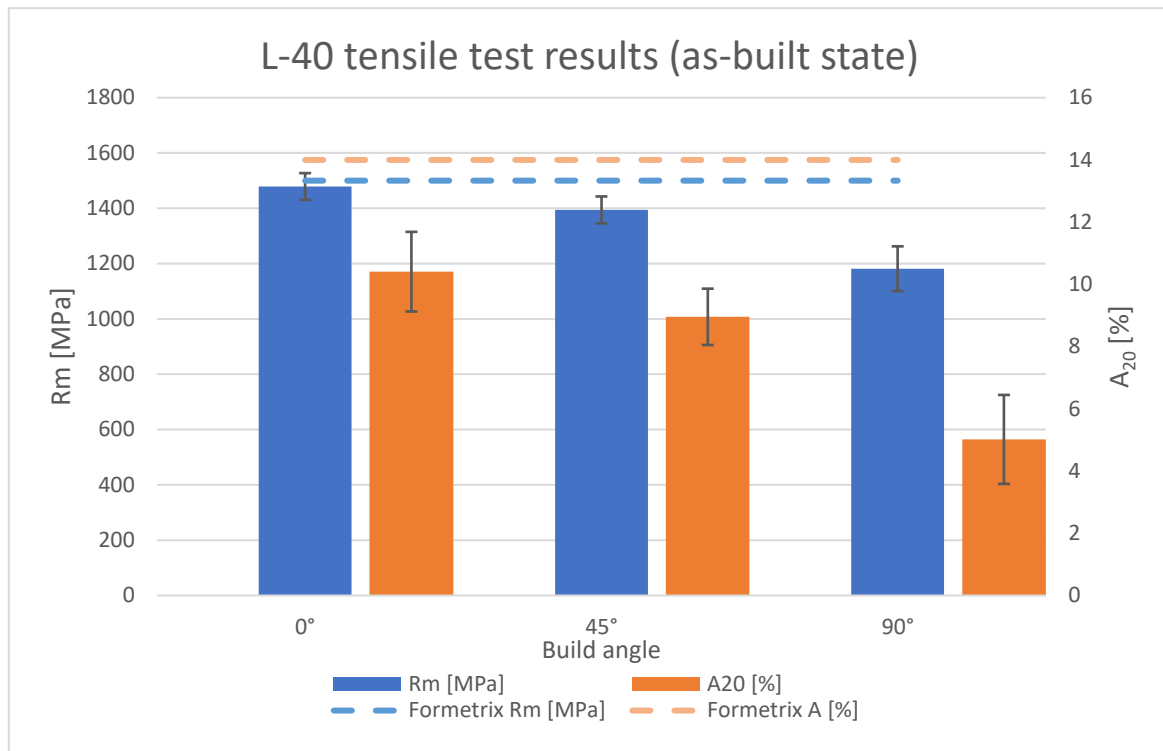


Figure 62: L-40 in as-built state - tensile test results for build angles 0°, 45° and 90°

From Table 18 and in Figure 62 is obvious trend of decreasing mechanical properties with increasing build angle ($R_{m0^\circ} > R_{m45^\circ} > R_{m90^\circ}$ and the same trend for elongation). Anisotropy topic of SLM manufactured parts was discussed in earlier chapters. Many publications dealt with anisotropy of SLM parts. As an example [78] and [79] can be mentioned. In both cases stainless steel 1.4404 (not tool steel) performed with the exact tendency of decreasing mechanical properties with increasing build angle. Especially tensile strength 0° build angle samples performed with the highest value. This tendency corresponds with epitaxial grain growth according to SLM manufacturing method, where the grains are interlocked in each layer. [78] Grains grow mostly in the direction of the heat source, so the shape is mostly needle-like (smallest dimension in the build direction). This fact is highly important in case of loading force on the sample, where perpendicular grains to the force are easier to break than parallel to the force. This is simply visualized in Figure 63.

As it was mentioned before, supplier (Formetrix) did not state, for which build direction the values are valid. It can be expected that the values are the best reachable throughout all directions (from previous discussion – 0° build angle).

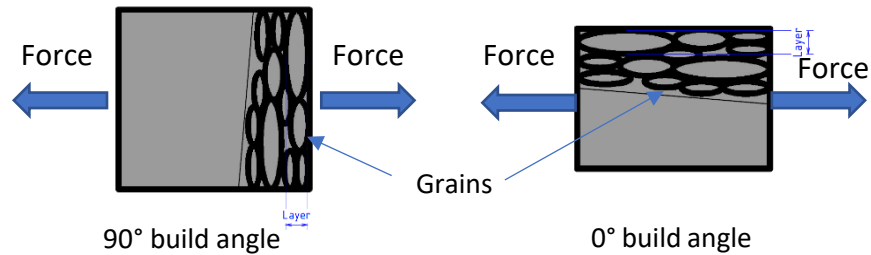


Figure 63: Simply visualized cause of samples anisotropy for different build angles

From Table 18 and Figure 62 can be generally said, that obtained mechanical properties are lower than the values clarified by the L-40 supplier. It is clear that samples were not in the proper inner condition to meet the specifications. That is also obvious from the following Figure 64, where broken tensile bars can be seen.

From Figure 64 can be said, that 90° build angle samples broke in perpendicular plane against the tensile force vector. This means that the crack was caused by the normal stress, not by the shear stress. This failure was most probably caused by any inner defects, that concentrated the stress and resulted into brittle fracture (right side of the Figure 64). Important fact also is, that the perpendicular fracture corresponds with the building planes from SLM printing process (grain interlocking discussed above).

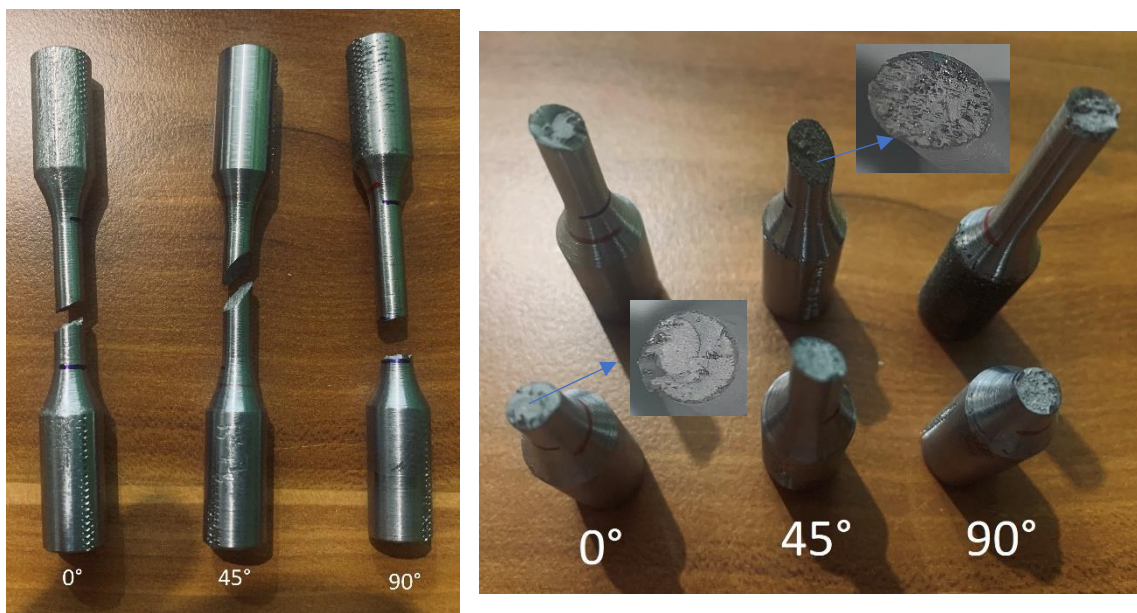


Figure 64: Broken L-40 SLM tensile samples for different build angles

The same issue can be observed for 45° build angle samples. The fracture plane again corresponds with the build plane direction. In the fracture surface we can again see brittle fracture with small stress accumulators (detail of the Figure 64).



Broken samples with 0° build angle performed with certain plastic strain in the fracture surface, but we can find again small stress accumulators. On the other hand, 2 samples even broke under the 45° angle which correspond with well-known fact of the maximum shear stress plane. From this fact we can assume that the material homogeneity and inner porosity was lowest for these samples. More complex discussion about the results will be placed after all mechanical testing.

Second realized test was Charpy impact test on the same 3 groups of samples (0°, 45°, 90° build angle), with U-type notch at room temperature. The resulted values are summarized in Table 19 and Figure 65.

Table 19: L-40 in as-built state – Charpy impact test results for build angles 0°, 45° and 90°

Build angle	KU [J]
0°	33 ± 2
45°	13,5 ± 2,5
90°	10 ± 0,5
Formetrix [2]	60*

*value was measured for V-notch (KV [J])

Charpy impact test results correspond with the tensile test results. The highest absorbed energy was achieved with the 0° build angle samples and the lowest absorbed energy was performed by 90° build angle samples ($KU_{0^\circ} > KU_{45^\circ} > KU_{90^\circ}$). Generally, is obvious, that

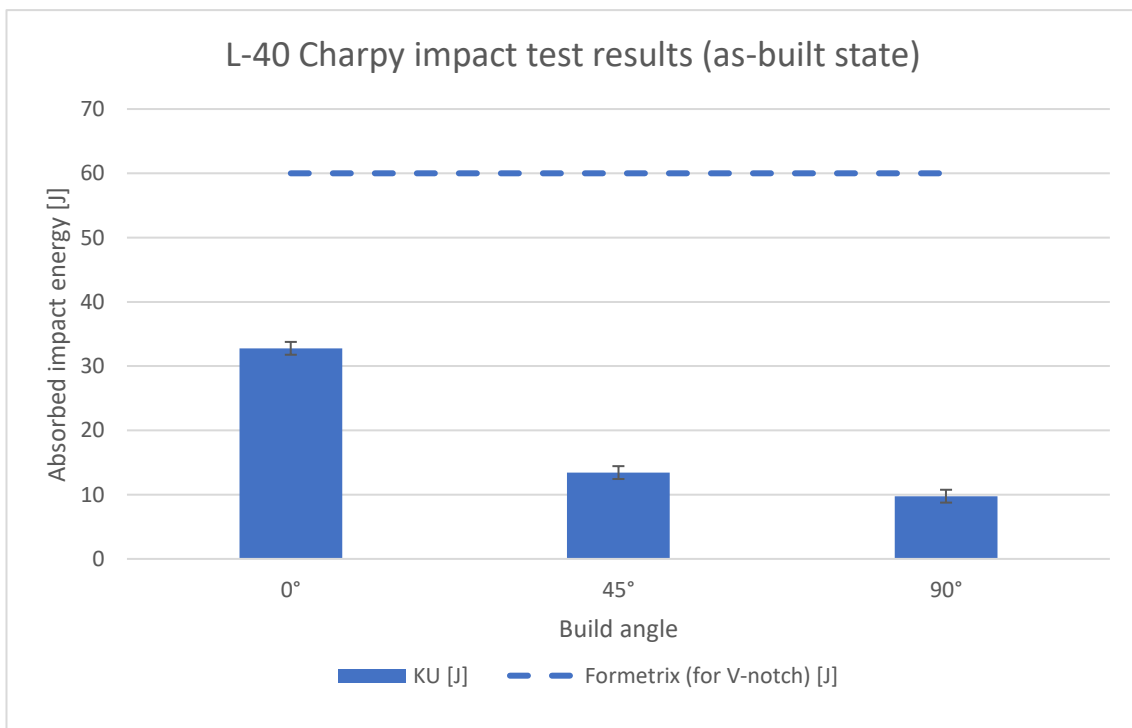


Figure 65: L-40 in as-built state – Charpy impact test results for build angles 0°, 45° and 90°



the values did not meet the specified value by the L-40 supplier. The closest value is approximately 59 % lower against the specified value. Especially values for 45° and 90° are critically low. On the other hand, if we compare the values with available study from EuroPM metallurgy conference (Table 9 on page 49) the difference is lower. As it was discussed in the study, for WA powder higher porosity amount was found in the samples (this fact leads to the lower absorbed energy values). We could also assume, that the porosity amount could interrupt the material integrity, so it is not able to stand under dynamic stress condition.

Generally, mechanical properties are lower in all build directions against the supplier's clarified values. Even if we focus on the best results in 0° build direction, the ductility of the material is not according to specifications. From the picture of the broken tensile samples (Figure 64) and observed fracture surfaces of Charpy samples, we can say that the prints were not in optimal inner quality. To sum it up, lower mechanical properties were affected by inner quality and also by anisotropy (for 45° and 90° build angles).

Despite the experiment part schedule and coronavirus restriction, author of this thesis could realize the light microscopy analysis to identify (prove) the cause of the failure and lower mechanical properties during the tensile and Charpy impact test. In Figure 66 the fracture surfaces can be seen. On the left of the Figure 66 is 45° build angle sample and on the right 90° build angle sample is displayed.

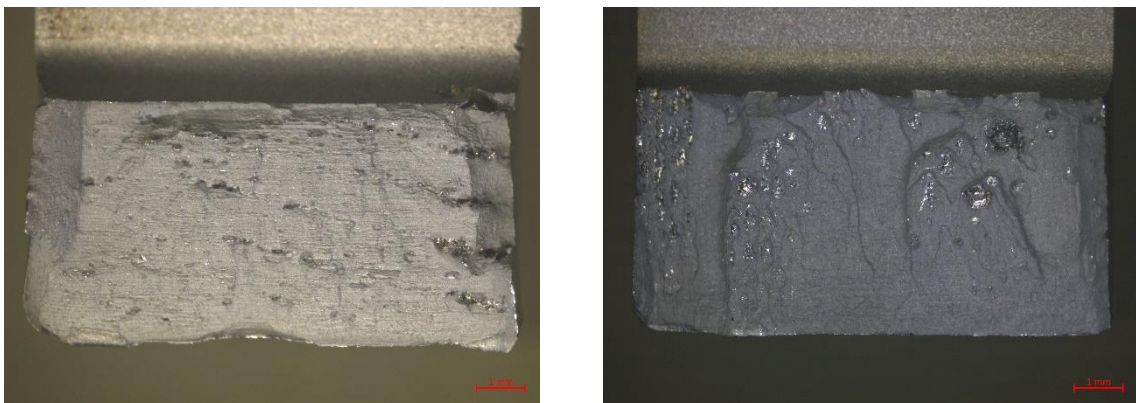


Figure 66: L-40 broken Charpy sample (fracture surface) – left 45° build angle, right 90° build angle



In Figure 66 defects from printing process can be found. It is obvious that these defects critically affected material behaviour during the Charpy impact test and failure was initiated especially in these areas. From the Figure 66 we can also assume that these defects are porosity resulted from the SLM process itself. To confirm this presumption, the light microscopy in perpendicular cut was observed. Results are shown in Figure 67.

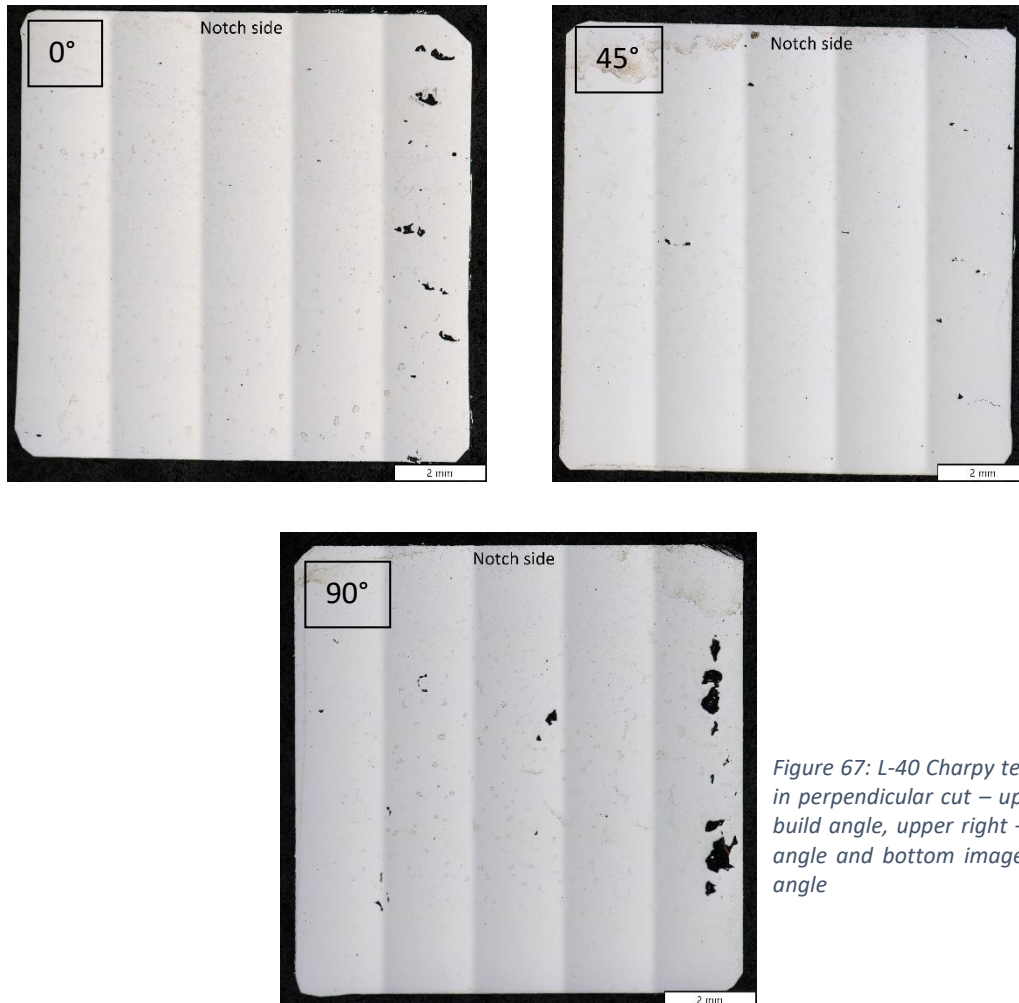


Figure 67: L-40 Charpy test samples in perpendicular cut – upper left 0° build angle, upper right – 45° build angle and bottom image 90° build angle

In Figure 67 the samples are captured as in the cubic samples experiment part (Chapter 5.3). The perpendicular cut was realized on 3 sample types in the same direction approximately 3 mm from the fracture surface. Build direction and notch side is marked on every picture. It is obvious, that porosity amount is higher than in the case of the cubic sample experiment (for the same parameters). The porosity is again irregular with locally nonmelted powder areas. Especially in 90° build angle sample porosity size is critical. As it can be also seen in the best Charpy test - 0° sample, the



porosity is concentrated dominantly on one side. This could be caused by the higher cooling rate in this area, which loses necessary energy for powder fusion. Another reason could be lower powder distribution on the sides of the build platform – that means porosity could be position based (printer based).

From previous comments we can say that probably no proper energy was delivered to the whole sample volume during the SLM process. For the small cubic sample, the energy input was enough, because surrounding heat absorbing volume was lower. Lower energy input causes porosity formation (previous investigation) and then lower mechanical properties of all testing samples. Based on this, author would recommend for future print use higher VED [J/mm^3] input, to fully fuse the volume sample. On the other hand, according to printed platform picture, VED should respect overheating and stress induction. Optimal value should be found between 150 and 167 J/mm^3 (or higher). Secondly would be suitable to surround the platform with cubic samples with the same process parameters and observe the porosity based on platform position (the second cause mentioned above – powder absence).

As the last part of this experiment part the total summary of the mechanical properties can be found in Table 20 with connection to the used VED [J/mm^3] value. All the resulted values were discussed in the previous chapters.

Table 20: Achieved properties with mechanical testing for tool steel L-40 processed by SLM

VED [J/mm^3]	Build angle	HRC	R _m [MPa]	A [%]	R _{p0,2} [MPa]	KU [J]
133	0°	44 ± 0,5	1479 ± 48	10,4 ± 1,2	1177 ± 72	33 ± 2
	45°		1394 ± 49	9,0 ± 0,9	-	13,5 ± 2,5
	90°		1182 ± 81	5,0 ± 1,4	-	10 ± 0,5
Formetrix values [2]		46-48	1500	>14	1300	60*

* value was measured with V-notch

If we put achieved values into previous graphic interpretation (Figure 39 and now updated Figure 68), it can be seen that the goals in a way of hardness were achieved. Because of usual L-40 dynamic process application (like HPDC dies), it is necessary to achieve higher impact energy. If we compare it with H13 as-built state [72], the resulted values are still more optimal for achieved L-40 results. Especially because L-40 can be



applied without any other heat treatment processing. Another important fact is that L-40 was easily printable at the room temperature without crack appearance. All these facts lead to more technical and economical tool manufacturing suitability. In Figure 68 L-40 achieved results are represented by the best 0° build angle values (H13 [72] and L-40 by Frometrix [2]). As it was discussed before, supplier most probably clarifies these values for the same direction (best results according to anisotropy). On the other hand, porosity content found in Charpy samples could lead to failure in the final tool during the application. It is almost necessary to follow mentioned recommendations and optimize the printing process to the best achievable inner quality.

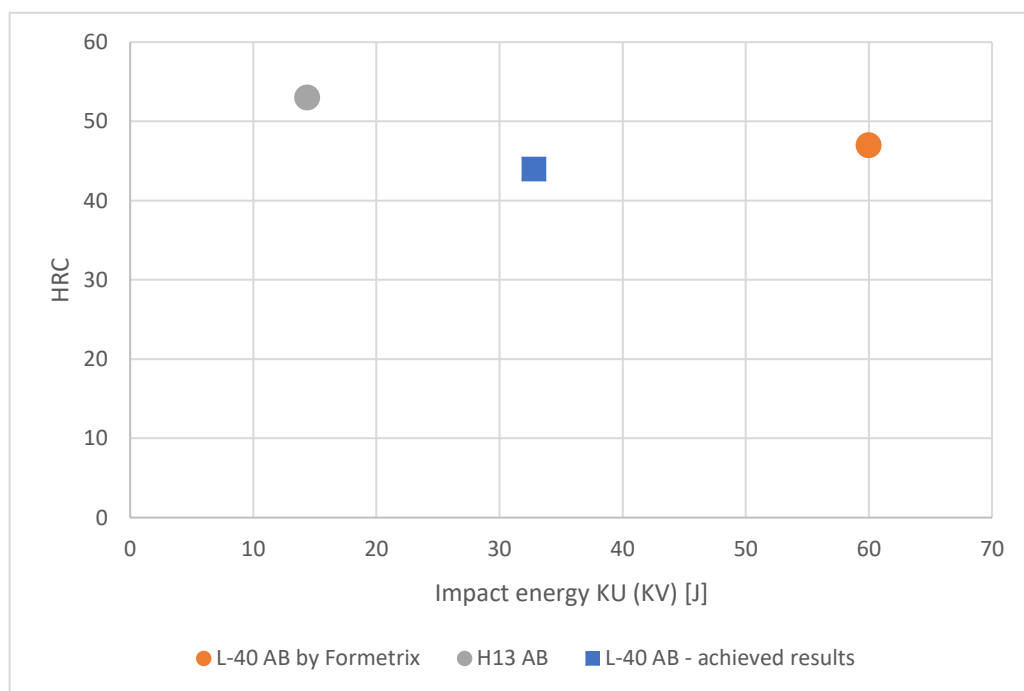


Figure 68: L-40 and H13 comparison in HRC and Impact energy ratio

5.5 Final L-40 application

Purpose of this thesis was to develop process parameters for SLM processing of tool steel L-40. As it was introduced, real application as tool or casting die was considered. Despite small defects found in the last mechanical samples print, final decision was to print the HPDC die core with followed recommendations (Chapter 5.4). Die core application was targeted for company Beneš a Lát a.s. especially for aluminium HPDC process. Visualized die core and die part assembly with cooling channels is shown in Figure 69.

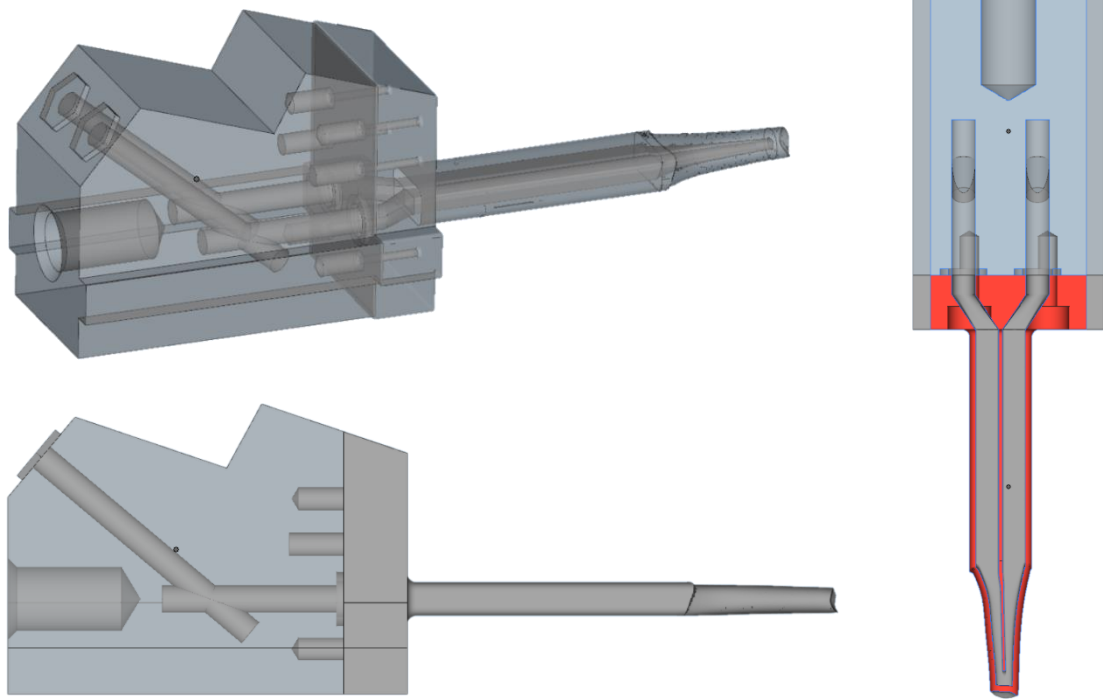


Figure 69: HPDC die assembly with selected L-40 core print application

HPDC die core print was finished after the thesis deadline submission date. The outlook is to test the core in the real casting process and to validate the benefits of the L-40 die part against the previous from different materials (like maraging steels etc.).

It can be said that the goals of the thesis were met except the porosity content in the mechanical testing samples (counter measurements were set). Final application of the casting core can be considered as beyond the scope of handed work. Real application of the research can be also considered as huge success for cooperation between Czech Technical University, NCC MATCA and industry companies like Beneš a Lát a.s. or Cardam Solution s.r.o.



6 Conclusion

Additive manufacturing technologies with focus on Selective laser melting were described. The process parameters and their importance were deeply introduced.

Tool steel L-40 in gas atomized powder was investigated as input material, followed by processing in form of single-tracks and cubic samples for different SLM process parameters. The investigation was finished with tensile and Charpy impact test for specific chosen process parameters. Some of the conclusions are suited for specific printer TruPrint 1000, but they can be adapted.

Conclusions from the experiment part are following:

- 1) Gas atomized powder particles are mostly spherical with few irregularities and no inner porosity. The particle size is $D_{50} = 30,1 \mu\text{m}$ and $D_{90} = 45,9 \mu\text{m}$. These values correspond with the suppliers' specifications and are suitable for SLM processing.
- 2) Chemical composition checked on EDX followed brief specifications by the supplier.
- 3) Single tracks performed with the best results for higher scanning speeds than 700 mm/s. This experiment was probably affected by the first layer thickness.
- 4) Cubic samples were successfully printed for Laser power 180-200 W, scanning speed 500-1400 mm/s, hatch spacing 60-90 μm and 40 μm layer thickness at the room temperature without crack appearance.
- 5) L-40 is printable at the room temperature without preheating.
- 6) Hatch distance of 90 μm is unsuitable parameter for L-40 processing (higher porosity content) on TruPrint 1000 printer.
- 7) Cubic samples with the best density values were achieved with process parameters resulting in VED 133-167 J/mm^3 (scanning speed 500 mm/s for laser power 180 and 200 W, 60 and 75 μm of hatch spacing and layer thickness 40 μm). Final part densities were between 99,94-99,98 %. Lower VED leads to unsuitable porosity.
- 8) The structure of L-40 tool steel in as-build state is formed by the combination of martensite, bainite and retained austenite with final hardness $44 \pm 0,5 \text{ HRC}$. This value approximately corresponds with the Formetrix (supplier's) specifications.



- 9) More efficient parameters with $h=75\ \mu\text{m}$, $P=200\ \text{W}$, $v=500\ \text{mm/s}$ and layer thickness $40\ \mu\text{m}$ were used for mechanical test samples print. These samples were printed in 3 build angle directions 0° , 45° and 90° .
- 10) The best print platform appearance showed 45° build angle samples. These samples performed with low overheat and no support cracks. That leads to the fact that supports under the whole sample transferred the heat successfully, so the stress induction was lower.
- 11) Obtained mechanical properties from all build angle samples were lower than the values clarified by the L-40 supplier (did not state for which build direction are clarified).
- 12) Best mechanical properties were achieved for 0° build angle, which corresponds with the published literature (influence by the grain shape and orientation). Elongation for these samples was $10,4 \pm 1,2\ \%$ and tensile strength $1479 \pm 48\ \text{MPa}$.
- 13) Charpy impact test followed the tensile test results. The values did not meet L-40 supplier's data. The closest value ($33 \pm 2\ \text{J}$) is approximately 59 % lower against the specified value. The values were affected by inner quality.
- 14) Charpy and tensile strength fracture surfaces performed inner defects that caused stress concentrations resulted in lower mechanical properties.
- 15) The light microscopy on all types of build angle samples showed higher porosity amount than in the case of the cubic sample experiment (for the same parameters). The porosity is again irregular with locally nonmelted powder areas. This could be caused by the higher cooling rate area or powder absence based on position on the build platform.
- 16) Based on the conclusion 15), author would recommend for future print use higher VED input, to fully fuse the volume sample – lower the hatch distance to $60\ \mu\text{m}$.
- 17) Goals of this thesis were almost reached, with further recommendations and final application beyond the thesis scope in the form of HPDC casting tool.



7 Literature

- [1] KEMPEN, K., L. THUIS, B. VRACKEN, S. BULS, J.V. HUMBEECK a J.-P. KRUTH. Producing crack-free, high density M2 HSS parts by Selective Laser Melting: Pre-heating the baseplate. *ResearchGate*. University of Leuven (KU Leuven) Department of Mechanical Engineering: University of Leuven (KU Leuven) Department of Mechanical Engineering, 2013, , 9.
- [2] *L-40 Tool Steel Powder for Metal 3D Printing: High-Performance Tool Steel for Powder Bed Fusion Platforms* [online]. In: . Formetrix, s. 2 [cit. 2020-09-23]. Dostupné z: <https://www.formetrixmetals.com/wp-content/uploads/2019/11/Formetrix-PRODUCT-DATA-SHEET-L-40-Fall-2019.pdf>
- [3] *Introduction to Additive manufacturing technology: A guide for Designers and Engineers* [online]. European Powder Metallurgy Association (EPMA): EPMA, Shrewsbury, 2019, [cit. 2020-02-16]. Dostupné z: <https://www.epma.com/epma-free-publications>
- [4] GIBSON, I., D. ROSEN a B. STUCKER. *Additive manufacturing technologies: 3D printing, rapid prototyping and direct digital manufacturing*. Second edition. London: Springer, 2015. ISBN 978-1-4939-2112-6.
- [5] ZHANG, J. a Y. JUNG. *Additive manufacturing: Materials, processes, quantifications and applications*. 1st. Cambridge, MA: Butterworth-Heinemann, 2018. ISBN 978-012-8123-270.
- [6] CHILDERHOUSE, T. a M. JACKSON. Near Net Shape Manufacture of Titanium Alloy Components from Powder and Wire: A Review of State-of-the-Art Process Routes. *Metals* [online]. 2019, **9**(6), 18 [cit. 2020-02-16]. ISSN 2075-4701. Dostupné z: doi:10.3390/met9060689



- [7] KIM, G., S. LEE, H. KIM et al. Three-Dimensional Printing: Basic Principles and Applications in Medicine and Radiology. *Korean Journal of Radiology*. 2016, **17**(2), 16. ISSN 1229-6929. Dostupné z: doi:10.3348/kjr.2016.17.2.182
- [8] 3D printing: The Complete Engineering Guide. In: *3DHUBS* [online]. Amsterdam, Netherlands.: 3D HUBS, 2020 [cit. 2020-02-19]. Dostupné z: <https://www.3dhubs.com/guides/3d-printing/#sla-dlp>
- [9] About Additive Manufacturing: Additive Manufacturing Research Group. In: *Loughbrough University* [online]. London/Loughborough University: Loughborough University, 2020 [cit. 2020-03-08]. Dostupné z: <https://www.lboro.ac.uk/research/amrg/about/the7categoriesofadditivemanufacturing/>
- [10] The impact of layer height on a 3D Print. In: *3DHUBS* [online]. Amsterdam: 3DHUBS, 2020 [cit. 2020-03-08]. Dostupné z: <https://www.3dhubs.com/knowledge-base/impact-layer-height-3d-print/>
- [11] Original PRUSA SL1. In: *PRUSA Research* [online]. Czech Republic: PRUSA 3D, 2020 [cit. 2020-03-08]. Dostupné z: <https://www.prusa3d.com/original-prusa-sl1/>
- [12] Prusa i3 printer: About us. In: *Prusa 3D* [online]. Prague: Prusa research, 2020 [cit. 2020-02-19]. Dostupné z: <https://www.prusa3d.com/about-us/>
- [13] *HP Metal Jet* [online]. California, USA: HP, 2020 [cit. 2020-03-08]. Dostupné z: <https://www8.hp.com/us/en/printers/3d-printers/products/metal-jet.html>
- [14] SLA vs. DLP: Compare Resin 3D Printers (2020 Guide). In: *FORMLABS* [online]. Somerville, MA 02143 USA: FORMLABS, 2020 [cit. 2020-02-19]. Dostupné z: <https://formlabs.com/blog/resin-3d-printer-comparison-sla-vs-dlp/>
- [15] What is FDM. In: *Stratasys* [online]. USA: Stratasys, 2020 [cit. 2020-02-19]. Dostupné z: <https://www.stratasys.com/fdm-technology>



- [16] Introduction to Material Jetting 3D Printing. In: *3DHUBS* [online]. 3DHUBS, 2020 [cit. 2020-02-20]. Dostupné z: <https://www.3dhubs.com/knowledge-base/introduction-material-jetting-3d-printing/>
- [17] Introduction to Binder Jetting 3D printing. In: *3D HUBS* [online]. 3D HUBS, 2020 [cit. 2020-02-26]. Dostupné z: <https://www.3dhubs.com/knowledge-base/introduction-binder-jetting-3d-printing/>
- [18] TruPrint série 1000 - Laser Metal Fusion (LMF): Additivní výrobní systémy. In: *TRUMPF: TruPrint* [online]. TRUMPF, 2020 [cit. 2020-03-02]. Dostupné z: https://www.trumpf.com/cs_CZ/produkty/stroje-systemy/systemy-aditivni-vyroby/truprint-serie-1000/
- [19] YANG, L., K. HSU, B. BAUGHMAN, D. GODFREY, F. MEDINA, M. MENON a S. WIENER. *Additive Manufacturing of Metals: The Technology, Materials, Design and Production*. 1. Cham: Springer International Publishing, 2017. Springer Series in Advanced Manufacturing. ISBN 978-3-319-55127-2.
- [20] JONES, G. Direct Metal Laser Sintering (DMLS). In: *ALL3DP: 3D printing magazine* [online]. All3DP, 2014 [cit. 2020-03-10]. Dostupné z: <https://all3dp.com/2/direct-metal-laser-sintering-dmls-simply-explained/>
- [21] DEMIR, A. a B. PREVITALI. Investigation of remelting and preheating in SLM of 18Ni300 maraging steel as corrective and preventive measures for porosity reduction. In: *The International Journal of Advanced Manufacturing Technology*. 2017, , s. 2697-2709. ISSN 0268-3768. Dostupné z: doi:10.1007/s00170-017-0697-z
- [22] SRIVATSAN, T.S. a T.S. SUDARSHAN. *Additive Manufacturing: Innovations, Advances, and Applications*. 1st. B/W Illustrations, 2015. ISBN ISBN 9781498714778.
- [23] MERTENS, R., B. VRANCKEN, N. HOLMSTOCK, Y. KINDS, J.-P. KRUTH a J. VAN HUMBEECK. Influence of Powder Bed Preheating on Microstructure and Mechanical Properties of H13 Tool Steel SLM Parts. In: *Physics Procedia*. 2016, , s. 882-890. ISSN 18753892. Dostupné z: doi:10.1016/j.phpro.2016.08.092



- [24] LI, Y., K. ZHOU, P. TAN, S. TOR, C. CHUA a K. LEONG. Modeling temperature and residual stress fields in selective laser melting. In: *International Journal of Mechanical Sciences*. 2018, , s. 24-35. ISSN 00207403. Dostupné z: doi:10.1016/j.ijmecsci.2017.12.001
- [25] Visualization of the shielding gas flow in SLM machines by space-resolved thermal anemometry. *Rapid Prototyping Journal* [online]. 2018, , 24 [cit. 2020-03-16]. ISSN 1355-2546. Dostupné z: doi:https://doi.org/10.1108/RPJ-07-2017-0149
- [26] REIJONEN, J., A. REVUELTA, T. RIIPINEN, K. RUUSUVUORI a P. PUUKKO. On the effect of shielding gas flow on porosity and melt pool geometry in laser powder bed fusion additive manufacturing. In: *Additive Manufacturing*. 2020, . ISSN 22148604. Dostupné z: doi:10.1016/j.addma.2019.101030
- [27] MILEWSKI, J. *Additive Manufacturing of Metals: From Fundamental Technology to Rocket Nozzles, Medical Implants, and Custom Jewelry*. First. Cham: Springer International Publishing, 2017. Springer Series in Materials Science. ISBN 978-3-319-58204-7.
- [28] MOSTAFAEI, A., C HILLA, E.L. STEVENS, P. NANDWANA, A.M. ELLIOT a M. CHMIELUS. *Comparison of characterization methods for differently atomized nickel-based alloy 625 powders: Powder Technology* [online]. , 180-192 [cit. 2020-03-14]. Dostupné z: doi:https://doi.org/10.1016/j.powtec.2018.04.014
- [29] PINKERTON, Andrew a Lin LI. The behaviour of water- and gas-atomised tool steel powders in coaxial laser freeform fabrication. *Thin Solid Films*. 2004, **453-454**(1), 600-605. ISSN 00406090. Dostupné z: doi:10.1016/j.tsf.2003.11.171
- [30] *Powder process: Particle Size Distribution (PSD)* [online]. Powder process, 2019 [cit. 2020-08-31]. Dostupné z: https://www.powderprocess.net/psd.html
- [31] YAP, C., C. CHUA, Z. DONG, Z. LIU, D. ZHANG, L. LOH a S. SING. Review of selective laser melting: Materials and applications. *Applied Physics Reviews* [online]. 2015, **2**(4) [cit. 2020-03-11]. ISSN 1931-9401. Dostupné z: doi:10.1063/1.4935926



- [32] LAAKSO, P., T. RIIPINEN, A. LAUKKANEN, T. ANDERSSON, A. JOKINEN, A. REVUELTA a K. RUUSUVUORI. Optimization and Simulation of SLM Process for High Density H13 Tool Steel Parts. In: *Physics Procedia*. Research Centre of Finland Ltd, 2016, , s. 26-35. ISSN 18753892. Dostupné z: doi:10.1016/j.phpro.2016.08.004
- [33] HAGEDORN-HANSEN, D., M.B BEZUIDENHOUT, D.M. DIMITROV a G.A. OOSTHUIZEN. THE EFFECTS OF SELECTIVE LASER MELTING SCAN STRATEGIES ON DEVIATION OF HYBRID PARTS: SLM. In: *South African Journal of Industrial Engineering* [online]. s. 363-376 [cit. 2020-03-15]. ISSN 2224-7890. Dostupné z: doi:https://doi.org/10.7166/28-3-1862
- [34] LIU, B., Bao-Qiang LI a Z. LI. Selective laser remelting of an additive layer manufacturing process on AlSi10Mg: Results in Physics. *Results in Physics* [online]. 2019, **12**(1), 982-988 [cit. 2020-03-15]. ISSN 2211-3797. Dostupné z: doi:https://doi.org/10.1016/j.rinp.2018.12.018.
- [35] CHENG, B., S. SHRESTHA a K. CHOU. Stress and deformation evaluations of scanning strategy effect in selective laser melting. In: *Additive Manufacturing* [online]. Part B. s. 240-251 [cit. 2020-03-15]. ISSN 2214-8604. Dostupné z: doi:https://doi.org/10.1016/j.addma.2016.05.007.
- [36] CHEN, Z., Z. WEI, P. WEI, S. CHEN, B. LU, J. DU, J. LI a S. ZHANG. Experimental Research on Selective Laser Melting AlSi10Mg Alloys: Process, Densification and Performance. In: *Journal of Materials Engineering and Performance*. 2017, , s. 5897-5905. ISSN 1059-9495. Dostupné z: doi:10.1007/s11665-017-3044-5
- [37] SUWAS, S. a D. KUMAR. Microstructure–Texture–Mechanical Property Relationship in Alloys Produced by Additive Manufacturing Following Selective Laser Melting (SLM) Technique. In: *Transactions of the Indian National Academy of Engineering*. ISSN 2662-5423. Dostupné z: doi:10.1007/s41403-019-00081-x
- [38] U2 Revision Hip Stem. In: *United Orthopedic Corporation* [online]. UOC USA INC. (USA Subsidiary) 20 Fairbanks, 2020 [cit. 2020-03-23]. Dostupné z:



www.uocusa.com/medical-professionals/products/hip-systems/u2-revision-hip-stem.aspx

- [39] ZHOU, L., T. YUAN, J. TANG, J. HE a Ruidi LI. *Mechanical and corrosion behavior of titanium alloys additively manufactured by selective laser melting – A comparison between nearly β titanium, α titanium and α β titanium*. In: . 2019, . ISSN 00303992. Dostupné z: doi:10.1016/j.optlastec.2019.105625
- [40] WEI, K., Z. WANG a X. ZENG. Preliminary investigation on selective laser melting of Ti-5Al-2.5Sn α -Ti alloy: From single tracks to bulk 3D components. In: *Journal of Materials Processing Technology*. 2017, , s. 73-85. ISSN 09240136. Dostupné z: doi:10.1016/j.jmatprotec.2017.01.032
- [41] ENGELI, R., T. ETTER, S. HÖVEL a K. WEGENER. Processability of different IN738LC powder batches by selective laser melting. In: *Journal of Materials Processing Technology*. 2016, , s. 484-491. ISSN 09240136. Dostupné z: doi:10.1016/j.jmatprotec.2015.09.046
- [42] Siemens 3D Prints Power Turbine Blades. In: *Digital Engineering: DE Magazine* [online]. Framingham, USA: DE Magazine, 2017 [cit. 2020-03-25]. Dostupné z: <https://www.digitalengineering247.com/article/siemens-3d-prints-power-turbine-blades/>
- [43] NI, X., D. KONG, L. ZHANG, C. DONG, J. SONG a W. WU. Effect of Process Parameters on the Mechanical Properties of Hastelloy X Alloy Fabricated by Selective Laser Melting. In: *Journal of Materials Engineering and Performance*. 2019, , s. 5533-5540. ISSN 1059-9495. Dostupné z: doi:10.1007/s11665-019-04275-w
- [44] Green Light for New 3D Printing Process: PRESS RELEASE. In: *FRAUNHOFER INSTITUTE FOR LASER TECHNOLOGY ILT* [online]. Aachen, Germany: Fraunhofer ILT, 2017 [cit. 2020-03-27]. Dostupné z: https://www.ilt.fraunhofer.de/content/dam/ilt/en/documents/Publication-and-Press/press_release/pr2017/PR_Green_Light_for_New_3D_Printing_Process.pdf



- [45] SINGER, F., D. DEISENROTH, D. HYMAS a M. OHADI. Additively manufactured copper components and composite structures for thermal management applications. In: *2017 16th IEEE Intersociety Conference on Thermal and Thermomechanical Phenomena in Electronic Systems (ITherm)*. IEEE, 2017, s. 174-183. ISBN 978-1-5090-2994-5. Dostupné z: doi:10.1109/ITHERM.2017.7992469
- [46] SPEIRS, M., X. WANG, S. VAN BAELEN, A. AHADI, S. DADBAKHSI, J.-P. KRUTH a J. VAN HUMBEECK. On the Transformation Behavior of NiTi Shape-Memory Alloy Produced by SLM. In: *Shape Memory and Superelasticity*. Springer Link, 2016, , s. 310-316. ISSN 2199-384X. Dostupné z: doi:10.1007/s40830-016-0083-y
- [47] PROCESSING HIGH CARBON STEELS BY SELECTIVE LASER MELTING (SLM). In: *FRAUNHOFER INSTITUTE FOR LASER TECHNOLOGY ILT* [online]. Fraunhofer ILT, 2018 [cit. 2020-03-27]. Dostupné z: [https://www.ilt.fraunhofer.de/content/dam/ilt/en/documents/annual_reports/AR17/TF2/AR17_P52_Processing-high-carbon-steels-by-selective-laser-melting-\(SLM\).pdf](https://www.ilt.fraunhofer.de/content/dam/ilt/en/documents/annual_reports/AR17/TF2/AR17_P52_Processing-high-carbon-steels-by-selective-laser-melting-(SLM).pdf)
- [48] MACEK, Karel. *Kovové materiály*. 2.vydání. V Praze: Nakladatelství ČVUT, 2006. ISBN 80-010-3513-1.
- [49] WU, W.J., S.B. TOR, K.F. LEONG, C.K. CHUA a A.A. MERCHANT. STATE OF THE ART REVIEW ON SELECTIVE LASER MELTING OF STAINLESS STEEL FOR FUTURE APPLICATIONS IN THE MARINE INDUSTRY. In: <https://dr.ntu.edu.sg/bitstream/10356/84425/1/State%20of%20The%20Art%20Review%20on%20Selective%20Laser%20Melting%20of%20Stainless%20Steel%20For%20Future%20Applications%20in%20The%20Marine%20Industry.pdf> [online]. Singapore, 2016 [cit. 2020-04-02]. Dostupné z: www.dr.ntu.edu.sg/bitstream/10356/84425/1/State%20of%20The%20Art%20Review%20on%20Selective%20Laser%20Melting%20of%20Stainless%20Steel%20For%20Future%20Applications%20in%20The%20Marine%20Industry.pdf
- [50] DEEV, A., P. KUZNETSOV, A. ZHUKOV a V. BOBYR. The Structure and Properties of the Samples Produced by Selective Laser Melting of 410L Steel-based Metal Powder. In:



- Physica Procedia*. 2017, , s. 31-38. ISSN 18753892. Dostupné z: doi:10.1016/j.phpro.2017.08.013
- [51] HSU, T.-H., Y.-J. CHANG, Ch.-Y. HUANG, H.-W. YEN, Ch.-P. CHEN, K.-K. JEN a A.-C. YEH. Microstructure and property of a selective laser melting process induced oxide dispersion strengthened 17-4 PH stainless steel. In: *Journal of Alloys and Compounds*. 2019, , s. 30-41. ISSN 09258388. Dostupné z: doi:10.1016/j.jallcom.2019.06.289
- [52] Benefits of Metal 3D Printing with 316L Stainless Steel. In: *Proto3000* [online]. 2019 [cit. 2020-04-02]. Dostupné z: <https://proto3000.com/3d-printing/metal-3d-printing-316l-stainless-steel/>
- [53] SALMAN, O.O., C. GAMMER, J. ECKERT, M.Z. SALIH, E.H ABDULSALAM, K.G. PRASHANTH a S. SCUDINO. Selective laser melting of 316L stainless steel: Influence of TiB₂ addition on microstructure and mechanical properties. In: *Materials Today Communications*. 2019, . ISSN 23524928. Dostupné z: doi:10.1016/j.mtcomm.2019.100615
- [54] ZWIREN, Alex, Chris SCHADE a Simon HOEGES. Economic Additive Manufacturing using Water Atomized Stainless Steel Powder. In: *GKN Powder Metallurgy* [online]. GKN Hoeganaes ,Cinnaminson: GKN Hoeganaes [cit. 2020-04-02]. Dostupné z: https://www.gknpm.com/globalassets/downloads/hoeganaes/technical-library/technical-papers/am/zwiren_economic-additive-manufacturing-using-water-atomized-stainless-steel-powder.pdf/
- [55] HOT-WORK TOOL STEELS WITH IMPROVED PROPERTIES FOR DIE CASTING APPLICATIONS. In: *ResearchGate* [online]. Edlstahl Witten-Krefeld GmbH: ResearchGate, 207 [cit. 2020-04-04]. Dostupné z: https://www.researchgate.net/publication/268264685_HOT-WORK_TOOL_STEELS_WITH_IMPROVED_PROPERTIES_FOR_DIE_CASTING_APPLICATIONS
- [56] MAPAL Innovations 2020: Innovations and product range additions 2020. In: *Mapal* [online]. Mapal, 2020 [cit. 2020-05-08]. Dostupné z:



https://www.mapal.com/fileadmin/mapal_ftp/Blaetterkataloge/index.html?catalog=MAPAL-Innovations-2020&lang=en_GB#page_1

- [57] KUNZ, J., J. SAEWE, S. HERZOG, A. KALETSCH, J. H. SCHLEIFENBAUM a Ch. BROECKMANN. Mechanical Properties of High-Speed Steel AISI M50 Produced by Laser Powder Bed Fusion. In: *Steel research international*. 2020. ISSN 1611-3683. Dostupné z: doi:10.1002/srin.201900562
- [58] SOBOTOVÁ, Jana. *Perspective tool steels*. <https://portal.cvut.cz/wp-content/uploads/2017/04/HP2016-24-Sobotova.pdf>, 2017. Czech Technical University, Prague.
- [59] *Designation systems for steels-Part1: Steel names: EN10027-1*. CEN. Brusel: European committee for standardization, 2005.
- [60] *Tool steels: EN ISO 4957:2000*. Second. Brussels: European comittee for standartization, 2000.
- [61] PTÁČEK, Luděk. *Nauka o materiálu II*. 2. opr. a rozš. vyd. Brno: CERM, 2002. ISBN 80-720-4248-3.
- [62] KUBÍN, Matěj. *HEAT TREATMENT OF TOOL STEELS*. BRNO UNIVERSITY OF TECHNOLOGY, 2017. Bachelor thesis. BRNO UNIVERSITY OF TECHNOLOGY. Vedoucí práce Vít Jan.
- [63] FEUERHAHN, F., A. SCHULZ, T. SEEFELD a F. VOLLERTSEN. Microstructure and Properties of Selective Laser Melted High Hardness Tool Steel. In: *Physics Procedia*. 2013, , s. 843-848. ISSN 18753892. Dostupné z: doi:10.1016/j.phpro.2013.03.157
- [64] BOES, J., A. RÖTTGER, C. MUTKE, C. ESCHER a W. THEISEN. Microstructure and mechanical properties of X65MoCrWV3-2 cold-work tool steel produced by selective laser melting. In: *Additive Manufacturing*. ScienceDirect, 2018, , s. 170-180. ISSN 22148604. Dostupné z: doi:10.1016/j.addma.2018.08.005



- [65] KENNEDY, R. a G. KRAUSS. *Tool Steels*. 5th Edition. ASM International, 1998. ISBN 9781615032013.
- [66] *INTRODUCTION TO HOT ISOSTATIC PRESSING TECHNOLOGY: A guide for Designers and Engineers* [online]. In: . EPMA, 2019, s. 36 [cit. 2020-05-08]. Dostupné z: <https://www.epma.com/epma-free-publications/product/introduction-to-hot-isostatic-pressing-brochure>
- [67] MASUCH, Thomas. *THE HENRY FORDS OF METAL POWDER FOR 3D PRINTING* [online]. Fromnext magazine, 2019 [cit. 2020-09-23]. Dostupné z: <https://fromnextmag.de/highlight-stories/2019/formetrix/?L=1>
- [68] *HIGH PERFORMANCE APPLICATIONS* [online]. 171 Forbes Boulevard, Suite 2000 Mansfield, MA 02048: FORMETRIX, INC., 2017 [cit. 2020-09-26]. Dostupné z: <https://www.formetrixmetals.com/applications/>
- [69] Combining Toughness, Thermal Resistance in HPDC Die Steel: Materials. In: *Foundry management and technology: Foundrymag* [online]. Foundrymag [cit. 2020-05-09]. Dostupné z: <https://www.foundrymag.com/materials/media-gallery/21932109/combining-toughness-thermal-resistance-in-hpdc-die-steel>
- [70] In Automotive, Is Additive Manufacturing an Answer for Die Cast Tooling?. In: *Additive Manufacturing: Magazine* [online]. Additive Manufacturing, 2019 [cit. 2020-05-09]. Dostupné z: <https://www.additivemanufacturing.media/articles/in-automotive-is-additive-manufacturing-an-answer-for-die-cast-tooling>
- [71] JOFFRE, Thomas, Nathalie MAILLOL a et. AL. Development of a New Tooling Steel (L40) for Laser Powder Bed Fusion: Influence of Exposure Parameters and Powder Atomization: Euro PM2019 – Beam Based Technologies I. In: *Euro PM2019 – Beam Based Technologies I*. Maastricht: European Powder Metallurgy Association (EPMA), 2019, s. 7.



- [72] REN, Bo a et. AL. Preparation and mechanical properties of selective laser melted H13 steel. *Journal of Materials Research*, [online]. 2019, , 1415-1425 [cit. 2020-09-23]. Dostupné z: doi:10.1557/jmr.2019.10
- [73] TAN, Chaolin, Kesong ZHOU a et. AL. Microstructural characterization and properties of selective laser melted maraging steel with different build directions. *Science and Technology of Advanced Materials* [online]. Taylor and Francis Group, 2018, , 14 [cit. 2020-09-23]. ISSN 1878-5514. Dostupné z: doi:10.1080/14686996.2018.1527645
- [74] A basic guide to particle characterization. In: *A basic guide to particle characterization* [online]. Grovewood Road, Malvern,: Malvern Instruments Limited, 2015, s. 24 [cit. 2020-08-31]. Dostupné z: https://www.cif.iastate.edu/sites/default/files/uploads/Other_Inst/Particle%20Size/Particle%20Characterization%20Guide.pdf
- [75] *Particle Sizer Analysette 22 NanoTec: University of chemistry and technology, Department of Glass and Ceramics* [online]. Prague: University of chemistry and technology, 2014 [cit. 2020-09-01]. Dostupné z: <http://tresen-old.vscht.cz/sil/cs/node/8204>
- [76] MACEK, Karel, František HNILICA a Vladimír STARÝ. *Experimentální metody v materiálovém inženýrství*. Praha: Nakladatelství ČVUT, 2008. ISBN 978-80-01-03934-2.
- [77] SOLA, Antonella a Alireza NOURI. Microstructural porosity in additive manufacturing: The formation and detection of pores in metal parts fabricated by powder bed fusion. *Journal of Advanced Manufacturing and Processing* [online]. 2019, **1**(3) [cit. 2020-09-17]. ISSN 2637-403X. Dostupné z: doi:10.1002/amp2.10021
- [78] HITZLER, L., J. HIRSCH, B. HEINE, M. MERKEL, W. HALL a A. ÖCHSNER. On the Anisotropic Mechanical Properties of Selective Laser-Melted Stainless Steel. *Materials* [online]. 2017, **10**(10) [cit. 2020-12-05]. ISSN 1996-1944. Dostupné z: doi:10.3390/ma10101136



- [79] MEIER, H. a Ch. HABERLAND. Experimental studies on selective laser melting of metallic parts. *Materialwissenschaft und Werkstofftechnik* [online]. 2008, **39**(9), 665-670 [cit. 2020-12-05]. ISSN 09335137. Dostupné z: doi:10.1002/mawe.200800327
- [80] FEI Quanta SEM FEG. In: *Thermo Fisher Scientific* [online]. [cit. 2020-09-28]. Dostupné z: <https://www.fei.com/products/sem/quanta-sem/#gsc.tab=0>
- [81] ZAYANI, W., S. AZIZI, K. S. EL-NASSER, I. ALI a H. MATHLOUTHI. Structural and electrochemical characterization of new co-doped spinel ferrite nanomaterial used as negative electrode in Ni/MH battery. In: *2018 9th International Renewable Energy Congress (IREC)* [online]. IEEE, 2018, s. 1-5 [cit. 2020-09-28]. ISBN 978-1-5386-0998-9. Dostupné z: doi:10.1109/IREC.2018.8362576



List of abbreviations and variables

<u>Abbreviation</u>	<u>Explanation</u>	<u>Units</u>
%	percentage (fraction)	-
wt. %	weight percentage	-
°	degree	-
µm	micro-meter	-
2D	Two dimensional	-
3D	Three dimensional	-
3DP	Three-Dimensional printing	-
A	Elongation	[%]
A ₁	Fe-Fe ₃ C eutectic temperature line	
ABS	Acrylonitrile Butadiene Styrene	-
A _{cm}	Fe-Fe ₃ C diagram temperature line	-
AISI	American Iron and steel Institute	-
Al	aluminium	-
AM	Additive Manufacturing	-
AMF	Additive manufacturing file	-
approx.	approximately	-
ASTM	American Society for Testing and Materials	-
BCC	Base Centred Cubic	-
BJ	Binder Jetting	-
C	carbon	-
°C	degree Celsia	-
CAD	Computer aided design	-
CCD	Charged-coupled device	-
CDLP	Continuous Digital Light Processing	-
Co	cobalt	-
Cr	chrome	-
Cu	copper	-
ČVUT/CTU	Czech Technical University	-
D _{10,50,90}	Particle size for certain % of powder	-
DLP	Digital Light Processing	-
DMLS	Direct Metal Laser Sintering	-



DOD	Drop on demand	-
e.g.	for example	-
EBAM	Electron beam additive manufacture	-
EBM	Electron Beam Melting	-
EDX	Energy Dispersive X-Ray	-
E_L	Energy linear density	[J/mm]
EN	European standard	-
et.al.	Et alii ("and others")	-
etc.	Et cetera ("and others")	-
FCC	Face Centred Cubic	-
FDM	Fused deposition modelling	-
Fe_3C	iron carbide	-
FFF	Fused Filament Fabrication	-
GA	Gas Atomized	-
GmbH	Company with limited liability	-
h	Hatching distance	[μm]
HAZ	Heat affected zone	-
HCP	Hexagonal Closed Packed	-
HIP	High Isostatic Pressing	-
HPDC	High pressure die casting	-
HRC	Rockwell Hardness -scale C	[N/mm ²]
HSS	High Speed Steel	-
ILT	Institute for Laser Technology	-
ISO	International Organization for Standard	-
J	joule	[N.m]
kg	kilogram	[N.s ² /m]
KV	Impact energy (V-notch)	[J]
KU	Impact energy (U-notch)	[J]
kV	kilo-Volts	-
LENS	Laser Engineered Net Shape	-
LMF	Laser Metal Fusion	-
LOM	Laminated Object Manufacturing	-
Mg	magnesium	-



min	minimum	-
MIT	Massachusetts Institute of Technology	-
MJ	Material Jetting	-
MJF	MultiJet fusion	-
mm	millimetre	-
mm ²	millimetre squared	-
mm ³	cubic millimetre	-
Mn	manganese	-
Mo	molybdenum	-
MPa	Megapascal	[N/mm ²]
N	newton	[kg.m/s ²]
Nb	niobium	-
NCC	National center of competence	-
Ni	nickle	-
NiTi	Nitinol	-
NPJ	Nanoparticle Jetting	-
Ød ₀	diameter of the tensile strength specimen	[mm]
P	Laser Power	[W]
P	phosphor	-
PH	Precipitation hardened	-
ppm	parts per million	-
PSD	Particle Size Distribution	-
R	Tension	[MPa]
R _m	Tensile strength	[MPa]
R _{p0,2}	Yield strength	[MPa]
S	sulphur	-
SEM	Scanning Electron microscope	-
SG	shielding gas	-
Si	Silicon	-
SLA	Stereolithography	-
SLM	Selective Laser Melting	-
SLS	Selective laser sintering	-
STL	Stereolithography	-



t	Layer thickness	[μm]
Ti	Titanium	-
USA	United States of America	-
UV	ultraviolet	-
v	Scanning Speed	[mm/s]
V	Vanadium	-
VED	Volume energy density	[J/mm ³]
W	Watt	[kg.m ³ /s ³]
WA	Water Atomized	-
α	alpha	-
β	beta	-
γ	gamma	-



List of figures

Figure 1: Tool steel L-40 processed in L-PBF printer	2
Figure 2: Additive manufactured part from Ti-alloy [6]	3
Figure 3: SL technology principle [7].....	4
Figure 4: SLA printed model parts [14]	6
Figure 5: FDM technology principle [8]	7
Figure 6: Prusa i3 printer [12]	7
Figure 7: Material jetting technology [16].....	8
Figure 8: Binder jetting technology [17]	9
Figure 9: LMF (SLM) process part production [18]	11
Figure 10: EBM process [5]	12
Figure 11: Printing process [20]	14
Figure 12: SLM part removing [19]	16
Figure 13: Process flow chart.....	16
Figure 14: SLM printer scheme [5]	17
Figure 15: Cracks elimination with preheating for M2 HSS steel [22].....	19
Figure 16 a) Gas atomized powder b) Water atomized of H13 tool steel [29]	21
Figure 17: PSD curve [3].....	22
Figure 18 SLM process parameters example.....	23
Figure 19: L-40 cubic samples from experiment	24
Figure 20: Types of scan strategies [34]	25
Figure 21: Angular offset scan strategy [19].....	25
Figure 22: Ti-6Al-4V hip system stem [38].....	28
Figure 23: SIEMENS 3D printed blade [42]	29
Figure 24: Copper AM processing [44]	30
Figure 25: High carbon steel processing in SLM [47].....	31
Figure 26: 316L additive manufactured part [52].....	34
Figure 27: 18Ni300 SLM printed samples [21]	34
Figure 28: MAPAL 3D printed bell tool [56].....	35
Figure 29: M2 HSS parts produced with a pre-heating temperature of 90°C (left), 150 °C (middle), 200 °C (right) [1]	38
Figure 30: HIP part effect [66]	42



Figure 31: Conventional tool heat treatment (normalizing is not suitable for every tool steel)	43
Figure 32: SLM manufactured tool heat treatment	43
Figure 33: L-40 bolt threading tool [2].....	44
Figure 34: L-40 application examples by Formetrix [68]	46
Figure 35: Approximate HPDC (aluminium) die thermal cycle.....	46
Figure 36: Die failure mechanisms [69]	47
Figure 37: Conventional cooling [70].....	47
Figure 38: Conformal cooling tool [70].....	48
Figure 39: Various tool steels comparison from various sources – left: HRC and elongation, right: HRC and Impact energy	50
Figure 40: TruPrint 1000 by Trumpf company [18]	51
Figure 41: Light scattering in laser diffraction measuring method for larger and smaller particles [74]	52
Figure 42: FEI Quanta 3D FEG [78].....	53
Figure 43: SEM peaks example [79].....	54
Figure 44: Single-track in software Magics.....	55
Figure 45: Deposited first layer.....	56
Figure 46: Cubic samples	56
Figure 47: Cubic samples set up	57
Figure 48: Printing process of the cubic samples	57
Figure 49: L-40 platform examples pre-processed in software Magics	58
Figure 50: PSD resulted curve (orange – cumulative, blue – differential)	60
Figure 51: L-40 powder particles in different magnifications [SEM]	61
Figure 52: Fixed, grained, polished L-40 powder particles [SEM]	62
Figure 53: Printed single tracks.....	64
Figure 54: The best achieved L-40 single track $P=200$ W and $v=1100$ mm/s.....	67
Figure 55: 3D scan of the best achieved L-40 single tracks	67
Figure 56: Final printed L-40 platform for 200 W – on the left de-powdering, on the left finished platform	68
Figure 57 Porosity based on VED value for all L-40 samples.....	69
Figure 58: Irregular shape porosity.....	69



Figure 59: L-40 as-built microstructure on the lowest porosity cubic sample, $44\pm 0,5$ HRC
..... 71

Figure 60: SLM printed platform examples from tool steel L-40 (total print time in hours:
left-13, middle-18, right 13,5)..... 73

Figure 61: L-40 machined SLM testing samples 73

Figure 62: L-40 in as-built state - tensile test results for build angles 0° , 45° and 90° ... 75

Figure 63: Simply visualized cause of samples anisotropy for different build angles 76

Figure 64: Broken L-40 SLM tensile samples for different build angles 76

Figure 65: L-40 in as-built state – Charpy impact test results for build angles 0° , 45° and
 90° 77

Figure 66: L-40 broken Charpy sample (fracture surface) – left 45° build angle, right 90°
build angle..... 78

Figure 67: L-40 Charpy test samples in perpendicular cut – upper left 0° build angle,
upper right – 45° build angle and bottom image 90° build angle 79

Figure 68: L-40 and H13 comparison in HRC and Impact energy ratio 81

Figure 69: HPDC die assembly with selected L-40 core print application 82



List of tables

Table 1: AM technologies - summary	5
Table 2: Printing parameters dealing in this thesis	26
Table 3: Alloy cold-work steels processed by SLM (examples)	37
Table 4: HSS processed by L-PBF examples	38
Table 5: Simplified comparison of the tool steel types [65].....	39
Table 6: Alloying elements in tool steels and their effect on properties [58].....	40
Table 7: L-40 chemical composition declared by Formetrix [2]	44
Table 8: L-40 mechanical and physical properties clarified by the company Formetrix [2]	45
Table 9: Resulted mechanical properties from various atomization powders in publication [71].....	49
Table 10: Various tool steels comparison from various sources.....	50
Table 11: Comparison of measured and specified powder particle size.....	60
Table 12: L-40 powder chemical composition control	63
Table 13: Groups of single tracks.....	65
Table 14: Single-tracks results for specific laser power and scanning speed.....	66
Table 15: L-40 cubic samples -porosity values for laser power 180 W in %.....	70
Table 16: L-40 cubic samples -porosity values for laser power 200 W in %.....	70
Table 17: Metallography pictures summary of samples up to $v=1100$ mm/s assigned to E [J/mm^3] and porosity value [%]	72
Table 18: L-40 as-built state mechanical properties – tensile test.....	74
Table 19: L-40 in as-build state – Charpy impact test results for build angles 0° , 45° and 90°	77
Table 20: Achieved properties with mechanical testing for tool steel L-40 processed by SLM.....	80